Experimental Assessment of Isotopic Trophic Transmission in an Insect Defoliator, the Eastern Spruce Budworm (*Choristoneura fumiferana*): Implications for Pest Dispersal Tracing.

Brent Holmes

Thesis submitted to the University of Ottawa
in partial fulfillment of the requirements for the
Master of Science in Biology

Department of Biology
Faculty of Biology
University of Ottawa

© Brent Holmes, Ottawa, Canada, 2026

PREFACE

This thesis represents original work completed in fulfillment of the requirements for the Master's of Science (Biology) degree at the University of Ottawa. Chapter 2 of this thesis is a manuscript currently under review for publication in the peer-reviewed journal Oecologia.

STATEMENT OF CO-AUTHORSHIP AND CONTRIBUTIONS

I am the primary author of this manuscript. Dr. Clement Bataille, Dr. Felipe Dargent, and I designed the studies. Brent Holmes, Felipe Dargent, and collaborators from the Canadian Forest Service and the Newfoundland Department of Fisheries, Forestry and Agriculture - Forest Insect and Disease Control Section, collected the samples. Brent Holmes, Isabela Marie Silva-Souza, Felipe Dargent, Megan Reich, and Petrus Le Roux performed the laboratory and analytical work. Brent Holmes, Isabela Marie Silva-Souza, Dr. Felipe Dargent, and Dr. Clement Bataille performed the statistical analyses. Jean-Noel Candau, Megan Reich, and Dr. Clement Bataille contributed methods and data. Dr. Clement Bataille and Dr. Felipe Dargent supervised Brent Holmes and gathered funding for this project.

ABSTRACT

Migration plays a vital role in the initiation, spread, and persistence of eastern spruce budworm (*Choristoneura fumiferana*; SBW) outbreaks, but the timing, frequency, and origins of migratory events remain difficult to trace and hinders efforts to manage the detrimental impacts of outbreak spread. A promising alternative is the application of stable isotope geolocation to identify the natal origjn of immigrant individuals, but this approach requires establishing trophic transfer relationships and spatially explicit environmental isotope baselines that have not been previously established for the SBW system. This thesis developed a robust biological and environmental framework necessary to support multi-isotope geolocation of SBW across eastern Canadian boreal forests.

Across eastern Canada, known-origin SBW and foliage samples were collected and analyzed for carbon ($\delta^{13}C$), nitrogen ($\delta^{15}N$), hydrogen ($\delta^{2}H$), sulfur ($\delta^{34}S$), and strontium ($^{87}Sr/^{86}Sr$) isotopes. The trophic transmission relationship between host foliage and SBW were quantified, and high-resolution foliar isoscapes were developed using environmental covariates and random forest models to characterize isotope variation.

$\delta^{15}N$, $\delta^{34}S$, and $^{87}Sr/^{86}Sr$ exhibited strong trophic transmission and pronounced geographic structure, identifying them as the most informative geolocators for SBW. $\delta^{2}H$ retained broad spatial gradients but exhibited weak trophic relationships due to high within-site variability, limiting their utility at regional scales. While $\delta^{13}C$ showed limited geographic discrimination despite measurable trophic transmission. These findings demonstrate that individual isotope systems capture complementary sources of environmental variation and highlights the potential of multi-isotope approaches to enhance isotope geolocation.

This work establishes the first species-calibrated multi-isotope framework for isotope geolocation in SBW and provides one of the first high-resolution foliar isotope baseline datasets spanning the eastern Canadian boreal forest. Beyond supporting future investigations of migratory connectivity and outbreak dynamics, these environmental baselines provide a resource for broader applications in wildlife ecology, biogeochemistry, and natural resource management, while laying the foundation for the application of isotope geolocation for SBW monitoring and management.

ACKNOWLEDGEMENTS

I would not be where, or who, I am today without the unconditional love and support of my parents, Barry and Cathy. I am profoundly grateful for the values you instilled in me, for your unwavering encouragement, patience, and belief in my abilities. I thank my siblings Ryan, Craig, and Kristen, for setting an example that I have always aspired to follow; I love and respect you more than you know. Thank you to my sister and brother-in-law, Monique and Mario, and for the joy brought by my amazing nieces and nephews you have provided. I am deeply thankful to Logan, Mark, and Nic for nearly two decades of friendship. I could not ask for better friends. Together you make me stronger.

I am especially indebted to by supervisor, Clement Bataille, for his mentorship, patience, and intellectual generosity. His guidance was instrumental in shaping both the conceptual framework of this thesis and my development as a researcher. Throughout my MSc, he encouraged me to think critically while challenging me to grow as a scientist. His patience, particularly during setbacks and moments of uncertainty, gave me the confidence and resilience to persevere and grow as an independent scientist, without his encouragement and example, none of this would have been possible.

I would like to extend my sincere gratitude to my co-supervisor, Heather Kharouba, for her guidance throughout my MSc. Having initially joined as a valued member of my thesis advisory committee before kindly agreeing to co-supervise my work, her distinct research background was incredibly beneficial. Her insights provided a unique and welcomed perspective on aspects of my project that might otherwise have been overlooked.

I am eternally grateful to Felipe for the guidance and mentorship that he has always so graciously provided. I would not have entered the field of stable isotope ecology without him. You have been an inspiration to me ever since I first took your Evolution of Sex course as an undergraduate and remain someone I deeply respect and consistently look up to.

To my defense examiners, Tom Sherratt and Kyra St. Pierre, thank you for their challenging questions and valuable insights. While preparing for my thesis defense was a demanding and stressful endeavor, our discussion provided a welcome intellectual challenge that ultimately strengthened the quality of this work.

I would also like to acknowledge the Veizer Lab, Smita and Nimal for their technical expertise, methodological training and willingness to share both time and knowledge. Their collaboration greatly accelerated my learning in stable isotope analysis and analytical practices.

Although I could have thanked my lab mates in the section above, as they became close friends over the course of our graduate studies, their support warrants special recognition. They were always willing to help in the lab, patiently teaching techniques that I would otherwise have struggled to master, and equally willing to spend time outside the lab over drinks and board games. Thank you for the memories we created together along the way, they will stay with me forever.

Obi and Luna, the best dogs in the whole world, deserve special recognition. Their constant companionship, (mostly) quietly resting at my feet while I worked at my desk, was an

essential source of stability and a reminder to rest, reflect, and maintain perspective. With persistent but gentle reminders to take a break to pet, walk, and play with them.

This thesis is dedicated to you Luna. You were the sweetest, gentlest companion I could have ever asked for. Losing you was heartbreaking, and I wish more than anything that you were still with me. You were taken away from me far too soon, and not a day goes by that I do not miss you. Your unwavering love, and unconditional companionship carried me through some of the most difficult moments of this journey, and your memory will always remain a part of it.

Finally, I wish to acknowledge myself, for perseverance in the face of significant adversity. The past several years has been the most challenging of my life, with my illness there were moments when abandoning this seemed inevitable. Although I stumbled along the journey I never gave up. However, this achievement is not mine alone. It is the result of the love and support of those closest to me, who helped me regain confidence and perspective when it was most difficult to do so. Without their guidance and encouragement, I would not have overcome the demands of graduate school. Together, you reminded me that perseverance is sustained not only by discipline, but by community.

Table of Contents

Preface ii

Statement of Co-Authorship and Contributions ii

Abstract iii

Acknowledgements v

List of Tables xiv

Chapter 1: Introduction 1

1.1 Insect Migration *1*

1.1 The eastern spruce budworm (Choristoneura fumiferana) *2*

1.1.1 Ecological and economic consequences 2

1.1.2 Ecology and life history 3

1.1.3 Management strategies 5

1.2 Migration and the challenges of tracking origins *7*

1.3 Stable isotopes as intrinsic markers of origin *9*

1.3.1 Principles of stable isotope ecology 9

1.3.2 1.Isotopes and fractionation 9

1.3.3 Trophic transmission and fractionation 10

1.3.4 Geographic variation in isotopic composition 12

1.3.5 Isotope geolocation 12

1.3.6 Multi-isotope geolocation 13

1.4 Isotope systems relevant to SBW tested in this thesis *14*

1.5 Spruce Budworm as a model system *17*

1.6 Knowledge gaps and rationale *18*

1.7 Objectives and hypotheses *19*

1.8 Overview of thesis structure *20*

Chapter 2: Not all isotopes make good geolocators: trophic transfer reveals contrasting geolocation potential in eastern spruce budworm **22**

2.1 Abstract *25*
2.2 Introduction *26*
2.3 Methods *31*
2.3.1 Foliar sample preparation and isotope analysis 33
2.3.2 Moth sample preparation and isotope analysis 37
2.3.3 Statistical analysis 39
2.3.4 Trophic Discrimination Factor 41
2.4 Results *42*
2.4.1 Carbon 42
2.4.2 Nitrogen 43
2.4.3 Hydrogen 45
2.4.4 Sulfur 49
2.4.5 Strontium 49
2.5 Discussion *52*
2.5.1 Carbon 52
2.5.2 Nitrogen 54
2.5.3 Hydrogen 56
2.5.4 Sulfur 57
2.5.5 Strontium 58
2.5.6 Limitations 61
2.6 Conclusion *61*
2.7 Declarations *63*

Chapter 3: Multi Isotope Geolocation Potential Across the Eastern Canadian Boreal Forest **64**

3.1 Abstract *65*
3.2 Introduction *67*
3.2.1 Objectives 72
3.3 Methods *73*

3.3.1 Foliar sample collection 73
3.3.2 Foliar sample preparation and isotope analysis 73
3.3.3 Isoscape development 78
3.3.4 Selecting the most discriminatory isotope for a given area 82
3.4 Results *84*
3.4.1 Carbon isotopes 84
3.4.2 Nitrogen isotopes 84
3.4.3 Sulfur isotopes 85
3.4.4 Hydrogen isotopes 86
3.4.5 Strontium isotopes 86
3.4.6 Isotope separability 87
3.5 Discussion *89*
3.5.1 Carbon isotopes 89
3.5.2 Nitrogen isoscape 90
3.5.3 Sulfur isoscape 91
3.5.4 Hydrogen isotopes 93
3.5.5 Strontium isotopes 94
3.5.6 Isotope geolocation potential 97
3.5.7 Implications for isotope-based geolocation 99
3.5.8 Limitations 100
3.6 Conclusion *103*
109

Chapter 4: Conclusion **112**

4.1 Summary of Main Findings *112*
4.2 Future Directions and Recommendations *115*
4.3 Use of Artificial Intelligence and Funding *117*

References **118**
Supplementary **134**

LIST OF FIGURES

Figure 1.1 - Generalized life cycle of the eastern spruce budworm *(Choristoneura fumiferana*). The dashed line represents the overwintering diapause stage. Life-stage illustrations were generated using Open AI ChatGPT from reference images and assembled by author. 5

Figure 2.1 - Known-origin sample sites for host conifer foliage (*Abies balsamea* and Picea spp.) and spruce budworm (*Choristoneura fumiferana*) across eastern Canada. Points indicate site location and lines point to the stable isotope analyzed for foliage and budworm tissues, including hydrogen (δ^2H), carbon (δ^{13}C), nitrogen (δ^{15}N), sulfur (δ^{34}S), and strontium (^{87}Sr/^{86}Sr). 30

Figure 2.2 - Linear relationships describing trophic transmission of (A) δ^{13}C and (B) δ^{15}N from host foliage (Pinaceae) to known-origin SBW tissues (*Choristoneura fumiferana*) across sites in eastern Canada (δ^{13}C: 7 sites, 38 moths; δ^{15}N: 7 sites, 38 moths). Each point represents a foliage sample, and its corresponding moth samples from the same site. Solid lines indicate population-level fixed effects from linear mixed-effects models (with site of collection treated as a random intercept) and marginal 95% confidence intervals (shaded ribbon), while the dashed lines denote the 1:1 relationship for reference. Error bars represent ±1 standard deviation of the internal reference material (C-55: glutamic acid) within the analytical run, reflecting analytical uncertainty. Marginal (R^2_m) and conditional (R^2_c) R^2 values reported. 40

Figure 2.3 - Linear relationships describing trophic transmission of (A) δ^2H, (B) δ^{34}S, and (C) ^{87}Sr/^{86}Sr from host foliage (Pinaceae) to known-origin SBW tissues (*Choristoneura fumiferana*) across sites in eastern Canada (δ^2H: 19 sites, 126 moths; δ^{34}S: 23 sites, 74 moths; ^{87}Sr/^{86}Sr$_{indiv.}$: 18 sites, 58 moths; ^{87}Sr/^{86}Sr$_{pool.}$: 12 sites). (A, B) Each point represents a foliage sample, and its corresponding moth samples from the same site. Solid lines indicate population-level fixed effects from linear mixed-effects models (with site of collection treated as a random intercept) and marginal 95% confidence intervals (shaded ribbon). Marginal (R^2_m) and conditional (R^2_c) R^2 values reported. (C) Includes both individual moth samples (filled circles) and site-level pooled samples (open circles) excluded from the individual sample regression. Solid (individual moths) and broken (pooled moths) lines represent ordinary least squares regressions with 95% confidence intervals (shaded). Dashed lines indicate the 1:1 relationship for reference. Error bars represent analytical uncertainty based on internal reference materials within each analytical run, reflecting analytical uncertainty. 45

Figure 2.4 - Residual patterns of ^{87}Sr/^{86}Sr trophic transfer as a function of ^{88}Sr signal intensity. (A) Residuals from the ordinary least-squares regression of ^{87}Sr/^{86}Sr$_{SBW}$ versus ^{87}Sr/^{86}Sr$_{foliar}$ for individual SBW samples plotted against ^{88}Sr signal intensity (a proxy for overall available Sr). (B) Equivalent residual plot for site-level pooled moth samples. Note that panels share a common y-axis but differ in x-axis range. Shaded envelopes represent the dispersion of residuals across the gradient of ^{88}Sr intensity, and bounds the maximum residual variance across the observed intensity. 47

Figure 3.1 - Sampling sites across the eastern Canadian boreal forest. Distribution of sampled individuals across 339 sites in the eastern Canadian forest. Numbers correspond to site identifiers listed in Table 1. The map highlights the provinces where sampling took place, with grey lines indicating provincial boundaries. Symbols represent sampled sites, and the colour represent the number of isotope systems that was analyzed for each. Symbol size is scaled according to the number of individuals sampled per site (see legend). Provincial boundaries were obtained from Natural Earth (2023). 102

Figure 3.2 - Random Forest regression performance, partial dependence plots (PDPs) and predictions for $\delta^{13}C$ in needles. (a) Relationship between observed and predicted $\delta^{13}C$ values, with a fitted regression line (black) and the 1:1 reference line (dotted). (b) PDPs of predictors on predicted $\delta^{13}C$. Solid black lines represent the average predicted response when varying each predictor independently. Histograms below each plot indicate the distribution of observed values for the corresponding variable, providing context on sampling density. 103

Figure 3.3 - Random Forest regression performance, partial dependence plots (PDPs) and predictions for $\delta^{15}N$ in needles. (a) Relationship between observed and predicted $\delta^{15}N$ values, with a fitted regression line (black) and the 1:1 reference line (dotted). (b) PDPs of predictors on predicted $\delta^{15}N$. Solid black lines represent the average predicted response when varying each predictor independently. Histograms below each plot indicate the distribution of observed values for the corresponding variable, providing context on sampling density. 105

Figure 3.4 - Random Forest regression performance, partial dependence plots (PDPs) and predictions for $\delta^{34}S$ in needles. (a) Relationship between observed and predicted $\delta^{34}S$ values, with a fitted regression line (black) and the 1:1 reference line (dotted). (b) PDPs of predictors on predicted $\delta^{34}S$. Solid black lines represent the average predicted response when varying each predictor independently. Histograms below each plot indicate the distribution of observed values for the corresponding variable, providing context on sampling density. 106

Figure 3.5 - Random Forest regression performance, partial dependence plots (PDPs) and predictions for $\delta^{2}H$ in needles. (a) Relationship between observed and predicted $\delta^{2}H$ values, with a fitted regression line (black) and the 1:1 reference line (dotted). (b) PDPs of predictors on predicted $\delta^{2}H$. Solid black lines represent the average predicted response when varying each predictor independently. Histograms below each plot indicate the distribution of observed values for the corresponding variable, providing context on sampling density. 107

Figure 3.6 - Random Forest regression performance, partial dependence plots (PDPs) and predictions for $^{87}Sr/^{86}Sr$ in needles. (a) Relationship between observed and predicted $^{87}Sr/^{86}Sr$ ratios, with a fitted regression line (black) and the 1:1 reference line (dotted). (b) PDPs of predictors on predicted $^{87}Sr/^{86}Sr$. Solid black lines represent the average predicted response when varying each predictor independently. Histograms below each plot indicate

the distribution of observed values for the corresponding variable, providing context on sampling density. 108

Figure 3.7 - Predicted mean foliar isoscapes for carbon ($\delta^{13}C$), nitrogen ($\delta^{15}N$), sulfur ($\delta^{34}S$), hydrogen ($\delta^{2}H$), and strontium ($^{87}Sr/^{86}Sr$) across eastern Canada. 109

Figure 3.8 - Scale-dependent dominance of isotope geolocation potential across eastern Canada. Maps show the isotopes with the highest relative separability at each location, ranking the isotope expected to provide the strongest geolocation power at a given spatial scale. Panel (a) displays dominance evaluated at a ~10 km scale, while panel (b) shows dominance at a ~100 km scale. 109

Figure S1 - Spatial distribution of predictive uncertainty (standard deviation) associated with the mean foliar isoscapes for carbon ($\delta^{13}C$), nitrogen ($\delta^{15}N$), sulfur ($\delta^{34}S$), hydrogen ($\delta^{2}H$), and strontium ($^{87}Sr/^{86}Sr$) across eastern Canada. Uncertainty estimates were derived from quantile random forest models and represent the expected pixel-wise variability of isotope predictions. 1

Figure S2 - Dominance strength of isotope geolocation potential at two spatial scales. Maps show the dominance strength, defined as the maximum fractional separability across all isotope systems (C, N, S, H, and Sr) at each pixel. Dominance strength quantifies how strongly the top-ranked isotope outperforms all alternatives at a given location. Panel (a) displays dominance strength evaluated at a ~10 km spatial scale, and panel (b) at a ~100 km scale. Values approaching 1 indicate areas where a single isotope provides strongly dominant geolocation information, whereas lower values indicate regions where multiple isotopes contribute comparably to geolocation potential. 1

Figure S3- Spatial distribution of isotope rank based on fractional separability evaluated at a 10 km spatial scale. Each panel shows, for an individual isotope system (carbon, nitrogen, sulfur, hydrogen, or strontium), its rank relative to all other isotopes at each pixel (rank 1 = highest geolocation potential; rank 5 = lowest). Ranks were derived by ordering isotope-specific fractional separability values from highest to lowest at each location. 2

Figure S4 - Spatial distribution of isotope rank based on fractional separability evaluated at a 100 km spatial scale. Each panel shows, for an individual isotope system (carbon, nitrogen, sulfur, hydrogen, or strontium), its rank relative to all other isotopes at each pixel (rank 1 = highest geolocation potential; rank 5 = lowest). Ranks were derived by ordering isotope-specific fractional separability values from highest to lowest at each location. 3

LIST OF TABLES

Table 3-1 - Summary of sample analyzed for each isotope system. 74

Table 3-2 - Auxiliary variables tested for developing the random forest regression for each isotope system..... 79

Table S1 – Known-origin foliage samples.....135

Table S2– Known Origin SBW Samples 136

CHAPTER 1: INTRODUCTION

1.1 Insect Migration

Insect migration is a widespread ecological phenomenon that can influence ecosystem structure and function across regional and continental spatial scales. Migratory insects contribute to nutrient redistribution, trophic interactions, pollination dynamics, and ecological connectivity by transporting biomass and biological material among geographically distant habitats (Holland et al., 2006; Hu et al., 2016). For example, 2.6 billion hoverflies (*Episyrphus* spp.) migrate across the English Channel annually, delivering important ecosystem services such as nutrient cycling, introducing 1,000–2,500 kg of nitrogen and 100–250 kg of phosphorus, while their first generation of larvae consumes an estimated 6.3 trillion aphids each spring, exerting top-down control on herbivore populations (Gilbert, 2019). Annual insect migrations can involve trillions of individuals, collectively representing a biomass that surpasses that of many vertebrate migrants, and through these movements' insects transport nutrients, species, and genes in ways that parallel the role of plankton in oceanic food webs (Johnson, 1969; Hu et al., 2016).

Despite its ecological importance, scientific understanding of insect migration remains limited relative to vertebrate migration, largely because of the challenges associated with tracking small-bodied organisms over long distances (Chapman et al., 2015). This gap is particularly important for migratory pest insects, whose dispersal can generate substantial ecological, economic, and public-health consequences. *Anopheles* mosquitoes, which vector malaria, have been documented migrating hundreds of kilometres, facilitating disease transmission beyond regions covered by localized public-health initiatives (Huestis et al.,

2019), and locust swarms containing 50 million individuals per km^2 can consume up to 200 tons of vegetation daily, posing major threats to food security (FAO, 2020). For pest insects, migration influences the spatial and temporal patterns of infestation and the severity of damage to economically important crops and forests, so identifying the origins, dispersal pathways, and drivers of migration can improve forecasting and support targeted management (Pedgley, 1993; Cardim Ferreira Lima et al., 2020). Yet the absence of methods capable of tracing pest migration and geographic origin at high spatio-temporal resolution continues to limit these efforts.

1.1 The eastern spruce budworm (*Choristoneura fumiferana*)

1.1.1 Ecological and economic consequences

The eastern spruce budworm (*Choristoneura fumiferana*; SBW) is the most severe pest of the North American boreal forest, causing extensive defoliation of spruce (*Picea* spp.) and balsam fir (*Abies balsamea*) stands during outbreak periods (Chang et al., 2012; MacLean, 2016). Recurrent outbreaks cause major socio-economic impacts, for example, 44 million m^3 of wood was lost annually during Quebec's last outbreak, alongside job losses (Sterner and Davidson, 1982), heightened forest-fire risk (James et al., 2017; Manzello, 2020), and increased CO_2 emissions from the decomposition of dead trees and reduced carbon capture (Dymond et al., 2010).

SBW populations exhibit highly cyclical dynamics, characterized by prolonged endemic periods interrupted by large-scale outbreaks occurring approximately every 30 to 40 years (Royama et al., 2017; Johns et al., 2026). Population amplitudes may exceed four orders of magnitude between outbreak troughs and peaks, making SBW one of the most eruptive

forest insects in North America (Cooke and Régnière, 2025). During endemic phases, populations are believed to be regulated primarily by a complex assemblage of predators, parasitoids, and pathogens that maintain low densities; during outbreaks these natural controls become overwhelmed, allowing rapid population growth and expansion (Royama et al., 2017).

The first reliable records of SBW outbreaks date to around 1770, with paleoecological evidence extending into the early Holocene (Greenbank, 1963b; Simard et al., 2006). In the 20th century alone, three major outbreaks occurred, including the severe 1967–1993 outbreak that affected more than 50 million hectares of forest and resulted in an estimated 238 million m^3 of timber losses and $12.5 billion in lost revenue (Kettela, 1983; Grondin et al., 1996). The most recent outbreak began in Quebec in 2006 and defoliated 13.5 million ha in Quebec alone by 2020 (Canada, 2013; Healthy Forest Partnership, 2019). These consequences have motivated the development of management programs aimed at reducing outbreak severity and spread.

1.1.2 Ecology and life history

SBW is a lepidopteran in the family Tortricidae whose distribution closely overlaps that of its primary hosts, with a transcontinental range extending from the Atlantic coast of North America to Alaska (Mattson et al., 1988; Saskatechewan Ministry of Environment, 2018). Throughout its range it is closely associated with forests dominated by balsam fir (*Abies balsamea*) and spruce (*Picea* spp.), with larvae feeding primarily on the current-year foliage of balsam fir, white spruce (*Picea glauca*), red spruce (*Picea rubens*), and black spruce (*Picea mariana*; Greenbank, 1963). In eastern Canada, SBW completes a univoltine life cycle (Figure

1.1) that is closely synchronized with host phenology, particularly budburst, shoot elongation, and needle development, ensuring larvae have access to high-quality foliage during development (Miller, 1963). Eggs are laid in late July to early August; first-instar larvae emerge and disperse to sheltered microsites where they construct silken hibernacula and overwinter as second-instar larvae in diapause (Régnière and Nealis, 2007; Royama et al., 2017). In spring, larvae mine within the previous year's needles before transitioning to developing buds and current-year foliage following budburst, developing through six instars before pupation in early to mid-summer and adult emergence (Miller, 1963; Régnière and Nealis, 2007; Wardlaw et al., 2022). Following emergence, females typically deposit a portion of their eggs before dispersing to new locations to lay the remainder, and because adults are capable of long-distance dispersal they facilitate population connectivity across geographically separated regions (Greenbank et al., 1980).

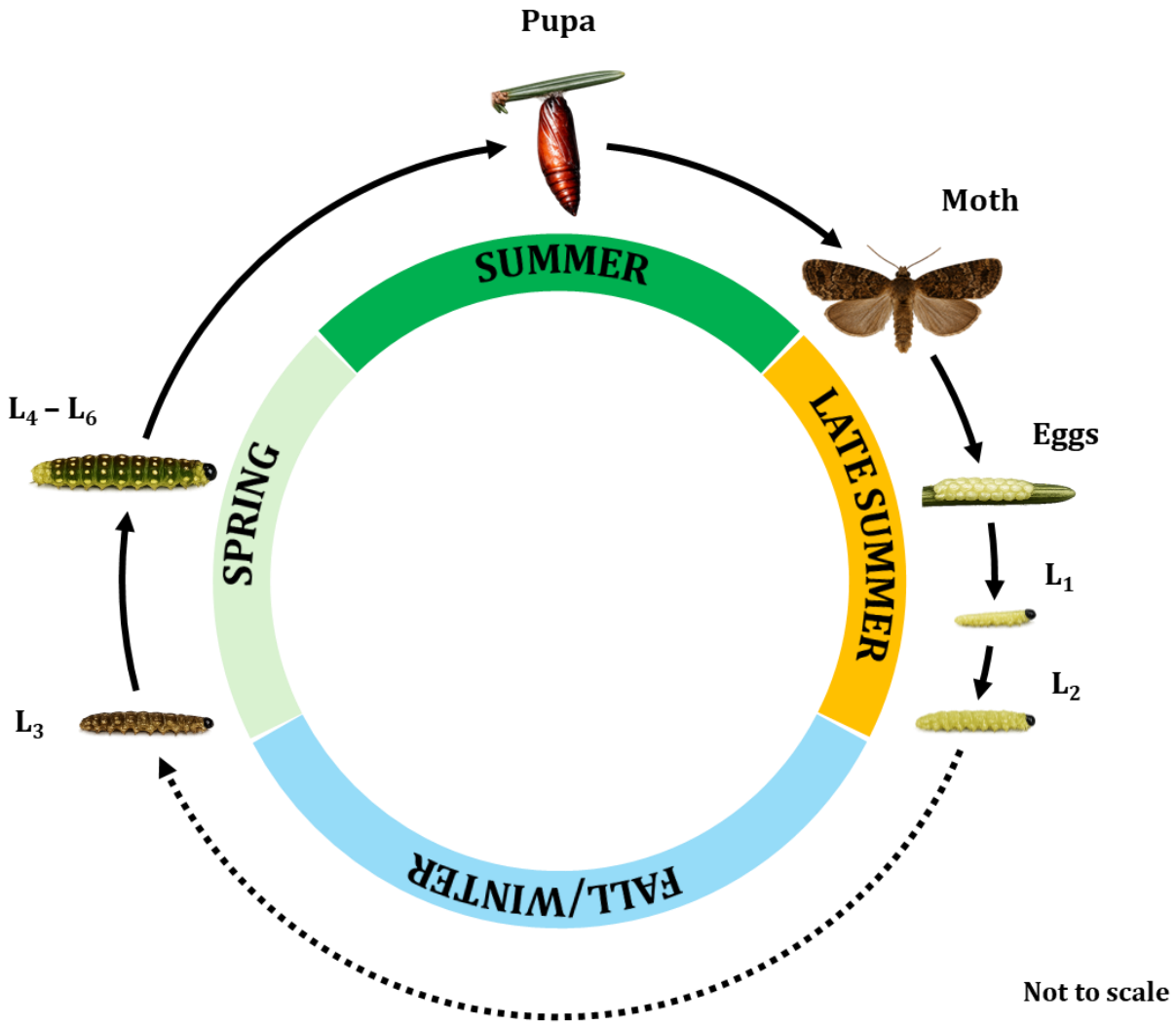

Figure 1.1 - Generalized life cycle of the eastern spruce budworm *(Choristoneura fumiferana*). The dashed line represents the overwintering diapause stage. Life-stage illustrations were generated using Open AI ChatGPT from reference images and assembled by author.

1.1.3 Management strategies

Management of SBW outbreaks has traditionally relied on the aerial application of biological insecticides, primarily *Bacillus thuringiensis kurstaki* (Btk) and the moulting regulator tebufenozide (Régnière et al., 2019). Two broad approaches have been developed to mitigate the ecological and economic impacts of outbreaks: the Foliage Protection Strategy (FPS) and the Early Intervention Strategy (EIS).

FPS aims to reduce tree mortality and timber losses by protecting high-value or high-risk stands once populations reach outbreak densities, suppressing larval feeding to maintain annual defoliation below levels associated with growth loss and mortality (Fuentealba et al., 2019; Liu et al., 2022; Johns et al., 2026). Although effective at preserving treated stands, control is applied after outbreak establishment and therefore does not prevent regional expansion; reinfestation by moths dispersing from nearby untreated sites is common and requires repeated applications (Bauce et al., 2004; Fuentealba et al., 2019).

EIS, by contrast, is a proactive, area-wide approach designed to suppress populations before outbreak establishment by targeting "hotspots", low-density but increasing populations, identified when L2 densities exceed seven larvae per 75 cm branch, the point at which populations begin to overcome Allee effects and are likely to grow rapidly (MacLean, 2016; Régnière and Nealis, 2019; Régnière et al., 2019). Trials show that EIS can substantially reduce hotspot abundance and limit outbreak expansion across large management areas (Johns et al., 2026). Its success, however, depends on detecting emerging hotspots before populations reach outbreak densities, and current detection relies on labour-intensive surveys of overwintering L2 that are costly and difficult to implement across large or remote landscapes (MacLean, 2016; Johns et al., 2019). Hotspots may form through local population growth, immigration, or a combination of both, and distinguishing among these requires knowing the geographic origins of adult moths, particularly when mass immigration events occur. However, conventional monitoring cannot easily and practically provide this information.

1.2 Migration and the challenges of tracking origins

Local SBW population density reflects not only survival and reproduction but also immigration and emigration, so recruitment can vary substantially among locations depending on regional dispersal (Royama et al., 2017). Although most SBW dispersal occurs over short distances and contributes to local connectivity, irregular long-distance migration events (>100 km) involving large numbers of gravid moths can seed previously uninfested or low-density populations, rapidly increasing larval densities the following year and potentially initiating new hotspots and outbreak expansion (Greenbank et al., 1980; Johns et al., 2019). Such pulses can overwhelm the natural controls of predation, parasitism, and stochastic mortality, so migration is recognized as a major driver of outbreak expansion and population connectivity (Ludwig et al., 1978; Pureswaran et al., 2016). Regional synchrony among geographically separated populations is thought to arise in part from spatially correlated, weather-driven variation in moth dispersal and egg recruitment, linking otherwise independent local populations into source and sink regions (Royama et al., 2017; Régnière and Nealis, 2019).

Climatic and meteorological conditions strongly influence the timing, magnitude, and direction of these events. SBW moths are strong, active fliers capable of flying 42 km unassisted, but under favourable winds they can disperse up to 450 km (Greenbank et al., 1980; Sturtevant et al., 2013), so migration depends on a complex combination of temperature, wind speed and direction, precipitation, atmospheric stability, and local density (Anderson and Sturtevant, 2011; Wainwright et al., 2017). While broad climatic conditions may influence the probability of migration, they do not identify where migrant moths

originate, so determining source regions remains a central challenge for SBW ecology and management and motivates the search for intrinsic markers of natal origin.

A range of approaches has been developed to investigate insect movement, each with strengths and limitations, but tracking SBW has proven especially difficult. Mark–release–recapture, in which insects are tagged, released, and subsequently recaptured to infer movement, provides direct individual-level information but suffers from low recapture rates for long-distance or low-density events and has not produced convincing results for SBW (Sanders, 1983; James et al., 2018). Radar entomology can monitor large-scale aerial movements in real time, and weather-surveillance radar has been used to track SBW exodus flights (Boulanger et al., 2017); however, radar cannot reliably distinguish among species, particularly small taxa, and Boulanger et al. (2017) acknowledged limitations in species identification, source-area determination, and reconstructing connectivity among populations. External tagging with passive transponders is costly, restricted to larger insects, and limited to detection ranges below ~1 km, making it unfeasible for moths the size of SBW (Chapman et al., 2011; Hobson and Wassenaar, 2019). Population genomic approaches infer connectivity from genetic differentiation but are ineffective in species with high gene flow and weak population structure, as is the case for SBW (Lumley et al., 2020). Ecological niche modelling can identify suitable establishment regions and potential source populations from occurrence and environmental data, but its accuracy depends on the quality of those datasets, which are often limited for insects (Menchetti et al., 2019; Nanini et al., 2024). Finally, wind-trajectory modelling simulates the movement of air parcels to infer potential dispersal pathways and has been applied to SBW (Sturtevant et al., 2013), but it depends on the accuracy of meteorological data and necessarily simplifies natural dispersal (Hopkinson

and Soroka, 2010). Collectively, these limitations highlight the need for a complementary, intrinsic marker capable of recording an individual's geographic origin.

1.3 Stable isotopes as intrinsic markers of origin

1.3.1 Principles of stable isotope ecology

Stable isotope analysis overcomes several limitations of traditional tracking methods. It does not require individuals to be captured, marked, and recaptured; it can be applied to small insects; and it does not require direct observation of migration events. Most importantly, stable isotopes can provide information about the geographic origin of individuals, allowing natal origins to be inferred retrospectively after capture (Bowen et al., 2005; Hobson and Wassenaar, 2019). Isotopes function as intrinsic markers because organisms naturally incorporate the isotopic composition of their local environment into their tissues during development (Peterson and Fry, 1987). As many isotope systems vary predictably across landscapes, tissues formed in different locations acquire distinct isotopic compositions, and comparing tissue values to isoscapes (i.e., spatially explicit models of isotope distribution) makes it possible to infer where an individual developed (Bowen et al., 2005; Bataille et al., 2021).

1.3.2 1.Isotopes and fractionation

Isotopes are forms of an element that differ in neutron number and atomic mass while sharing the same number of protons and chemical properties; stable isotopes are non-radioactive forms whose relative abundances vary naturally among environmental materials (Michener and Lajtha, 2007; Sharp, 2007). Because isotopic differences are extremely small, composition is expressed using delta (δ) notation as the deviation of a sample's heavy-to-light isotope ratio from an internationally recognized reference material, in parts per

thousand (‰); positive values indicate enrichment in the heavy isotope relative to the standard, and negative values indicate depletion (Peterson and Fry, 1987; Michener and Lajtha, 2007).

Natural variation arises because isotopes do not participate equally in physical, chemical, and biological processes, a phenomenon termed fractionation (Hoefs, 2021). Most fractionation reflects differences in isotope mass, which influence bond strength and reaction kinetics, causing lighter isotopes to participate more readily in processes such as diffusion, evaporation, photosynthesis, nutrient uptake, and enzymatic reactions (Michener and Lajtha, 2007; Sharp, 2007; Hoefs, 2021). Kinetic fractionation occurs when lighter isotopes react or move more rapidly than heavier ones, enriching reaction products in the lighter isotope, whereas equilibrium fractionation partitions isotopes unequally between compounds or phases at equilibrium, producing predictable differences between reactants and products (Michener and Lajtha, 2007). These processes generate predictable isotopic differences among water, soils, plants, and animals, and underlie both the spatial and the trophic patterns central to stable isotope ecology (Sharp, 2007; Hobson and Wassenaar, 2019; Hoefs, 2021).

1.3.3 Trophic transmission and fractionation

Trophic transmission describes the transfer of isotopic composition from environmental resources to consumer tissues through feeding relationships (Michener and Lajtha, 2007). As organisms consume and assimilate food, the isotopic composition of those resources is incorporated into newly synthesized tissues, allowing isotopic information acquired at lower trophic levels to propagate through food webs (Deniro and Epstein, 1978; Peterson and Fry,

1987). Although values are modified during assimilation and metabolism, broad environmental and spatial patterns are frequently conserved during transfer (Hobson, 1999; Wunder, 2012; Hobson and Wassenaar, 2019). For migratory organisms this is critical: if isotopic variation is transferred predictably between trophic levels, consumer tissues can serve as intrinsic records of the environment in which they formed.

Isotopic compositions are rarely transferred unchanged, however. During digestion, assimilation, metabolism, tissue synthesis, and excretion, processes may preferentially retain or eliminate certain isotopes, producing offsets between consumers and their diet that are commonly termed trophic discrimination (or enrichment) factors (Deniro and Epstein, 1978, 1981). The magnitude and direction of these factors vary among isotope systems, nitrogen, for example, typically becomes enriched with trophic level through preferential excretion of lighter isotopes during protein metabolism, whereas carbon shows smaller trophic shifts but also vary with species, developmental stage, tissue type, diet quality, nutritional stress, and metabolic activity (Martínez Del Rio et al., 2009; Sato and Azuma, 2016; Stephens et al., 2022). Discrimination factors derived from one species or system are therefore not always transferable to another (Martínez del Rio et al., 2009). As isoscapes are usually built from primary dietary resources (e.g., water, plants), a pre-requisite to deploy isotope geolocation is therefore to understand how the composition of those dietary resources is transmitted or modified during trophic transfer to ensure that spatial patterns present in dietary resources is conserved in consumer tissues (Wunder, 2012; Magozzi et al., 2019). In the case of SBW, it is critical to quantify the trophic transmission and fractionation between host foliage and SBW tissues before deploying the isotope geolocation framework in this system.

1.3.4 Geographic variation in isotopic composition

Another key component of applying isotope geolocation is that the isotope system used displays strong and predictable geographic variation (Wunder, 2012; Hobson and Wassenaar, 2019). Across landscapes, isotope composition varies in response to atmospheric, hydrological, geological, biological, and anthropogenic processes that generate spatially structured patterns, which can be modelled to predict isotope distributions across regions (Bowen, 2010; West et al., 2010; Bataille et al., 2021). However, the dominant drivers differ among systems, for example, hydrogen is governed largely by precipitation and climate, sulfur by marine-aerosol deposition and coastal proximity, strontium by underlying geology, and carbon and nitrogen by ecosystem processes and anthropogenic inputs. Each system therefore provides distinct but complementary geographic information that can be integrated to improve the accuracy of isotope geolocation (Bataille et al., 2021). Although trophic fractionation may alter absolute values, the underlying geographic structure is usually conserved in consumer tissues, which is precisely what allows organisms to retain a record of where they were born or developed their tissues (Hobson, 1999; Hobson and Wassenaar, 2019). The specific drivers on each isotope system tested in this thesis are detailed later in this introduction.

1.3.5 Isotope geolocation

Isotopic compositions vary predictably across landscapes and are transmitted to organisms (West et al., 2010). As a result, tissue composition can indicate the environmental conditions and region in which a tissue formed (Bowen et al., 2005; Hobson and Wassenaar, 2019). This is the basis of isotope geolocation, which uses spatial variation in isotopic composition to probabilistically assess potential regions of origin for individuals (Hobson et al., 2019b). By

comparing an individual's isotope composition to expected local isotope baselines, geolocation can distinguish residents from migrants and reconstruct natal origins. In holometabolous insects, metabolically inert, low-turnover tissues such as wings can preserve larval isotopic compositions throughout adult dispersal, allowing geolocation to approximate natal origin (Dargent et al., 2023, 2026; Lindroos et al., 2023). Isotope geolocation is quantitatively applied using Bayesian probability, by comparing the isotope composition of the sample of unknown origin to an isoscape mean and uncertainty (Wunder and Norris, 2008; Wunder, 2010; Ma et al., 2020; Courtiol, 2022). This comparison produces posterior probability surfaces which are usually not extremely precise for a given isotope. Those surfaces usually display broad high probability areas of potential origin because isotope composition are redundant on the landscape (Bataille et al., 2021) Fortunately, different isotope systems are governed by different processes and vary independently across space, therefore, combining multiple isotope systems can substantially improve geolocation precision by constraining origin across several environmental dimensions simultaneously (Bowen, 2010; West et al., 2010; Bataille et al., 2021).

1.3.6 Multi-isotope geolocation

Recent studies demonstrate the potential of applying multi-isotope geolocation for investigating insect migration and population connectivity. Reich et al., (2021, 2024, 2025) used δ^2H and $^{87}Sr/^{86}Sr$ to study the connectivity of monarch butterflies (*Danaus Plexippus*) across the US and painted ladies (*Vanessa cardui*) across the Afro-Palearctic revealing a multi-generational latitudinal migration of those species. For the painted ladies, they reconstructed the detailed migratory pathways and strategy of the species across the Sahara revealing connectivity and migratory leapfrog behavior that were impossible to identify

previously (Larsen, 1975). Recent preliminary work on SBW by Dargent et al. (2023) showed that dual-isotope analysis (δ^2H and ^{87}Sr/^{86}Sr) could distinguish local from immigrant SBW and identify immigration events at regional scales. However, no isoscapes could help identify the regions of origin of those immigration events. These studies show that isotope geolocation can resolve individual-level connectivity and that combining systems improves geolocation precision, while also underscoring that such applications depend on well-characterized, species-specific transfer relationships and environmental baselines that do not yet exist for SBW.

1.4 Isotope systems relevant to SBW tested in this thesis

In this thesis, we test several well-known isotope geolocators for deploying isotope geolocation technology for SBW. We describe the known drivers of isotope variations of those elements.

Hydrogen (δ^2H). δ^2H is the most widely used isotope geolocator because of its predictable spatial gradients associated with climatic and hydrological processes (Bowen, 2010; Hobson and Wassenaar, 2019). Spatial variations of hydrogen isotopes arise mainly through temperature-dependent fractionation during phase changes in the hydrological cycle: as an air mass moves inland, rises in elevation, or reaches higher latitudes, heavier isotopes preferentially precipitate first, progressively depleting ^{2}H in the remaining atmospheric moisture through the “rainout effect” (Bowen and Revenaugh, 2003; Bowen et al., 2005). Seasonal and regional climate further modulate δ^2H, with higher values in warmer months and in regions of lower precipitation (Michener and Lajtha, 2007). These processes generate

large-scale, spatially predictable gradients spanning hundreds of kilometres, making δ^2H a powerful tool for provenance studies.

Sulfur (δ^{34}S). δ^{34}S variation is influenced by geological, biological, and atmospheric processes, with coastal proximity playing a major role (Newton, 2021) . Marine-derived sulfur is enriched in ^{34}S (approximately +21‰), so coastal soils and vegetation typically show elevated δ^{34}S relative to inland environments (Peterson and Fry, 1987; Sparks et al., 2019; Bataille et al., 2021). As marine deposition declines inland, regional sulfur pools are increasingly shaped by local geology, weathering, permafrost and wetness conditions, microbial activity, and anthropogenic sulfur from industry and fossil-fuel combustion, generally yielding lower delta values more inland. Additionally, sulfur is transmitted through trophic levels with minimal fractionation (<1‰) (McCutchan et al., 2003), and plant and consumer δ^{34}S reflect these combined inputs, providing information on both large-scale coastal gradients and localized geological or anthropogenic influence (Britton, 2010).

Strontium (^{87}Sr/^{86}Sr). ^{87}Sr/^{86}Sr ratios show high spatial heterogeneity, often varying at fine scales (~1 km) in response to underlying geology (Bataille and Bowen, 2012). Variation is driven primarily by bedrock age and lithology, because radiogenic ^{87}Sr is produced by the slow radioactive decay of ^{87}Rb: older rocks with high Rb/Sr ratios exhibit elevated ^{87}Sr/^{86}Sr, whereas younger rocks generally show lower ratios (Faure and Powell, 1972; Michener and Lajtha, 2007). Local values can be modified by mineral weathering rates and atmospheric deposition (Crowley et al., 2017; Bataille et al., 2021). Strontium undergoes minimal fractionation during trophic transfer and this mass-dependent fractionation is, in any cases, corrected for during analysis (Flockhart et al., 2015). As a result, local bioavailable strontium

isotopes tend to follow patterns related to the underlying geological units, making $^{87}Sr/^{86}Sr$ particularly valuable for high-resolution provenance studies in geologically heterogeneous regions (Bataille et al., 2021).

Carbon ($\delta^{13}C$). While less used for isotope geolocation due to their strong fractionation with trophic and physiological processes, carbon isotopes also show some spatial variations. The spatial distribution of $\delta^{13}C$ is shaped primarily by photosynthetic pathway: plants discriminate against ^{13}C relative to atmospheric CO_2, with the magnitude of discrimination depending on whether a C3 or C4 pathway is used (Michener and Lajtha, 2007; Hoefs, 2021). However, boreal and temperate forests are dominated by C3 vegetation, therefore, most of the spatial variation in plant $\delta^{13}C$ are driven by factors affecting stomatal conductance and photosynthetic activity, such as water availability, salinity, temperature, light intensity, altitude, and nutrient stress (O'Leary, 1981; Farquhar et al., 1989; Diefendorf et al., 2010). Stressors that reduce stomatal conductance, such as water limitation, generally increase $\delta^{13}C$ by lowering internal CO_2 concentrations and limiting discrimination during fixation (Heaton, 1999; Codron et al., 2013). $\delta^{13}C$ therefore integrates physiological and environmental conditions, making it a useful indicator of regional environmental variation.

Nitrogen ($\delta^{15}N$). $\delta^{15}N$ is also rarely used as isotope geolocator due to the very large trophic fractionation and dietary mixing dominating the system. However, for SBW that consumes a relatively homogenous diet and are primary consumers, nitrogen isotopes might offer an additional source of geolocation information. Nitrogen isotope patterns are influenced by the cycling of nitrogen in biological and edaphic processes, including fixation, nitrification, and denitrification (Handley et al., 1994; Hoefs, 2021). Fractionation during nitrification and

denitrification can enrich soils in ^{15}N, with poorly aerated or suboxic conditions amplifying this enrichment, so factors such as temperature, water stress, salinity, soil composition, sea-spray influence, and anthropogenic disturbance all affect $\delta^{15}N$ across landscapes (Handley and Raven, 1992; Robinson, 2001; Codron et al., 2013). Plant $\delta^{15}N$ reflects the available nitrogen sources, which vary with forest harvesting, fertilization, root depth, soil organic matter, and microbial and mycorrhizal activity (Högberg, 1997; Michener and Lajtha, 2007). As plant material is consumed, $\delta^{15}N$ is enriched at each trophic level through discrimination during assimilation and excretion, allowing it to trace trophic interactions as well as environmental conditions during tissue formation (Quinby et al., 2020).

1.5 Spruce Budworm as a model system

SBW is an ideal species to apply isotope geolocation:

1) The development and diet of SBW are tailored to geolocation. During the larval stage, budworm individuals are relatively sedentary and complete their development feeding extensively on host foliage within a localized environment. As a result, larval tissues are expected to incorporate isotopic compositions that reflect the geochemical and environmental conditions of their localized natal habitat without integrating multiple dietary sources from distinct regions (Miller, 1963). Additionally, adult moths do not feed under natural conditions and are therefore not incorporating other dietary sources than their larval diet (Miller, 1987). As wing tissues are relatively inert (Lindroos et al., 2023), the isotopic composition of adult wings should be preserved following emergence and throughout migration. Those characteristics of SBW provide a well-constrained opportunity to evaluate whether host-foliage compositions are transferred into SBW tissues and can be used to infer geographic origin.

2) SBW regularly undertake long-distance migration across regions of pronounced geological, climatic, and ecological heterogeneity across eastern Canada. This environmental diversity should lead to strong spatial isotope variability across the eastern SBW range, facilitating the application and deployment of isotope geolocation for this system.

3) The periodic nature and economic significance of outbreaks have produced extensive monitoring networks, pheromone traps, aerial defoliation surveys, and population inventories, that provide independent, multi-decadal data on population dynamics and dispersal against which novel tracking approaches can be evaluated.

Collectively, strong spatial isotope gradients, localized larval development, retention of the natal signal into adulthood, extensive monitoring infrastructure, and ecologically significant migratory behaviour make SBW a particularly powerful system for developing and testing isotope geolocation, while addressing questions of direct relevance to outbreak monitoring and management.

1.6 Knowledge gaps and rationale

Despite decades of research on SBW ecology and dispersal, two linked gaps continue to limit understanding of migratory connectivity and outbreak dynamics. First, the natal origins of immigrant moths and the connectivity among outbreak regions remain largely unresolved: although long-distance migration is well supported by field observation, radar, and atmospheric modelling, existing methods cannot determine where immigrants originate or directly link source and recipient populations, leaving the contribution of different areas to regional dynamics unclear. Second, and underlying the first, the tools required to trace this

insect do not yet exist for this system. Isotope geolocation offers considerable potential, but preliminary studies (e.g., Dargent et al., 2023) assume that environmental isotopic variation is transferred predictably into consumer tissues, an assumption rarely validated across multiple isotope systems or ecological conditions. In the case of SBW, no species-specific trophic transfer functions or high-resolution environmental baselines have been established for eastern Canada. Without these validations, the accuracy of isotope geolocation cannot be evaluated for SBW.

This thesis therefore focuses on the prerequisites for isotope-based geolocation of SBW rather than on migration tracking itself. Before origins can be assessed, two foundations must be in place. The trophic transfer of each candidate isotope system from host foliage into SBW tissues must be quantified to identify which systems behave as reliable geolocators, and spatially explicit foliar isoscapes must be developed across the species' eastern Canadian range to serve as the environmental baseline against which tissue values are compared. Establishing this biological and environmental framework is the necessary first step toward deploying multi-isotope geolocation to reconstruct natal origins and, ultimately, toward supporting outbreak monitoring and management.

1.7 Objectives and hypotheses

Objectives. The objectives of this research were to (1) evaluate the trophic transmission of carbon, nitrogen, hydrogen, sulfur, and strontium isotopes from host foliage into SBW and assess their utility as isotope geolocators; and (2) develop high-resolution foliar isoscapes across the SBW distribution in eastern Canada, providing the basis for applying isotope geolocation to track this pest.

Hypothesis 1. Given that SBW larvae are specialist folivores that feed on a single host throughout development, I hypothesized that the isotopic composition of SBW tissues would correlate strongly with that of host foliage, because environmental isotopic signals incorporated into host trees should be predictably transferred into SBW tissues. Isotopic offsets between host trees and SBW tissues were expected to reflect physiological and behavioural processes that drive isotopic discrimination during assimilation and tissue formation.

Hypothesis 2. I hypothesized that host-foliage composition would exhibit distinct, predictable spatial patterns driven by regional climatic, geological, hydrological, and ecological gradients across eastern Canada, and that geolocation performance would vary among systems according to their dominant controls. As δ^{2}H, δ^{34}S, and $^{87}Sr/^{86}Sr$ exhibit strong spatial structure associated with climatic, coastal, and geological gradients, respectively, these systems were expected to provide the greatest geographic discriminatory power. In contrast, δ^{13}C and δ^{15}N are known to be more strongly influenced by localized ecological and physiological processes and were thus expected to show weaker large-scale structure only providing complementary geolocation information in specific environmental conditions.

1.8 Overview of thesis structure

Chapter 2 quantifies the trophic transmission of carbon, nitrogen, hydrogen, sulfur, and strontium isotopes from host foliage to SBW using known-origin samples, identifying which systems behave as reliable geolocators. Chapter 3 develops high-resolution foliar isoscapes across the eastern Canadian boreal forest and evaluates their combined potential for isotope

geolocation. Chapter 4 synthesizes these findings and outlines future directions toward operational isotope-based monitoring of SBW.

CHAPTER 2: NOT ALL ISOTOPES MAKE GOOD GEOLOCATORS: TROPHIC TRANSFER REVEALS CONTRASTING GEOLOCATION POTENTIAL IN EASTERN SPRUCE BUDWORM

Brent Holmes[1,2], Jean-Noel Candau[3], Petrus Le Roux[4], Megan S. Reich[1,2,5], Clement P. Bataille*[1,2,5], Felipe Dargent* [2,3]

[1] University of Ottawa, Department of Biology, K1N 6N5, Ottawa, ON, Canada.

[2] University of Ottawa, Department of Earth and Environmental Sciences, Advanced Research Complex building, 25 Templeton St., K1N 7N9, Ottawa, ON, Canada.

[3] Natural Resources Canada, Canadian Forest Service, Great Lakes Forestry Centre, P6A 2E5, Sault Ste. Marie, ON, Canada.

[4] Department of Geological Sciences, University of Cape Town, Rondebosch, South Africa

[5] Purdue University, Forestry and Natural Resources, 47907, West Lafayette, Indiana, USA

Corresponding author:

*Clement P. Bataille and Felipe Dargent contributed equally as co-senior authors.

Clement P. Bataille, cbataill@purdue.edu

Brent Holmes,

Felipe Dargent, felipe.dargentbocanegra@nrcan-rncan.gc.ca

Keywords boreal forest; *Choristoneura fumiferana*; multi-isotope geolocation; stable isotope transfer function; trophic discrimination

Author contribution statement BH, CPB and FD designed the study. BH and FD collected the samples. BH and PLR performed the laboratory and analytical work. BH, FD and CPB performed the statistical analyses. JNC and MSR contributed methods and data. BH wrote the first draft. All authors contributed to revisions and approved the final manuscript. CPB and FD supervised BH and gathered funding for this project.

ORCID iDs:

Brent Holmes : 0009-0006-2105-8801

Jean-Noel Candau : 0000-0001-9356-3950

Petrus Le Roux : 0000-0002-5930-4995

Megan S. Reich : 0000-0002-0597-4854

Clement P. Bataille : 0000-0001-8625-4658

Felipe Dargent: 0000-0002-4510-0086

This chapter is based on the paper “Not all Isotopes make good Geolocators: Trophic Transfer reveals contrasting geolocation potential in eastern spruce budworm” which is currently under review at Oecologia (Manuscript #: OECO-D-26-00672) (Holmes et al., 2026)

2.1 Abstract

Stable isotope geolocation of insects assumes that environmental isotope signals are transferred predictably from host plants to consumer tissues, yet this assumption is rarely tested. Using known-origin samples from eastern Canada, we quantified the transfer of δ^2H, δ^{13}C, δ^{15}N, δ^{34}S, and ^{87}Sr/^{86}Sr from host Pinaceae foliage to *Choristoneura fumiferana* (eastern spruce budworm, SBW) with linear and mixed-effects models. δ^{15}N showed strong, near-proportional transfer (R^2 = 0.84) with a large but consistent trophic discrimination factor (5.32 ± 0.76‰). δ^{34}S showed near-proportional transfer (R^2 = 0.88), minimal fractionation (−0.43 ± 1.15‰), and strong regional structure. ^{87}Sr/^{86}Sr tracked geological variation, but individual moths were close to analytical detection limits; pooled samples recovered near-proportional transfer (R^2 = 0.85). δ^{13}C showed moderate coupling (R^2 = 0.48) with high intra-site variance, and δ^2H was weakly related to foliage (R^2 = 0.08), with residual scatter (8.96‰) far exceeding analytical uncertainty (±1.7‰). δ^{34}S and ^{87}Sr/^{86}Sr, which have well-characterized baselines across eastern Canada, are therefore strong geolocators for SBW and likely for other species in the region. δ^{15}N is transmitted with high fidelity, but its geolocation potential depends on foliar baselines that remain to be mapped. δ^{13}C and δ^2H have limited value at this scale. The weak performance of δ^2H, a standard geolocator, and the strong performance of δ^{15}N show that the suitability of an isotope for geolocation is not an intrinsic property of the isotope but emerges from the interaction of environmental spatial structure, trophic transfer, and organismal biology.

2.2 Introduction

Multi-isotope geolocation has become a promising tool for studying migratory insect ecology (Bowen and West, 2019; Hobson, 2019). Insects are notoriously difficult to track using traditional methods because they are small, short-lived, and occur in large populations, which limits our ability to forecast and manage insect-mediated benefits and threats across biodiversity conservation, agriculture, forestry, and public health (Holland et al., 2006; Chapman et al., 2015; Hu et al., 2016). Stable isotopes help overcome these limitations by providing intrinsic markers that insects acquire from their natal environment and enabling the reconstruction of movement and connectivity (Hobson, 1999).

Using multiple isotopes simultaneously has advanced insect migration ecology because combining isotopes that have independent patterns of variation allows finer geolocation resolution and more precise ecological inferences on insect mobility at regional to continental scales. For example, Reich et al. used δ^2H and ^{87}Sr/^{86}Sr ratios to reveal moderate migratory connectivity of *Vanessa cardui* (painted lady butterflies) across the Afro-Palearctic, confirming a broad multigenerational parallel migration across the Sahara (Reich et al., 2024). Similarly, Dargent et al. used dual isotope analysis (δ^2H and ^{87}Sr/^{86}Sr) to confirm spruce budworm immigration events and distinguish between local and immigrant populations over fine spatial scales (Dargent et al., 2023). However, isotopes are not equally suitable for geolocation: some are strongly structured by stable geographic variables such as precipitation (e.g., δ^2H) (Bowen et al., 2005) or bedrock geology (e.g., ^{87}Sr/^{86}Sr) (Bataille et al., 2020), whereas others are more heavily influenced by trophic and metabolic processes

that introduce biological noise and weaken spatial signals (e.g., $\delta^{13}C$) (Martínez Del Rio et al., 2009) .

Isotopic geolocation relies on the transfer of environmentally structured isotope compositions from substrates to the base of the food chain (e.g., water, minerals to plants) through food webs, and into organism tissues (West et al., 2010). The core principle is that ecosystems exhibit predictable isotope compositions that vary geographically according to climatic, hydrological, and geological conditions at the site of growth, and those compositions are integrated into an organism's tissues, so that it can be used to trace back its origin (West et al., 2010). Ideally, isoscapes for geolocation would be developed using a known-origin dataset (i.e., individuals with verified origin) for the focal species; however, for herbivorous insects this is often impractical and expensive, as it would require rearing individuals across their entire range (West et al., 2010). As a result, isotope baselines are typically generated from environmental substrates (e.g., local water) or primary producers directly linked to those substrates because they can be sampled broadly (Hobson et al., 1999a). For isotopic geolocation to be valid, however, the isotopic composition of these baseline substrates must be reliably related to the isotope composition of the focal organism's tissues (West et al., 2010). Establishing robust baseline-tissue transfer functions is therefore a prerequisite for interpreting geographic origin in insect isotope studies.

In herbivorous insects, spatial isotope patterns are expected to transfer from host plants into insect tissues, allowing direct comparisons between tissue isotopes and environmental isoscapes to infer natal origin (Hobson et al., 1999c, 2019a). Tissues with slow turnover, such as chitinous wings, preserve the isotopic composition of the environment in which they

formed and are therefore commonly used to determine the natal origin of individuals, particularly after long-distance dispersal (Lindroos et al., 2023). However, during assimilation and incorporation of plants into herbivore tissues, isotopic fractionation produces predictable but non-identical isotope values between consumers and their diets (Deniro and Epstein, 1978, 1981). These offsets, known as trophic discrimination factors (TDFs), arise from trophic metabolic processes such as differential routing of dietary macromolecules or preferential excretion of lighter isotopes (Minagawa and Wada, 1984). Additional differences can arise because isotopes are measured in tissues that differ compositionally and biochemically from the baseline substrates(Gannes et al., 1997). For example, insect wings are primarily made of chitin, a long-chain structural polymer, whereas host foliage consists largely of carbohydrates, and these substrates differ in their isotopic composition prior to any metabolic fractionation (Lindroos et al., 2023). As a result, baseline-tissue differences reflect both physiological fractionation and inherent differences in the bulk chemical composition of the tissue being analyzed. TDFs vary among elements: TDFs are generally ~+1‰ for carbon (Deniro and Epstein, 1978), ~+3.4‰ for nitrogen (Deniro and Epstein, 1981; Minagawa and Wada, 1984; McCutchan et al., 2003), and between -1.5 and 1.5‰ for sulfur (Raoult et al., 2024), although they are often difficult to properly determine due to dietary, metabolic, or ontogenic processes overprinting (McCutchan et al., 2003). While strontium isotopes fractionate during trophic processes, this mass-dependent fractionation is normalized during analysis (Bataille et al., 2020). The transmission of isotope compositions from primary producers to herbivorous insects is rarely validated empirically, introducing a significant source of uncertainty, particularly for multi-isotope frameworks that rely on accurate and predictable baseline-tissue relationships.

Quantifying baseline-tissue uncertainty is essential for developing robust, interpretable, and biologically calibrated isoscapes (Hobson et al., 2010). The predictive performance of multi-isotope geolocation frameworks depends, in large part, on the predictable trophic fractionation leading to strong, consistent correlations between foliage and tissue isotopes (Wunder et al., 2005; Wunder and Norris, 2019). The remaining uncertainty in baseline-tissue transfer is incorporated into the geolocation framework itself with poor correlation strongly decreasing the geolocation potential of the isotope. R packages such as assignR (Ma et al., 2020) and IsoriX (Courtiol et al., 2019) incorporate transfer-function uncertainty into the isoscape calibration process, propagating both environmental variation and biological error terms into probability-based geographic assignments(Wunder, 2012). However, these best practices are rarely followed, and transfer functions are often derived from very limited datasets of unrelated species and applied as fixed corrections, without fully accounting for the true uncertainty in trophic transmission. In a multi-isotope context, failing to propagate this uncertainty can overweight poorly constrained isotopes, inflate apparent spatial precision, and produce erroneous geolocation.

Here, we use *Choristoneura fumiferana*, the eastern spruce budworm (SBW), as a model system to test the assumptions that isotopic compositions are transferred predictably from their host foliage, and evaluate whether trophic fractionation is sufficiently predictable for use in isotope geolocation application. SBW are the most damaging pest in the North American boreal forest and undergo recurrent outbreaks every 30-40 years, resulting in extensive defoliation of their spruce (Picea spp.) and balsam fir (*Abies balsamea*) hosts, and leading to major ecological and socio-economic consequences (Chang et al., 2012; MacLean, 2016). SBW outbreak expansion is thought to be triggered by massive but sporadic long-

distance dispersal events (>100 km) where gravid females can seed new infestation areas (Johns et al., 2019). Isotopes are a very promising approach for tracking these long-distance dispersal events and to better manage outbreaks (Dargent et al., 2023, 2026).

In this study, we evaluate whether isotopes of hydrogen, carbon, nitrogen, sulfur, and strontium effectively trace SBW origin by measuring the strength and consistency of isotopic transmission from foliage to moth tissues. A strong, predictable correlation would indicate limited metabolic overprinting and support the use of these isotopes as geolocators. Given that SBW are host-specialist folivores that feed almost exclusively on needles of a few species without switching trees, we hypothesize that SBW tissue will reflect local foliar isotopic compositions with consistent offsets due to trophic fractionation. Suitable geolocators must meet three key requirements. First, the environmental baseline must be spatially structured at the scale of the animal range. Second, baseline signal must be transmitted from foliage to consumer tissue with a predictable and near-proportional transfer. Third, the variance introduced within a site (intra-site), by microhabitat heterogeneity, individual physiology, or analytical error, must be small relative to the isotopic contrast between sites. We evaluate each of the five isotopes to propose a hierarchy of isotopes for geolocation in eastern Canada.

2.3 Methods

Since adult SBW are non-feeding and only live for ~10 days, we expect a strong correlation between the isotopic composition of SBW and their host plants. We assessed TDFs between host foliage and SBW by collecting SBW pupae from up to three adjacent trees at 19 sites in Ontario, and 12 sites in Newfoundland (Fig. 1; "known-origin" samples). The sites span a diverse range of environmental conditions which can influence the cycles of our target isotopes systems (Contina et al., 2022). Rather than rearing SBW on isotopically enriched diets in the laboratory, we prioritized field samples to estimate the uncertainty of this relationship under natural conditions. At each known-origin site, we collected needles from either the same trees or within 10 meters of the sampled SBW. In most cases, needles from multiple trees from the same site were pooled for foliar analysis. Known-origin moths in our dataset were collected in the field as pupae, and a few as late-stage L6 larvae, and allowed to eclose in paper bags in the laboratory (~22°C). At the collection sites we recorded the geographic coordinates and date of collection. To evaluate the degree of intra-site isotope variations, we intended to analyze three to five moths per site, yet some sites did not have enough pupae whereas others had unsuccessful eclosions or Hymenoptera parasitoidism.

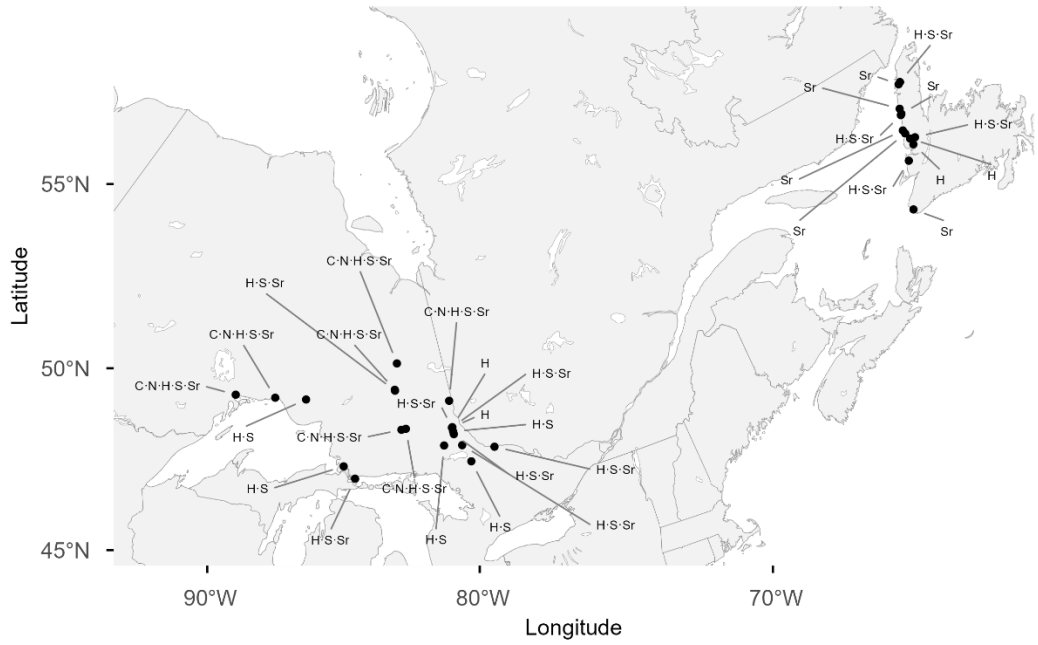

Figure 2.1 - Known-origin sample sites for host conifer foliage (*Abies balsamea* and Picea spp.) and spruce budworm (*Choristoneura fumiferana*) across eastern Canada. Points indicate site location and lines point to the stable isotope analyzed for foliage and budworm tissues, including hydrogen ($\delta^{2}H$), carbon ($\delta^{13}C$), nitrogen ($\delta^{15}N$), sulfur ($\delta^{34}S$), and strontium ($^{87}Sr/^{86}Sr$).

2.3.1 Foliar sample preparation and isotope analysis

2.3.1.1 General preparation

Analyses of foliar $\delta^{2}H$, $\delta^{13}C$, $\delta^{15}N$, $\delta^{34}S$ were performed at the Jan Veizer Stable Isotope Laboratory (University of Ottawa). Dry needles were aggregated by site, rinsed twice with deionized water to remove surface particulates, and dried at 50°C for 48 h. Dried needles were then homogenized to a fine powder and stored in glassine envelopes.

2.3.1.2 Carbon and nitrogen

Carbon and nitrogen isotope analyses were run separately in August 2023 because of the very large amount of carbon complicating the nitrogen analysis. Ground foliage samples (C% = 48.7 ± 1.3; N% = 1.2 ± 0.3) were micro-weighed to a target mass of 0.60 ± 0.06 mg into tin capsules (Elemental Microanalysis). Samples were combusted in a vario EL cube elemental analyser (Elementar, Germany) via flash combustion at 1800°C°, equipped with oxidation and reduction reactors packed with copper oxide wires, silver wool, and copper reagents (Elemental Microanalysis, United Kingdom). Combustion was performed using 4.5 O_2 as the combustion gas (Messer, Germany) and 5.0 He (Messer, Germany), as the carrier gas, with gas flows and temperatures set according to manufacturer specifications. Following combustion, water was removed using a Sicapent trap (Merck, Germany) and N_2 was purified by removing $CO_2$with an Ascarite trap (Merck, Germany). For $\delta^{13}C$ analyses, after N_2 was completely evacuated from the system, the trapped CO_2 was desorbed from the Ascarite trap and analyzed independently. The resulting gases travelled sequentially via a Conflo IV interface (Thermo, Germany) to an isotope ratio mass spectrometer (IRMS, DeltaPlus Advantage, Thermo, Germany), operated using Isodat 3.0 (Thermo, Germany). Corrections

for ^{17}O contributions to CO_2 were applied using the Santrock-Studley-Hayes algorithm. Isotopic deltas were derived relative to a working gas (4.0 CO_2, 4.8 N_2, Messer, Germany) introduced using the Conflo IV and were normalized using LIMS for Light Stable Isotopes (USGS, United States).

Isotopic ratios are reported in δ notation relative to the Vienna Pee Dee Belemnite (V-PDB) scale for carbon and relative to atmospheric N_2 (AIR) for nitrogen. Values were calibrated using a three-point calibration with internal standards: C-51 Nicotiamide (Acros Organics, Belgium; $\delta^{13}C$: -22.95‰; $\delta^{15}N$: 0.07‰), C-52 mix of ammonium sulphate and sucrose (Merck, Germany; $\delta^{13}C$: -11.94‰; $\delta^{15}N$: 16.58‰), C-54 Caffeine (Alfa Aesar, United Kingdom; $\delta^{13}C$: -34.46‰; $\delta^{15}N$: -16.61‰). Those internal standards were previously calibrated against international standards IAEA-CH-6 (-10.45 ± 0.03‰), NBS-22 (-30.02 ± 0.04‰), USGS-40 (-26.39 ± 0.04‰) and USGS-41 (+37.63 ± 0.05‰) for $\delta^{13}C$ and IAEA-N1 (+0.43 ± 0.07‰), IAEA-N2 (+20.41 ± 0.12‰), USGS-40 (-4.52 ± 0.06‰), and USGS-41 (+47.57 ± 0.11‰;) for $\delta^{15}N$. Analytical precision was monitored using a blind internal standard C-55 L-glutamic acid (Merck, Germany; $\delta^{13}C$: -28.5 ±0.1‰, n = 3; $\delta^{15}N$: -3.9 ± 0.1‰, n = 2) and calibrated against the same international standard above. A full set consisting of each of the calibration and blind reference materials was analyzed at the beginning and end of the run, as well as distributed every 30 samples. Calibration and blind reference material were weighted to provide 300 ± 15µg C and 100 ± 5 µg N. The C-55 L-glutamic acid reference material was analyzed at a range of masses (0.53 -2.11 mg) in the middle of each run for linearity. For each run, the analysed $\delta^{13}C$ and $\delta^{15}N$ values of C-55 glutamic acid fell within the range of accepted calibrated values.

2.3.1.3 Hydrogen

Bulk ground foliage samples (H% = 6.3 ± 0.3) were micro-weighed to a target mass of 0.25 ± 0.025 mg into silver capsules. Hydrogen isotopic measurements were conducted via high-temperature flash pyrolysis at 1400°C using a temperature conversion elemental analyzer (Elementar Germany) equipped with a zero blank autosampler. He flushing was conducted in the autosampler for 4h prior to any analysis to remove potential water vapor. After pyrolysis, the purified H_2 was introduced to a Thermo Fisher Delta Plus XP isotope ratio mass spectrometer (ThermoFinnigan, Germany) via a Conflo IV interface. Three-point calibration was performed using reference standards: CBS (caribou hoof; -157 ± 0.9‰), KHS (kudu horn; -35.3 ± 1.1‰), and USGS-43 (human hair; -44.4 ± 2.0‰). Analytical precision was monitored using a keratin reference standard, USGS42 (human hair; measured: -71.9 ± 1.1‰, n = 3; standard: -72.9 ± 2.2‰), and two internal standards, *Lymantria dispar* ground wings to act as a chitin matrix match (measured: -62.0 ± 1.57‰, n = 3; long-term average: -64.0 ± 0.8‰) and G-744 (keratin; measured: -58.8 ± 1.2‰, n =18; long-term average: -60.5‰ ± 0.8‰) distributed throughout analytical runs. δ^2H values were determined by comparative equilibration against the keratin reference materials listed above, which were equilibrated alongside the samples under identical ambient conditions. Reported δ^2H values therefore refer to the non-exchangeable hydrogen fraction. One limitation of this analytical approach is that bulk leaf tissue has a different exchangeable-H fraction than keratin but no standard currently exists for plant material. Analytical precision, assessed from repeated measurements of USGS42 and internal chitin standards, was better than ±1.7‰. All δ^2H values are reported relative to the VSMOW-SLAP international scale.

2.3.1.4 Sulfur

Sulfur isotope data used in this study were derived from the same foliar and SBW samples reported in Dargent et al. (2026). As the datasets are shared between studies, sample preparation, EA-IRMS procedures, calibration, and quality control were identical. No additional sulfur isotope analyses were performed for this study.

2.3.1.5 Strontium

Foliage samples were cleaned to remove surface dust, lipids, and contaminants by rinsing twice with deionized water followed by an ultrasonic cleaning in a deionized water bath. Samples were then dried at 50°C for 48 h°. Dried foliage samples were digested by microwave digestions using 1 mL of concentrated nitric acid (16 M; Trace Metal Grade distilled for moths; Fisher Chemical, Canada) for 15 min at 250C° using an Anton Paar Multiwave 7000 microwave system (Austria) in Organic High setting. Complete digestion was confirmed by the presence of clear, particle-free solutions. Foliage samples were transferred to 7 ml Savillex PTFE vials. For Sr concentration determination, a 200 µL aliquot of each digest was transferred to a separate Savillex vial, dried, and re-dissolved in 2,000 µL 2% v/v nitric acid with 20 ppb indium as an internal standard. Sr concentrations were measured using an Agilent 8800 triple-quadrupole inductively coupled plasma mass spectrometer (ICP-MS) at the Department of Earth and Environmental Science, University of Ottawa. Calibration standards were prepared from certified single element standards (SCP science; Montreal, Canada). The digest (~1 mL) was dried and re-dissolved in 1 mL 6 M nitric acid for chromatographic Sr preparation. Strontium purification was performed using 100 µL microcolumns packed with Sr-spec Resin™ (100-150 µm; Eichrom Technologies, USA).

Columns were conditioned with 0.5 mL of 6 M nitric acid prior to sample loading. Based on ICP-MS concentration results, foliage sample volumes were adjusted to achieve a target Sr load of ~ 100 ng. The entire moth digest was used. Matrix elements were removed using 6 M nitric acid, and Sr was subsequently eluted using 0.05 M nitric acid. Purified Sr fractions were dried and re-dissolved in 2% v/v nitric acid for isotopic analysis. For foliage, $^{87}Sr/^{86}Sr$ were measured at the MC-ICP-MS Facility, Department of Geological Sciences, University of Cape Town, using a Nu Plasma HR MC-ICP-MS. ^{87}Rb interference was corrected by monitoring ^{85}Rb and applying an established $^{87}Rb/^{85}Rb$ ratio. Kr interferences of ^{84}Sr and ^{86}Sr were corrected by subtracting contributions based on the measured On-Peak Zero in the 2% HNO_3 solution used to prepare all standards and samples for analysis. Instrumental mass fractionation was corrected by normalizing $^{86}Sr/^{88}Sr$ to 0.1194 using the exponential law. Strontium isotope compositions are reported as $^{87}Sr/^{86}Sr$ ratios. Foliage samples were run at a concentration of ~200 ppb with all $^{87}Sr/^{86}Sr$ data referenced to bracketing analyses of NIST SRM987 (0.710255 ± 0.000023; 2 SD; (Waight et al., 2002). The worst within-run precision was ± 0.000039 (1 SD, n =16). Chitin standard (Alfa Aesar chitin) was also run 0.714016 ± 0.000038 (1 SD; n = 10).

2.3.2 Moth sample preparation and isotope analysis

Moth cleaning was done following Dargent et al. (2026). Briefly, moths were washed in beakers containing a 2:1 v/v chloroform:methanol solution to remove lipids, dust, and contaminants. Each individual moth was gently swirled a few times and submerged in the solution for 30 min, followed by subsequent transfers in fresh solution for 3 h, and 15 min. Clean moths were air dried in a class-100 fume hood and stored in glassine envelopes. For hydrogen, carbon, and nitrogen analyses we used wings, which are generally expected to

exhibit limited or negligible tissue turnover (Lindroos et al. 2023). Due to extremely low sulfur concentrations in SBW moth wings (<0.01%; Dargent et al., 2026), the head and thorax were used instead for $\delta^{34}S$ analyses, Similarly, since strontium concentrations are low in SBW (Dargent et al. 2023) we used full individuals.

Analyses for $\delta^{2}H$, $\delta^{13}C$, and $\delta^{15}N$ were similar to those for needles but at lower masses ($\delta^{2}H$: 0.25 ± 0.025 mg; joint $\delta^{13}C$ and $\delta^{15}N$: 0.5 ± 0.05 mg). A matrix-match standard of ground and homogenized spongy moth (*Lymantria dispar*, Linnaeus, 1758) wings was used for blind quality control (measured: -63.5 ± 0.8‰, n = 5; long-term average = -64 ± 0.8‰) for $\delta^{2}H$ analyses. The C-55 glutamic acid internal standard was used as blind quality control for $\delta^{13}C$ and $\delta^{15}N$ with $\delta^{13}C$ = -28.5 ± 0.1‰ (n = 3) and $\delta^{15}N$ = -3.9 ± 0.1‰ (n = 2). Procedures for strontium isotope analysis in moths were similar to foliar analyses. Strontium concentration in SBW tissues is very low (<1 ppm) and required ultra-clean laboratory procedures to minimize contamination including the use of ultra-clean distilled Trace Metal Grade (Fisher Chemical, Canada) nitric acid for Teflon cleaning, sample digestion and Sr separation. A small, digested aliquot (50 µL) was sampled for Sr concentration analysis, to maximize the remaining amount of Sr for isotope analysis. The Sr concentrations were used to tune the sensitivity of the Nu-Plasma II high-resolution multi-collector inductively coupled plasma mass spectrometer (MC-ICP-MS; Nu Instruments) coupled to a desolvating nebulizer (Aridus II™, CETAC Technologies) at the Pacific Center for Isotopic and Geochemical Research (PCIGR, University of British Columbia). At the PCIGR, standards were run in the range of moth concentrations with reproducibility of $^{87}Sr/^{86}Sr$ measurement for 5 ppb NIST SRM987 is 0.71025 ± 0.000023 (1 SD, n =138) and for 1.4 ppb NIST SRM987 0.71019 ± 0.00011 (1

SD, n = 48). Chitin standards, 5 ppb Alfa Aesar chitin, yielded a mean $^{87}Sr/^{86}Sr$ of 0.714073 ± 0.000128 (1 SD; n = 10).

For sulfur isotope preparation and analysis, the SBW samples used in this study were derived from the same individuals and preparation procedures reported in Dargent et. (2026).

2.3.3 Statistical analysis

To quantify trophic transmission relationships between isotope values in host foliage and moth tissue, we used a series of regression-based approaches. For each isotope system, we fitted linear regression models in the form:

$$Moth_{isotope} = \beta_0 + \beta_1 \times Foliage_{isotope} + \epsilon$$

where β_1 represents the slope (i.e., the transfer function) and β_0 represents the intercept. Because needles were in most cases pooled by site prior to analysis, most sites contribute a single foliar value against which several individual moths are compared. Foliar isotope composition is therefore effectively a site-level predictor. We therefore report simple linear regression (SLR) statistics as descriptive summaries of the foliage-consumer relationship and treat the linear mixed-effects models described below as the inferential models. In the mixed models, foliar isotope composition and the site random intercept are strongly collinear for the same reason, so we interpret the comparison as a test of whether site-level foliage explains differences among site mean moth values, and not as a test of intra-site trophic transmission. Model assumptions were evaluated using residual diagnostics. The strength and reliability of each isotope system was assessed using the coefficient of determination (R^2), regression slope and intercept values, and residual standard error. Isotopes with high R^2, consistent slopes, and low unexplained variance were considered better geolocators.

Linear mixed-effects models (LMM) were fitted with site included as a random intercept, allowing baseline isotope values to vary among sites while maintaining a common foliage-SBW relationship across all locations. First, we fitted a null mixed-effects model containing only a random intercept for site:

$$Moth_{isotope} \sim 1 + (1|site)$$

This model was fit to quantify baseline variance partitioning and assess the degree of spatial clustering in isotope values and was used to estimate intraclass correlation coefficients (ICC), providing a measure of the proportion of total SBW isotope variance attributable to inter-site variation (i.e., site-level clustering). We then incorporated foliage isotope values as a fixed effect while retaining site as a random intercept:

$$Moth_{isotope} \sim Foliage_{isotope} + (1|Site)$$

This modelling framework allowed foliage isotope values to explain systematic variation in SBW isotope composition while accounting for unmeasured environmental or ecological differences among collection sites. For every isotope system we report the same three models, the simple linear regression (SLR), the null mixed model with site as a random intercept (null LMM), and the mixed model with foliage added as a fixed effect (full LMM), so that model comparisons are consistent across systems. LMMs were fitted using restricted maximum likelihood estimation (REML) to estimate parameters and report them. LMMs were then refitted using maximum likelihood (ML) to allow comparison of models with different fixed-effect structures via Akaike's Information Criterion with a correction for small sample sizes (AICc).

All statistical analyses were performed in R 4.4.1 (R Core Team 2024) using packages tidyverse (Wickham et al., 2019), ggplot2 (Wickham, 2016), lme4 (Bates et al., 2015) and lmerTest (Kuznetsova et al., 2017).

2.3.4 Trophic Discrimination Factor

Trophic discrimination factors were calculated for each isotopic system as the difference between site-level foliar isotope value and isotope value for each individual SBW collected from the same site. Individual TDFs were calculated as:

$$\mathrm{TDF}_{\mathrm{individual}} = \delta\mathrm{SBW}_{\mathrm{individual}} - \delta\mathrm{foliar}_{\mathrm{site}}$$

where $\delta\mathrm{SBW}_{\mathrm{individual}}$ is the isotope value of an individual moth and $\delta\mathrm{foliar}_{\mathrm{site}}$ is the foliar isotope value for the corresponding site. Individual TDFs were then averaged within each site to obtain site-level TDFs before averaging site-level TDFs across all sampling locations to calculate the mean TDF for each isotopic system.

2.4 Results

2.4.1 Carbon

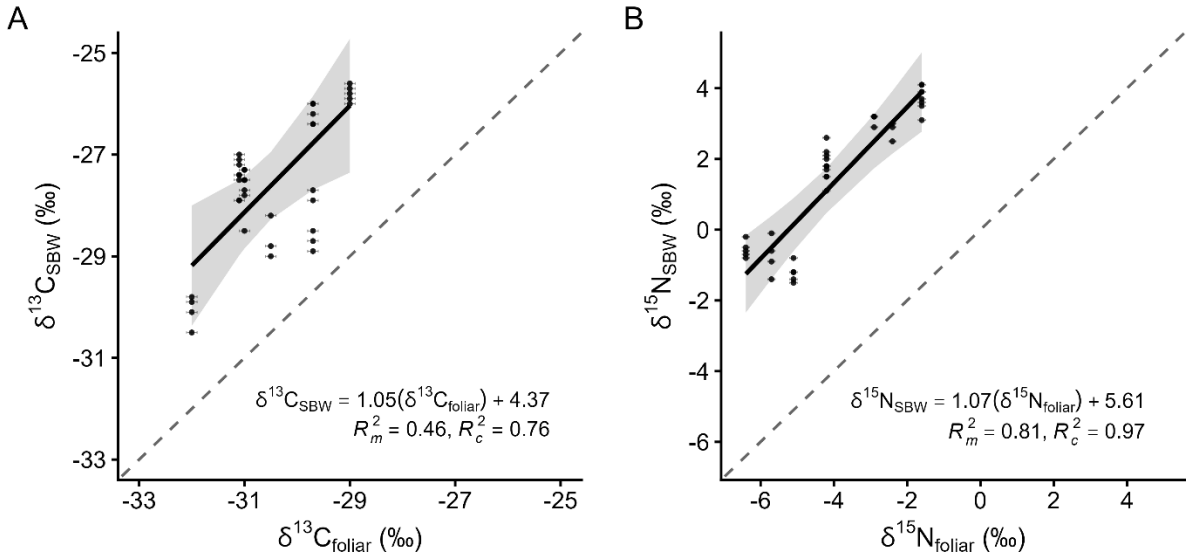

Figure 2.2 - Linear relationships describing trophic transmission of (A) δ^{13}C and (B) δ^{15}N from host foliage (Pinaceae) to known-origin SBW tissues (*Choristoneura fumiferana*) across sites in eastern Canada (δ^{13}C: 7 sites, 38 moths; δ^{15}N: 7 sites, 38 moths). Each point represents a foliage sample, and its corresponding moth samples from the same site. Solid lines indicate population-level fixed effects from linear mixed-effects models (with site of collection treated as a random intercept) and marginal 95% confidence intervals (shaded ribbon), while the dashed lines denote the 1:1 relationship for reference. Error bars represent ±1 standard deviation of the internal reference material (C-55: glutamic acid) within the analytical run, reflecting analytical uncertainty. Marginal (R^2_m) and conditional (R^2_c) R^2 values reported.

Carbon isotope composition ranged from -32.0‰ to -29.0‰ in foliage ($\delta^{13}C_{foliar}$), and -30.5‰ to -25.6‰ in known-origin SBW moths ($\delta^{13}C_{SBW}$). The average trophic discrimination factor (TDF) was 2.88 ± 0.81‰. A positive linear relationship was observed between foliar and moth $\delta^{13}C$ values ($F_{1,36} = 33.17$, $p < 0.001$, $R^2 = 0.48$, n = 38 moths from 7 sites). The simple linear regression model (SLR) estimated a slope of 0.96 ± 0.17 ($t = 5.76$, $p < 0.001$) and a non-significant intercept of 1.71 ± 5.09‰ ($t = 0.34$, $p = 0.74$), and a residual standard error of 0.94‰, consistent with transfer of $\delta^{13}C$ from foliage to moth tissues. The null linear mixed effect model (LMM) exhibited strong among-site variation in $\delta^{13}C_{SBW}$ (ICC = 0.77, conditional $R^2 = 0.77$). Including $\delta^{13}C_{foliar}$ reduced among-site variance by 62% (from 1.64 in the null LMM to 0.63 in the full LMM, and SD 1.28‰ and 0.79‰, respectively) and reduced the ICC to 0.56. Within-site residual variation remained qualitatively unchanged between the LMMs (from 0.491 in the null LMM to 0.492 in the full model) with residual SD of 0.7‰. The full LMM (AICc = 101.73) outperformed both the null (ΔAICc = 4.73) and SLR models (ΔAICc = 5.81). This model showed a positive association between $\delta^{13}C_{foliar}$ and $\delta^{13}C_{SBW}$ (slope = 1.05 ± 0.35, t = 3.01, p = 0.03; Figure 2.2A), with $\delta^{13}C_{foliar}$ (i.e., the fixed effect) explaining 46% of the variation (marginal $R^2 = 0.46$) in $\delta^{13}C_{SBW}$, and the full model explaining 76% of the total variation (conditional $R^2 = 0.76$).

2.4.2 Nitrogen

$\delta^{15}N_{foliar}$ values ranged from -6.4‰ to -1.6‰, while $\delta^{15}N_{SBW}$ values ranged from -1.5‰ to 4.1‰. The average TDF was 5.32 ± 0.76‰. A strong, positive linear relationship was observed between foliar and moth $\delta^{15}N$ values ($F_{1,36} = 183.7$, $p < 0.001$, $R^2 = 0.84$, n = 38 moths from 7 sites). The SLR estimated a slope of 1.05 ± 0.08 ($t = 13.55$, $p < 0.001$) with an intercept of 5.57 ± 0.33‰ ($t = 16.79$, $p < 0.001$), and a residual standard error of 0.79‰,

indicating proportional transfer of $\delta^{15}N$ from foliage to moth tissues. The null LMM exhibited substantial among-site variation in $\delta^{15}N_{SBW}$ (ICC = 0.97, conditional R^2 = 0.97). Inclusion of $\delta^{15}N_{foliar}$ as a fixed effect reduced among-site variance by 85% (from 4.26 in the null LMM to 0.65 in the full LMM, and SD 2.06‰ and 0.81‰, respectively) and reduced ICC to 0.83. As with $\delta^{13}C$, within-site residual variation remained the same between the LMMs (both 0.129) with a relatively small residual SD of 0.34‰. The full LMM (AICc = 59.57) outperformed both the null (ΔAICc = 11.71) and SLR models (ΔAICc = 34.73). This model showed a strong positive association between $\delta^{15}N_{foliar}$ and $\delta^{15}N_{SBW}$ (slope = 1.07 ± 0.19, t = 5.75, p < 0.01;Figure 2.2B), with $\delta^{15}N_{foliar}$ explaining 81% of the variation (marginal R^2 = 0.81) in $\delta^{15}N_{SBW}$, and the full model explaining 97% of the total variation (conditional R^2 = 0.97).

2.4.3 Hydrogen

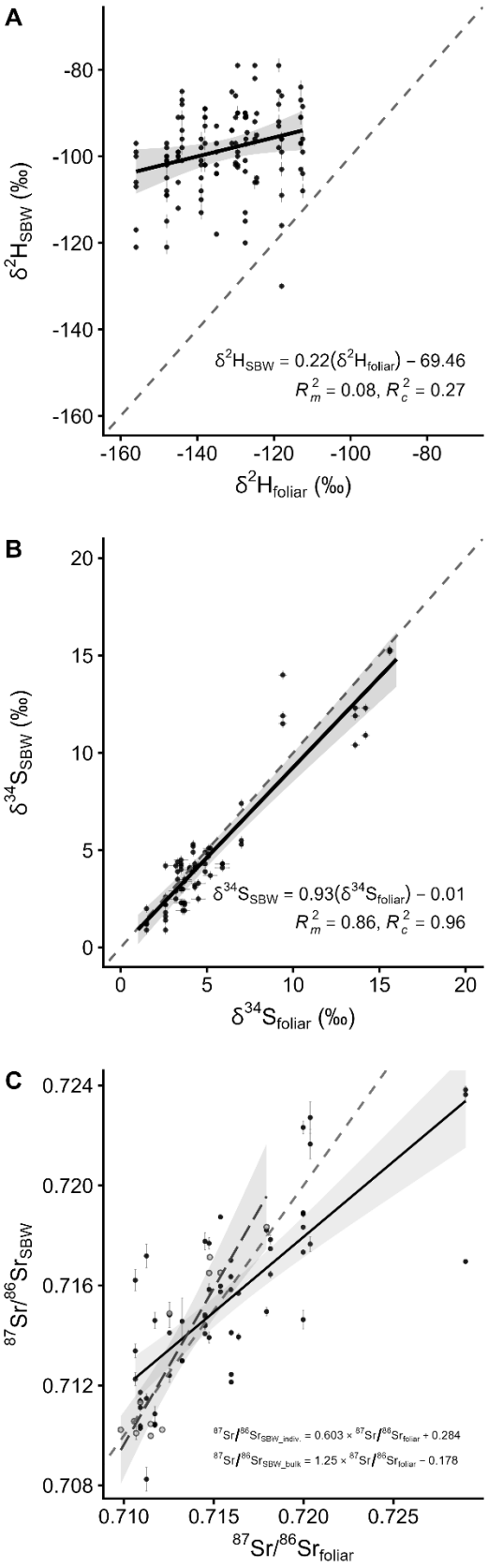
A
-80
-100
-120
-140
-160
δ²H_SBW (‰)
δ²H_SBW = 0.22(δ²H_foliar) – 69.46
R²_m = 0.08, R²_c = 0.27
-160
-140
-120
-100
-80
δ²H_foliar (‰)
B
20
15
10
5
0
δ³⁴S_SBW (‰)
δ³⁴S_SBW = 0.93(δ³⁴S_foliar) – 0.01
R²_m = 0.86, R²_c = 0.96
0
5
10
15
20
δ³⁴S_foliar (‰)
C
0.724
0.720
0.716
0.712
0.708
⁸⁷Sr/⁸⁶Sr_SBW
⁸⁷Sr/⁸⁶Sr_SBW_indiv. = 0.603 × ⁸⁷Sr/⁸⁶Sr_foliar + 0.284
⁸⁷Sr/⁸⁶Sr_SBW_bulk = 1.25 × ⁸⁷Sr/⁸⁶Sr_foliar – 0.178
0.710
0.715
0.720
0.725
⁸⁷Sr/⁸⁶Sr_foliar

Figure 2.3 - Linear relationships describing trophic transmission of (A) δ^2H, (B) $\delta^{34}S$, and (C) $^{87}Sr/^{86}Sr$ from host foliage (Pinaceae) to known-origin SBW tissues (*Choristoneura fumiferana*) across sites in eastern Canada (δ^2H: 19 sites, 126 moths; $\delta^{34}S$: 23 sites, 74 moths; $^{87}Sr/^{86}Sr_{indiv.}$: 18 sites, 58 moths; $^{87}Sr/^{86}Sr_{pool.}$: 12 sites). (A, B) Each point represents a foliage sample, and its corresponding moth samples from the same site. Solid lines indicate population-level fixed effects from linear mixed-effects models (with site of collection treated as a random intercept) and marginal 95% confidence intervals (shaded ribbon). Marginal (R^2_m) and conditional (R^2_c) R^2 values reported. (C) Includes both individual moth samples (filled circles) and site-level pooled samples (open circles) excluded from the individual sample regression. Solid (individual moths) and broken (pooled moths) lines represent ordinary least squares regressions with 95% confidence intervals (shaded). Dashed lines indicate the 1:1 relationship for reference. Error bars represent analytical uncertainty based on internal reference materials within each analytical run, reflecting analytical uncertainty.

SBW moths (δ^2H_{SBW} range -130.0‰ to -79.0‰) and their corresponding foliage samples (δ^2H_{foliar} range -156.0‰ to -112.5‰) showed a significant but very weak positive linear relationship ($F_{1,124}$ = 10.16, p < 0.01, R^2 = 0.076, n = 126 moths from 19 sites). The SLR estimated a slope of 0.21 ± 0.07 (t = 3.19, p < 0.01) with an intercept of -70.99 ± 8.74‰ (t = -8.12, p < 0.001), and a residual standard error of 8.96‰. The null LMM exhibited some among-site variation in δ^2H_{SBW} (ICC = 0.26, conditional R^2 = 0.26). Inclusion of δ^2H_{foliar} as a fixed effect reduced among-site variance by 24% (from 22.22 in the null LMM to 16.83 in the full LMM, and SD 4.71‰ and 4.1‰, respectively) and reduced ICC to 0.21. Within-site residual variation was similar and relatively high between the LMMs (64.38 and 64.2) and thus had a relatively large residual SD of ~8‰. The full LMM (AICc = 907.29) outperformed both the null (ΔAICc = 2.79) and SLR models (ΔAICc = 6.9). This model also had a weak positive association between δ^2H_{foliar} and δ^2H_{SBW} (slope = 0.22 ± 0.1, t = 2.24, p < 0.04;Figure 2.3A), with δ^2H_{foliar} explaining only 0.8% of the variation (marginal R^2 = 0.08) in δ^2H_{SBW}, and the full model explaining 27% of the total variation (conditional R^2 = 0.27). Given the large degree of within-site variation in δ^2H_{SBW} we aggregated SBW individual values to site

averages and explored whether it improved the fit of foliar-to-moth δ^2H relationship. This approach is not feasible for our LMMs since the number of sites would equal the number of observations. Aggregating the data improved model fit ($F_{1,18}$ = 5.62, p = 0.03, R^2 = 0.24, p = 0.03, 20 moth averages from 20 sites) but explained less variation in δ^2H than the full LMM. Despite this improvement in the SLR fit, the slope remained the same and far from 1 indicating strong attenuation of δ^2H transmission.

2.4.4 Sulfur

As in Dargent et al. (2026) a strong positive linear relationship was observed between $\delta^{34}S_{foliar}$ and $\delta^{34}S_{SBW}$ ($F_{1,72}$ = 517, p < 0.001, R^2 = 0.88, n = 74 moths from 23 sites), with SLR regression yielding a slope of 0.94 ± 0.04 (t = 22.74, p < 0.001), an intercept not significantly different from 0 (−0.07 ± 0.25‰, t = -0.27, p = 0.79), and a residual standard error of 1.21‰, consistent with proportional isotopic transfer. The average TDF was −0.43 ± 1.15‰. The null LMM showed strong among-site variation in $\delta^{34}S_{SBW}$ (ICC = 0.96, conditional R^2 = 0.96). The inclusion of $\delta^{34}S_{foliar}$ as a fixed effect reduced model variance by 92% (from 13.5 in the null LMM to 1.11 in the full LMM, and SD 3.67‰ and 1.05‰, respectively) and reduced ICC to 0.68. Within-site residual variation remained the same in both LMMs (both 0.51) with residual SD of 0.71‰. The full LMM (AICc = 213.55) outperformed both the SLR (ΔAICc = 28.5) and null models (ΔAICc = 53.2). This model shows qualitatively the same foliar to SBW relationship as the SLR, that is, a strong, positive and near proportional association between $\delta^{34}S_{foliar}$ and $\delta^{34}S_{SBW}$ (slope = 0.93 ± 0.06, t = 14.48, p = 0.03; intercept not significantly different from 0;Figure 2.3B), with $\delta^{34}S_{foliar}$ explaining 86% of the variation (marginal R^2 = 0.86) in $\delta^{34}S_{SBW}$, and the full model explaining 96% of the total variation (conditional R^2 = 0.96).

2.4.5 Strontium

$^{87}Sr/^{86}Sr_{foliar}$ ranged from 0.710630 to 0.729022, whereas $^{87}Sr/^{86}Sr_{SBW}$ values ranged from 0.708252 to 0.723825. We first analysed individual moth $^{87}Sr/^{86}Sr$ ratios. Although we expected to see no fractionation between foliage and moths (see Discussion), the average TDF offset between foliar, and moth was at -0.00033 ± 0.00231. SLR regression showed a positive relationship between foliar and SBW moth $^{87}Sr/^{86}Sr$ ratios ($F_{1,56}$ = 82.64, p < 0.001,

R2 = 0.60, n = 58 moths from 18 sites). The simple linear regression model (SLR) estimated a slope of 0.60 ± 0.07 (t = 9.09, p < 0.001), an intercept of 0.28 ± 0.05 (t = 5.99, p < 0.001), and a residual standard error of 0.002, consistent with partial isotopic transfer from foliage to SBW tissues (Figure 2.3C). The null linear mixed effect model (LMM) exhibited strong among-site variation in $^{87}Sr/^{86}Sr_{SBW}$ (ICC = 0.62, conditional R^2 = 0.62). Including $^{87}Sr/^{86}Sr_{foliar}$ (marginal R^2 = 0.58) reduced among-site variance by 92% (from 7.16 x 10-6 in the null LMM to 6.04 x 10-7 in the full LMM, and SD 2.68 x 10-3 and 7.77 x 10-4, respectively), reduced the ICC to 0.12, but explained a similar amount of variance (conditional R^2 = 0.63). Within-site residual variation remained qualitatively unchanged between the LMMs (from 4.35 x 10-6 in the null LMM to 4.33 x 10-6 in the full model) with residual SD of 2.08 x 10-3. Nonetheless, the SLR (AICc = -540.33) outperformed both the full (ΔAICc = 1.88) and null LMM models (ΔAICc = 26.97). To evaluate whether low sample mass or analytical precision influenced these results, pooled SBW samples were prepared by amalgamating multiple known-origin moths per site into a single homogenous sample. Pooled $^{87}Sr/^{86}Sr$ ratios ranged from 0.709985 to 0.718336, while foliage ratios for the same set of sites ranged from 0.709819 to 0.717943. Pooled samples exhibited a stronger, near proportional relationship between $^{87}Sr/^{86}Sr_{foliar}$ and $^{87}Sr/^{86}Sr_{SBW}$ ($F_{1,10}$ = 58.24, p < 0.001, R^2 = 0.85, n = 12 pooled-moth samples from 12 sites). This SLR estimated a slope of 1.25 ± 0.16 (t = 7.63, p < 0.001), an intercept not significantly different from 0 (-0.18 ± 0.12, t = -1.52, p = 0.16), and a residual standard error of 0.001 (Figure 2.3C). An ANCOVA showed that approach for strontium extraction (single vs. pooled moths) significantly influenced the detected relationship between foliar and SBW $^{87}Sr/^{86}Sr$ ratios (interaction term: t(66) = -2.44, p = 0.017). The pooled-moth samples had a significantly steeper slope than the individual SBW data, which

is better aligned with $^{87}Sr/^{86}Sr$ trophic transfer expectations. Visual inspection of residuals from both SLR models against a proxy of available strontium in a sample (i.e., ^{88}Sr intensity) indicates that individual SBW samples contain lower concentrations of strontium, and that lower ^{88}Sr intensity was associated with higher error in the SLR models.

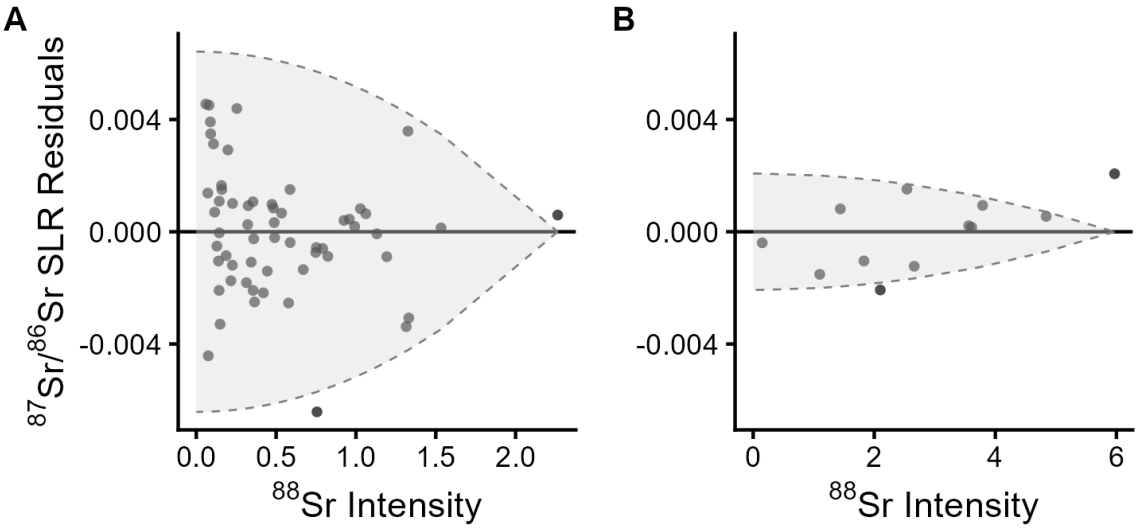

Figure 2.4 - Residual patterns of $^{87}Sr/^{86}Sr$ trophic transfer as a function of ^{88}Sr signal intensity. (A) Residuals from the ordinary least-squares regression of $^{87}Sr/^{86}Sr_{SBW}$ versus $^{87}Sr/^{86}Sr_{foliar}$ for individual SBW samples plotted against ^{88}Sr signal intensity (a proxy for overall available Sr). (B) Equivalent residual plot for site-level pooled moth samples. Note that panels share a common y-axis but differ in x-axis range. Shaded envelopes represent the dispersion of residuals across the gradient of ^{88}Sr intensity, and bounds the maximum residual variance across the observed intensity.

2.5 Discussion

2.5.1 Carbon

Across heterogeneous environmental conditions, $\delta^{13}C_{SBW}$ exhibited a positive but moderate relationship with $\delta^{13}C_{foliar}$, indicating variable trophic transmission of carbon isotope signals from host foliage to SBW tissues. Although the relationship was statistically significant, approximately a quarter of the variance in $\delta^{13}C_{SBW}$ remained unexplained. Site accounted for a significant component of variation, and inclusion of $\delta^{13}C_{foliar}$ as a fixed effect significantly improved model performance. Nevertheless, substantial intra-site and inter-site variability remained, limiting the utility of $\delta^{13}C$ for provenance applications at the spatial scale examined here.

This variability is likely driven in part by the inherent sensitivity of $\delta^{13}C_{foliar}$ to fine-scale environmental heterogeneity. Foliar $\delta^{13}C$ integrates photosynthetic discrimination processes governed by the ratio of intercellular to atmospheric CO_2, which responds to stomatal conductance and carboxylation capacity (Farquhar et al., 1989; Diefendorf et al., 2010). Consequently, water availability, vapour pressure deficit, precipitation seasonality, irradiance, canopy microclimate, and edaphic conditions can all influence foliar $\delta^{13}C$ values (Farquhar et al., 1989; Diefendorf et al., 2010). Many of these processes operate at microhabitat scales and can generate approximately 1‰ variation within stands and even among branches of the same tree. Additional heterogeneity may arise from within-canopy gradients in atmospheric CO_2 concentration and isotopic composition generated by canopy photosynthesis and inputs of isotopically light CO_2 from soil respiration (Farquhar et al., 1989). These processes can produce substantial local variation in $\delta^{13}C_{foliar}$, weakening the

assumption of site-level baseline homogeneity required for isotope-based geographic assignment.

At the consumer level, SBW development is expected to introduce additional variance through ontogenetic shifts in carbon allocation and fractionation. $\delta^{13}C$ in insect tissues can shift during growth, starvation, and metamorphosis due to preferential catabolism of ^{13}C-depleted lipid reserves and changes in assimilation and respiration(Doi et al., 2007). These processes can generate within-population $\delta^{13}C$ differences of ~1‰ (Doi et al., 2007), which are consistent with the intra-site variability we observed in SBW and the high TDF (mean TDF of 2.88 ± 0.81‰) relative to other Lepidoptera raised in the laboratory (Quinby et al., 2020). Larval feeding conditions in the field are likely heterogeneous, and thus $\delta^{13}C_{SBW}$ may reflect variation in both foliar baseline signals and individual physiological state, reducing geographic specificity. This variability is consistent with evidence that $\delta^{13}C$ trophic discrimination is less predictable than for other isotope systems and is strongly influenced by metabolic routing and macronutrient composition rather than trophic position alone (McCutchan et al., 2003).

Although foliar $\delta^{13}C$ exhibits broad climatic gradients and site explained a significant component of variation in our LMM, substantial intra-site variability, variable trophic transmission, and additional physiological fractionation at the consumer level reduced the geographic specificity of the signal. Consequently, despite the presence of broad spatial structure, $\delta^{13}C$ does not provide sufficient resolution for reliable standalone geolocation of individual SBW across the spatial extent examined here.

2.5.2 Nitrogen

$\delta^{15}N_{foliar}$ explained most of the variation observed in $\delta^{15}N_{SBW}$ and reduced unexplained inter-site variance by 85% showing a near proportional relationship. These findings indicate that spatial variation in $\delta^{15}N$ was primarily driven by differences among sites and that these differences were largely captured by $\delta^{15}N_{foliar}$. The strong performance of both the LMM model, and even the SLR, demonstrates that geographic variation in host-tree isotopic baselines is transferred predictably to SBW tissues. This result is consistent with the literature showing that plant $\delta^{15}N$ reflects ecosystem-level nitrogen cycling processes that vary across climatic, edaphic, and biogeochemical gradients (Amundson et al., 2003) Consequently, where geographically structured foliar $\delta^{15}N$ baselines occur, as reported across many terrestrial ecosystems and supported by our limited $\delta^{15}N_{foliar}$, these patterns should be expressed predictably in $\delta^{15}N_{SBW}$, fulfilling the requirements for isotope geolocation. The strong agreement between foliar and moth $\delta^{15}N$ values suggests that uncertainty associated with $\delta^{15}N$ geolocation will arise primarily from modeling the foliar isotope landscape rather than from the trophic transfer itself.

This is surprising considering that the TDF observed between moths and their host trees exceeds commonly reported values of approximately 2-4‰ for herbivorous vertebrates (Minagawa and Wada, 1984) and insects (Quinby et al., 2020). Although elevated, this value falls within the upper range reported for Lepidoptera reared in laboratory studies using artificial diets (Tibbets et al., 2008). The consistency of this TDF across environmentally distinct sites suggests that it is largely governed by stable physiological processes rather than local differences in diet quality or environmental conditions affecting nutritional stress and elevating consumer $\delta^{15}N$ through increased protein catabolism(McCutchan et al., 2003).

Several non-exclusive mechanisms may contribute to the elevated TDF observed in SBW. First, metamorphosis in holometabolous insects involves extensive tissue reconstruction and nitrogenous waste production, processes that can substantially alter isotopic composition (Tibbets et al., 2008). During pupation, isotopically depleted exuviae and meconium are expelled, enriching remaining tissues in ^{15}N and producing isotopic shifts of up to 5‰ enrichment in other insects (Doi et al., 2007; Tibbets et al., 2008). Second, temperature may indirectly affect fractionation through its influence on metabolic rate, protein turnover, and nitrogen excretion pathways. Increased growth and protein cycling enhance deamination and preferential loss of ^{14}N, thereby enriching tissues in ^{15}N (Deniro and Epstein, 1981). Consistent with this mechanism, *Spodoptera littoralis* exhibits a $\delta^{15}N$ increase of approximately 1.5‰ under rapid growth conditions (Charberet et al., 2023). Whatever its cause, this large TDF did not weaken the strong foliar-moth relationship observed in our study, indicating that it is both predictable and readily accommodated within a transfer-function for isotope geolocation.

Although the transfer function identified here is highly promising, several steps are required before $\delta^{15}N$ can become an effective geolocator. First, broader geographic sampling is needed across the SBW range to characterize the magnitude and spatial structure of $\delta^{15}N_{foliar}$ (Amundson et al., 2003; Craine et al., 2009; Souza-Silva et al., 2026). Second, the effects of physiology and nutritional stress on $\delta^{15}N_{SBW}$ should be quantified more explicitly. Adult SBW are short lived and do not feed following emergence, relying entirely on nutrient reserves acquired during larval development. Consequently, catabolism during adulthood or migration could theoretically modify isotopic composition (Doi et al., 2007). Experimental studies examining nutritional stress could potentially identify isotopic changes associated

with catabolism which are likely to occur in migratory individuals. Third, the temporal stability of foliar and moth $\delta^{15}N$ values should be evaluated across years and outbreak phases. Although nitrogen cycling in boreal forests is generally conservative and tightly regulated (Amundson et al., 2003), climatic variability and severe SBW outbreaks may alter local nitrogen dynamics through enhanced nutrient recycling from frass and insect carcasses (Christenson et al., 2002). Quantifying the magnitude of these temporal effects will be necessary to determine how much year-to-year variation contributes to geolocation uncertainty.

Nitrogen isotopes are rarely considered as geolocators because mixed diets and physiological variability frequently obscure geographically structured isotopic signals. In host-specialist insects such as SBW, however, the combination of a highly restricted larval diet, limited intra-site isotopic variability, and the absence of adult feeding following emergence creates unusually favorable conditions for $\delta^{15}N$ geolocation. Our results demonstrate that $\delta^{15}N$ signals are transferred predictably from host foliage to adult moths, retain strong site-level structure, and exhibit a highly consistent trophic discrimination factor across diverse environmental conditions. These findings suggest that $\delta^{15}N$ may represent an underappreciated candidate for reconstructing the mobility of SBW across eastern Canada. The remaining task is to characterize the spatial and temporal structure of foliar $\delta^{15}N$ baselines across the full geographic range of the species.

2.5.3 Hydrogen

$\delta^{2}H_{SBW}$ was only weakly related to $\delta^{2}H_{foliar}$ ($R^2 = 0.08$), and within-site residual variation (SD ~8‰) greatly exceeded analytical uncertainty. Three factors likely contribute. First, the

range of δ^2H_{foliar} among our sites (~44‰) is small relative to continental precipitation gradients, so within-site variance is large compared with the spatial signal at this scale. Second, hydrogen in consumer tissues derives from both dietary organic hydrogen and body water, and their relative contributions vary with physiology and development (Hobson et al., 1999c; Magozzi et al., 2019). Third, bulk foliage and chitin differ in their proportion of exchangeable hydrogen, which normalization of bulk foliage against keratin standards may not fully correct (Soto et al., 2017; Magozzi et al., 2021). Replacing foliar δ^2H_{foliar} with precipitation δ^2H did not improve the relationship. δ^2H remains effective at continental scales, where isotopic gradients exceed within-site variance, but at the regional scale examined here its signal-to-noise ratio is too low for reliable geolocation of individual SBW.

2.5.4 Sulfur

$\delta^{34}S_{SBW}$ values closely tracked the isotopic composition of host foliage (Dargent et al., 2026). A near-zero mean TDF (-0.43 ± 1.15‰), is consistent with the established theory that sulfur exhibits negligible trophic fractionation due to the conservation of essential dietary amino acids (i.e., cysteine and methionine; Trust and Fry, 1992). When disentangling the trophic transfer effects from the underlying spatial structure, we found strong site-level structuring, indicating that $\delta^{34}S_{SBW}$ variability is attributable to inter-site rather than intra-site variation. Inclusion of $\delta^{34}S_{foliar}$ reduced unexplained inter-site variance by 92%, and the full model explained 96% of the total variance, as expected if $\delta^{34}S_{SBW}$ variation was predominantly structured by baseline foliar $\delta^{34}S_{foliar}$ composition. The large variation in $\delta^{34}S_{foliar}$ across the study region (1.5‰ to 15.6‰) is consistent with environmentally driven sulfur cycling controlled primarily by atmospheric deposition and marine aerosols as observed on the larger scale $\delta^{34}S_{foliar}$ isoscape (Dargent et al., 2026). The low trophic discrimination, high-

transfer fidelity, and strong regional structure make sulfur isotopes a strong geolocator for tracking SBW movements (e.g., Dargent et al., 2026).

2.5.5 Strontium

$^{87}Sr/^{86}Sr_{SBW}$ covaried positively with $^{87}Sr/^{86}Sr_{foliar}$ ratios, indicating that SBW retain geographically derived strontium isotopes from their larval host foliage. This result is consistent with the theoretical basis of strontium isotope geolocation, with bioavailable Sr being directly transferred from bedrock to soils, plants, and primary consumers (Capo et al., 1998; Bataille and Bowen, 2012). The wide range of $^{87}Sr/^{86}Sr_{foliar}$ across sites further reflects the strong geological heterogeneity of eastern Canada, where ancient Precambrian rocks occur alongside younger sedimentary and Appalachian formations that generate distinct bioavailable $^{87}Sr/^{86}Sr_{foliar}$ (Le Corre et al., 2025).

Despite this clear baseline relationship, the regression suggests attenuation from $^{87}Sr/^{86}Sr_{foliar}$ to $^{87}Sr/^{86}Sr_{SBW}$. No fractionation of Sr isotopes is expected because mass-dependent fractionation is corrected for during analysis. Therefore, the difference between $^{87}Sr/^{86}Sr_{foliar}$ and $^{87}Sr/^{86}Sr_{SBW}$ usually occur with mixing of two isotopically distinct sources or analytical limitations. Based on the stronger but scattered model residuals at lower ^{88}Sr signal intensity (Figure 2.4), we hypothesize that this attenuation was best explained by analytical limitations. Sr concentrations in individual SBW approached the lowermost limits of the best MC-ICP-MS sensitivity, often close to 1 ng of Sr. Under such low Sr concentrations, the signals for ^{87}Sr and ^{86}Sr are extremely low and error rapidly propagates in the $^{87}Sr/^{86}Sr$ ratios. Contamination and blanks are unlikely to be the cause as the residuals are scattered

without clear bias supporting our findings that procedural blank contribution was less than 5% for most samples.

To overcome these analytical limitations, we pooled individuals by site to increase the amount of Sr available during purification and analysis. This approach produced a stronger foliage-moth correlation (R^2 = 0.85) and a slope whose 95% confidence interval fell within the expected 1:1 relationship (Figure 2.3C). Pooled samples exhibited higher signal intensity and reduced dispersion relative to individual ones (Figure 2.4), and residual magnitude declined with increasing ^{88}Sr signal intensity, consistent with an analytical rather than a biological source of error when operating at the edge of the instrument's detection limit. Additionally, pooling samples might also average out biological micro-variation among individuals feeding at the same site.

The biological characteristics of SBW further support the use of $^{87}Sr/^{86}Sr$ as a geolocator for this particular species. Adult moths do not feed after emergence and have relatively short lifespans, meaning that their tissue Sr is derived almost entirely from larval feeding sites (Dargent et al., 2023). The contribution of sites in the LMM, along with the well-characterized spatial structure of $^{87}Sr/^{86}Sr$ across eastern Canada (Le Corre et al., 2025) further support the use of $^{87}Sr/^{86}Sr$ as a geolocator. $^{87}Sr/^{86}Sr$ ratios provide direct information on natal habitat that is largely independent of climatic influences that affect other isotope systems, such as hydrogen, carbon, and nitrogen (Reich et al., 2021). Because geological variation often occurs over relatively fine spatial scales, strontium isotopes can provide geographic resolution that complements climate-driven tracers (Bataille et al., 2021; Reich et al., 2021). Although similar lithologies may generate isotopically indistinguishable regions at

continental scales, integrating $^{87}Sr/^{86}Sr$ with complementary isotope systems has repeatedly been shown to improve geolocation accuracy and precision (Bataille et al., 2021; Crowley et al., 2021; Reich et al., 2021).

Our results demonstrate that $^{87}Sr/^{86}Sr$ ratios exhibit conservative trophic transmission from host foliage to SBW and retain information derived from underlying geological substrates. The principal limitation for insect geolocation identified in this study was analytical rather than ecological, arising from the low Sr concentrations present in individual moths. Consequently, future applications should focus on increasing analytical precision through larger sample masses, pooled analyses, or methodological developments that improve measurement sensitivity at low Sr concentrations. Once these constraints are addressed, $^{87}Sr/^{86}Sr$ has considerable potential as a geolocation tracer for SBW, particularly when incorporated into multi-isotope geolocation frameworks.

2.5.6 Limitations

First, sample sizes differ substantially among isotope systems and are small for carbon and nitrogen (7 sites) relative to sulfur (23 sites), hydrogen (19 sites) and strontium (18 sites), so the strength of evidence is not uniform across the systems we compare; the nitrogen result, which we identify as among the most promising, rests on the smallest dataset in the study. Second, different tissues were analysed for different elements, wings for $\delta^{2}H$, $\delta^{13}C$ and $\delta^{15}N$, head and thorax for $\delta^{34}S$, and whole individuals for $^{87}Sr/^{86}Sr$, because of differences in elemental concentration; the resulting transfer functions are therefore not strictly comparable across systems, and each incorporates a tissue-specific offset in addition to any physiological fractionation. Third, foliage was pooled by site prior to analysis, so intra-site foliar heterogeneity was not quantified and foliar composition acts as a site-level predictor. This matters most for $\delta^{13}C$, where we attribute intra-site variance in moth values to within-canopy heterogeneity and ontogenetic effects, but where unmeasured foliar heterogeneity is an equally plausible and untested explanation. Fourth, sampling was restricted to Ontario and Newfoundland and does not span the full SBW range, so the transfer functions reported here should be treated as regionally calibrated.

2.6 Conclusion

Isotope geolocation in insects is limited by the effective propagation of isotopes from the environment to the animal, yet this step is rarely investigated. By quantifying it directly in a host-specialist insect herbivore, we show that the five isotope systems most commonly used show different levels of suitability for geolocation. $\delta^{34}S$ and $\delta^{15}N$ display near-proportional transfer with a consistent trophic discrimination factor and low intra-site variance and are

the strongest geolocators in this system. However, unlike $\delta^{34}S$ which has a well-established isoscape across eastern Canada, the $\delta^{15}N$ patterns still need to be characterized and confirmed before $\delta^{15}N$ could be used as a geolocator. Sr isotopes are transmitted conservatively, as expected, but their limitation for tiny-insect ecology is analytical rather than biological. $\delta^{13}C$ and $\delta^{2}H$ are poorly propagated due to microhabitat variation in photosynthetic discrimination and by mixed dietary and environmental hydrogen sources respectively, and neither has strong geolocator potential at the study scale presented here. Although $\delta^{2}H$ is among the most widely used isotopes for continental-scale geolocation, the high intra-site variance observed here substantially reduced its discriminatory power at the spatial scale examined, illustrating that isotope performance depends strongly on the geographic scale of application. The $\delta^{15}N$ result is the least expected. Nitrogen isotopes are seldom used to infer geographic origin because mixed and shifting diets usually decouple consumer values from any single baseline. In SBW that decoupling does not occur because larvae feed on the needles of one or a few host trees, adults do not feed at all, and the tissues we measure are formed before dispersal begins. The life history that makes this insect so difficult to track by conventional means is precisely what makes its $\delta^{15}N$ applicable for geolocation. The same reasoning should extend to other host-specialist herbivores with non-feeding adults, a life history shared by many of the lepidopteran pests whose movements are hardest to observe. More generally, our results caution against applying published baseline isoscapes to a new species without first measuring the transfer function and considering the study scale. A large but highly consistent trophic offset, as we observe for nitrogen, is no obstacle to geolocation, whereas a small but variable one, as we observe for carbon, is challenging to overcome.

2.7 Declarations

Funding This study was funded through an Early Intervention Strategy against Spruce Budworm Phase III funding through Natural Resources Canada - Canadian Forest Service - Pest Risk Management awarded to Felipe Dargent and Jean-Noël Candau and an Early Intervention Strategy against Spruce Budworm Phase III Small Scale Research Program awarded to Clement P. Bataille. The project was also covered by the Healthy Forest Partnership Early Intervention Strategy against Spruce Budworm Phase II Contribution Program awarded to the Invasive Species Centre by Natural Resources Canada - Canadian Forest Service - Pest Risk Management and contracted to Clement P. Bataille. Clement P. Bataille also received funding from the Natural Sciences and Engineering Research Council of Canada (NSERC) Discovery Grant RGPIN-2019-05709, Purdue College of Agriculture Start-up fund and USDA North Central Integrated Pest Management sub-award number 026461GG.

Competing interests The authors declare no competing interests.

Ethics approval This study involved insects and conifer foliage only and did not require ethics approval.

Data availability The datasets generated and analysed during this study, and the R code used to produce the results, are available at:

Acknowledgements We thank the field and laboratory personnel who contributed to sample collection and preparation, and the staff of the Jan Veizer Stable Isotope Laboratory (University of Ottawa), the Pacific Centre for Isotopic and Geochemical Research, and the MC-ICP-MS Facility at the University of Cape Town.

CHAPTER 3: MULTI ISOTOPE GEOLOCATION POTENTIAL ACROSS THE EASTERN CANADIAN BOREAL FOREST

Brent Holmes[1], Isabela M. Souza-Silva[2,3], Kala Studens[4], Megan Reich[3,5], Felipe Dargent[3,4], Jean-Noel Candau[4], Petrus Le Roux[5], Clement P. Bataille[1,3,6]

[1] University of Ottawa, Department of Biology, K1N 6N5, Ottawa, ON, Canada.

[2] Center for Nuclear Energy in Agriculture, University of Sao Paulo, SP 13416-000, Brazil

[3] University of Ottawa, Department of Earth and Environmental Sciences, Advanced Research Complex building, 25 Templeton St., K1N 7N9, Ottawa, ON, Canada.

[4] Natural Resources Canada, Canadian Forestry Service, Great Lakes Forestry Centre, P6A 2E5, Sault Ste. Marie, ON, Canada.

[5] University of Cape Town, Department of Geological Sciences, Geological Sciences Building, Rondebosch 7701, South Africa

[6] Purdue University, Forestry and Natural Resources, 47907, Lafayette, Indiana, USA

Corresponding author:

Clement P. Bataille **cbataill@purdue.edu**

KEWORDS
Isotopes, Migration, Forestry, Geolocation, Isoscapes, Conservation, Provenance

3.1 Abstract

Rapid climate and land-use change are reshaping species mobility in the boreal forest but tools for reconstructing mobility remain limited for small-bodied and remote taxa. We developed a multi-isotope geolocation framework for eastern Canada using foliar isoscapes to inform forestry and conservation applications. Needles of conifers were collected across eastern Canada (2019–2022) and analyzed for carbon, nitrogen, sulfur, hydrogen and strontium isotopes. Random forest regressions integrated foliar isotopes with geospatial predictors representing climate, geology, atmospheric deposition, vegetation, soils, and forest properties. Model performance (10-fold CV) was moderate for carbon and nitrogen isotopes (RMSE = 0.97‰, MAE = 0.77‰, R^2 = 0.36; RMSE = 1.67‰, MAE = 1.33‰, R^2 = 0.33, respectively), strong for strontium and hydrogen isotopes (RMSE = 0.0045, MAE = 0.00230, R^2 = 0.59; RMSE = 9.4‰, MAE = 7.4‰, R^2 = 0.59, respectively) and excellent for sulfur isotopes (RMSE = 1.52‰, MAE = 1.12‰, R^2 = 0.89). Carbon and nitrogen isotopes showed high intra-site variability driven by species differences, needle chemistry, plant physiology and microenvironmental conditions but retained significant geographic structure linked to insolation, stand age, and moisture conditions (for carbon) and to moisture and edaphic conditions (for nitrogen). Hydrogen isotopes exhibited high intra-site variation, but spatial patterns were well-predicted by climate. Strontium isotopes showed limited intra-site variation and followed underlying geology though predictive accuracy was constrained by the complexity of eastern Canadian bedrock. Sulfur isotopes displayed the lowest intra-site variance and were dominated by spatial changes in marine sea-salt deposition. We then introduce a separability-based framework (i.e., the ratio of spatial variance to predictive uncertainty at biologically relevant scales) enabling direct comparison among isotopes and

explicit evaluation of scale dependence. Across the region, sulfur and strontium isotopes provide the strongest geolocation potential at large scales (~100 km), while strontium dominates at finer spatial scales (~10km) where lithological heterogeneity is high. Carbon and nitrogen offer supplemental discriminatory power in regions structured by forest properties or edaphic conditions, particularly where other isotopes show limited spatial contrast. The geolocation potential of hydrogen isotopes is limited to a few regions where strong climatic gradients are present. Our work provides robust isotope baselines for tracing provenance and mobility of boreal species along with a scale-explicit decision-support tool to optimize isotope selection in ecological studies across the eastern Canadian boreal biome.

3.2 Introduction

Rapid global change and intensifying human impacts are altering the seasonal movements of many species (Cooke et al., 2024), often with adverse consequences for population dynamics and ecosystem functioning (Tucker et al., 2018; Kubelka et al., 2022). Quantifying these changes in mobility is essential to inform management of pests and invasives for biosecurity purposes and support conservation practises for connectivity and habitat protection for species of concern. However, understanding the mobility habits of key pests and endangered species is difficult: long-term tagging or GPS deployments remain logistically challenging for taxa with small body sizes and large populations (e.g., many insects and small birds), and/or for species that occupy remote or sensitive habitats (e.g., Arctic and boreal mammals). Assessing changes in mobility and its impact on population dynamics require baselines ecological data spanning the timescales at which the key drivers of mobility (climate, land use, human disturbances) operate, which are often decadal to centennial. This need for baseline data is especially prominent for taxa that experience large natural demographic fluctuations such as cyclical spruce budworm outbreaks (Royama, 1984), boom-and-bust caribou population cycles (Gunn, 2003), and irruptive songbird species population (Koenig and Knops, 2001). Such natural variability often makes it challenging to disentangle human impacts from intrinsic population dynamics to develop effective management plans.

The boreal forest, a circumpolar biome comprising roughly 27-30% of global forest area, shelters an extraordinary share of Earth's biodiversity (Ruckstuhl et al., 2008; Brandt et al., 2013). Each summer, billions of migratory songbird and insect species converge on the boreal region to breed, generating one of the planet's largest seasonal pulses of biological productivity (Ruckstuhl et al., 2008; Wells, 2011; Hu et al., 2016). Resident species, including

caribou and spruce budworm, further shape boreal ecosystems through their dispersal, trophic interactions, and cyclical population dynamics. The boreal biome has become a global hotspot for climate change and land-use pressures linked to natural resource development (Gauthier et al., 2015, 2023). High-latitude regions are warming faster than the global average, driving rapid shifts in fire regimes, permafrost thaw, insect outbreaks, and biotic range expansions (Kittel et al., 2000; Schuur and Mack, 2018; Stralberg et al., 2020; Foster et al., 2022). These dynamics pose mounting risks and are changing the behavior of native species and seasonal migrants that rely on this biome. At the same time, climate and land-use disturbances are enabling some pest and invasive species to expand their ranges, colonize new habitats, or undergo outbreaks with major ecological and socio-economic impacts on the boreal landscape (Wolken et al., 2011; Langor et al., 2014; Nealis, 2016; Marini et al., 2022).

Stable isotope analysis provides a powerful intrinsic method for reconstructing past movements and geographic origins of individuals at scales ranging from sub-annual to lifetime (Brennan et al., 2019; Wooller et al., 2021). Compared with other tracking approaches, isotope analyses are logistically practical, relatively inexpensive, and can be conducted on deceased animals or archived biological materials. They offer a means of reconstructing ecological baselines of mobility during periods when climate or human disturbances did not shape population dynamics, and they enable tests of how past analogue disturbances affected movement ecology and population processes in both extant and extinct species (Rubenstein and Hobson, 2004; West et al., 2010; Hobson et al., 2019b).These unique strengths make stable isotopes an approach of choice for ecological inference, particularly in

remote boreal landscapes where tagging opportunities and long-term baseline data are limited (Rubenstein and Hobson, 2004; West et al., 2010; Hobson et al., 2019b).

The principle of isotope geolocation is to compare the isotope composition of animal tissues with predicted spatial isotope landscapes (isoscapes) to infer the probable region of origin of an individual (Bowen et al., 2005; West et al., 2010; Hobson et al., 2019b). Hydrogen and oxygen isotopes ($\delta^{2}H$, $\delta^{18}O$) are widely used because tissue hydrogen and oxygen often reflect precipitation or source water at the site where the tissue was formed (Hobson and Wassenaar, 2019). However, assignments based on a single isotope system typically produce broad, low-specificity origin areas due to shallow spatial gradients, redundant values and high uncertainties of single isoscapes (Wunder, 2010). Integrating additional, complementary isotope systems can dramatically improve spatial resolution (Wunder, 2010). While carbon and nitrogen isotopes ($\delta^{13}C$, $\delta^{15}N$) are rarely used in geolocation studies due to the strong influence of physiological and trophic isotope fractionation on their variations, they often show broad spatial variations in forests linked to climate and edaphic conditions that have been leveraged for tracing habitat and mobility (Amundson et al., 2003). More recently, strontium isotopes ($^{87}Sr/^{86}Sr$), which track underlying geology at fine spatial scales (Bataille and Bowen, 2012), and sulfur isotopes ($\delta^{34}S$) which vary with sea-spray and atmospheric deposition gradients, have shown strong potential to enhance the precision of isotope geolocation (Bataille et al., 2021; Dargent et al., 2026).

The independent power of each isotope can be leveraged quantitatively in a multi-isotope geolocation framework. In this framework continuous maps of probable origin are generated by incorporating the predictive power and uncertainty associated with each isotope

(Wunder, 2010; Wassenaar, 2019). Those posterior probability maps are then intersected because each isotope varies independently (Wunder, 2010; Vander Zanden et al., 2014). The method can substantially refine origin estimates and has allowed ground-breaking ecological discoveries (Wunder, 2010; Vander Zanden et al., 2014). For example, dual $\delta^{2}H$ and $^{87}Sr/^{86}Sr$ assignments in juvenile North American raptors revealed strong structuring in migratory connectivity along western flyways (Crowley et al., 2021). $\delta^{2}H$ combined with $^{87}Sr/^{86}Sr$ elucidated Afro-Palearctic migratory connectivity across the Sahara and revealed a leapfrog migration behavior in painted lady butterflies (Reich et al., 2024). Beyond contemporary systems, multi-isotope mapping (e.g., $^{87}Sr/^{86}Sr$ and $\delta^{18}O$) has reconstructed lifetime movement histories of several late Pleistocene megafauna species demonstrating their changing mobility behavior with changing climate and human pressures (Gigleux et al., 2019; Rowe et al., 2024). Multi-isotope geolocation is also useful to trace and certify the provenance of wood products (Truszkowski et al., 2025; Martinelli et al., 2026).

However, a persistent limitation in effectively designing isotope geolocation studies is the lack of *a priori* knowledge on the discriminatory power of each isotope system for the focal species and region. Because isotopes vary across landscapes at different spatial scales and in response to distinct environmental processes, their ability to resolve origin differs geographically and taxonomically. Strontium isotopes, for example, may vary at sub-kilometer resolution in geologically complex regions but remain nearly homogeneous across hundreds of kilometers of broad carbonate platforms. Sulfur isotopes exhibit steep gradients in coastal environments due to exponential declines in marine sulfate deposition (Bataille et al., 2021), or high micro-scale variability in permafrost-dominated landscapes driven by redox heterogeneity (Bataille and Skierszkan, 2025; Stevens et al., 2025) but can have limited

discriminatory power in some inland boreal forests (Dargent et al., 2026). Even δ^2H, typically characterized by broad, continental-scale gradients, can show fine-scale variation in mountainous regions or areas with strong microclimatic effects. Knowing the geolocation potential of each isotope system within the study area is essential for directing analytical resources toward the isotope systems that offer the strongest and most practical discriminatory power.

Eastern Canada is an excellent natural laboratory to develop multi-isotope geolocation frameworks and to test the discriminatory potential of different isotope systems in ecological applications. First, the eastern boreal forest is home to many species of concern both for conservation and biosecurity. Second, boreal and mixed-boreal habitats in the region are experiencing rapid disturbance and climate-driven change (wildfire, insect outbreaks, and shifting biogeography), underscoring the need for scalable movement tools to anticipate and manage population responses. Third, many focal taxa are highly mobile, small-bodied, and/or inhabit remote areas limiting conventional telemetry but tractable for isotope-based approaches that can be applied to small tissue amounts (e.g., insect wings, feathers, hairs) and to post-mortem material from monitoring programs or collections. Fourth, eastern Canada spans diverse environments, geologies and climates, conditions that produce strong, complementary spatial signals in hydrogen, carbon, nitrogen, strontium, and sulfur isotopes, and are a prerequisite for precise assignments. However, developing isotope geolocation studies to effectively investigate migratory pathways and connectivity of important pest, invasive, and conservation-priority species across this vast landscape requires to optimize the allocation of analytical and economic resources towards the isotope combinations with the best discriminatory power.

3.2.1 Objectives

Here we first collect foliar samples from two of the most common tree species of the boreal forest, Spruces (*Picea* spp.) and Balsam Fir (*Abies balsamea*), across eastern Canada. We then analyze those foliar samples for carbon, nitrogen, sulfur, hydrogen, and strontium isotopes. We use those data along with geospatial predictors to map each isotope across the boreal forest. We finally compare the discriminatory power of each isoscape across the landscape to support the design of ecological geolocation studies.

3.3 Methods

3.3.1 Foliar sample collection

Since plants are primary producers that integrate local ecosystem resources that reflects the local isotope ratio distributions and are at the base of trophic webs, we expect a predictable relationship between the local isotope composition of plants and herbivores. Thus, isoscapes can be readily constructed from the isotope composition of plants as far as the relationship between the herbivores and the plant baseline is well-characterized (Dargent et al., 2026; Holmes et al., 2026). To develop isoscapes for eastern Canada, we collected mature needles from the host plants of spruce budworm, balsam fir (*Abies balsamea*) and spruce (*Picea sp.*), across, mostly, eastern Canada, from sites encompassing a broad range of environmental, geological, geographic, anthropogenic and climatic conditions (Figure 3.1). These samples were collected between 2019 and 2022 by collaborators and volunteers at 260 sites, and their latitude and longitude were recorded. At 50 of these sites, we collected branches at ~1.5 meters above ground from three trees less than 10 meters apart. At the remaining sites, only one tree was sampled. In the laboratory, each branch was subsampled and, when possible, species was recorded before the samples were stored in kraft envelopes in a dry room. We calculated intra-site variance from the sites where multiple samples were collected. At 8 sites, we also collected needles from both spruce and balsam fir needles and immature vs. mature foliage to test the potential drivers of intra-site isotope variability.

3.3.2 Foliar sample preparation and isotope analysis

Needles were aggregated by site, rinsed twice with deionized water to remove surficial particles, and dried at 50 °C for 48h. Dry needles were ground to a fine powder and stored in glassine envelopes. Not all the isotopes were analyzed for each specimen at each site for cost

reasons (Table 1). Some samples were also analyzed for sulfur and strontium isotopes as part of previous publications ((Le Corre et al., 2025; Dargent et al., 2026); Table 3-1).

Table 3-1 - Summary of samples analyzed for each isotope system.

Isotope system	Number of samples analyzed for this study	Number of samples compiled from previous compilation and reference	Number of individual sites
	267	0	215
N ($\delta^{15}N$)	267	0	215
S ($\delta^{34}S$)	341	313 (Dargent et al., 2026)	211
Sr ($^{87}Sr/^{86}Sr$)	298	126 (Le Corre et al., 2025)	260

Carbon and nitrogen stable isotopes were analyzed at the Jan Veizer Stable Isotope Laboratory at the University of Ottawa across multiple runs between 2023 and 2024. The methods and standards for each run were identical. Carbon and nitrogen could not be run simultaneously because the C:N ratio in foliar material exceeded 10:1 which complicate proper instrument tuning and analytical precision. We micro-weighed a target mass of 0.6 ± 0.03 mg of conifer needle powder for carbon and a target mass of 6.0 ± 0.3 mg of conifer needle powder for N into tin capsules (Elemental Microanalysis, United Kingdom). Samples were combusted at 950C through an Elemental Analyser (Vario EL cube, Elementar, Germany) packed with copper oxide wires and silver wool (Elemental Microanalysis, United Kingdom) in the combustion reactor and a mix of copper granules and copper wires (Elemental Microanalysis, United Kingdom) in the reduction reactor. Combustion was performed using 4.5 O_2 (Messer, Germany) for the combustion and 5.0 He (Messer, Germany)

as the carrier gas. Gas flows and temperatures used were in accordance with instrument manufacturer specifications. For the carbon analysis, water was removed using a Sicapent trap (Merck, Germany). For the nitrogen analysis, CO_2 and water were removed with a trap consisting sequentially of Ascarite (Merck, Germany) and Sicapent. The resulting N_2 and CO_2 travelled through an interface interfaced (Conflo IV, Thermo, Germany) to an isotope ratio mass spectrometer (IRMS, DeltaPlus Advantage, Thermo, Germany) controlled using Isodat 3.0 (Thermo, Germany), and SSH used to correct for ^{17}O in CO_2. Isotopic deltas were derived relative to a working gas (4.0 CO_2 or 4.8 N_2, Messer, Germany) introduced using the Conflo IV and were normalized using LIMS for Light Stable Isotopes (USGS, United States). $\delta^{15}N$ and $\delta^{13}C$ were calibrated through a three-point calibration using internal standards C-51 Nicotiamide (Acros Organics, Belgium) $\delta^{15}N$=0.07, $\delta^{13}C$ =-22.95‰), C-52 mix of ammonium sulphate (Merck, Germany) + sucrose (Merck, Germany) ($\delta^{15}N$=16.58‰, $\delta^{13}C$ =-11.94‰), C-54 caffeine (Alfa Aesar, United Kingdom, $\delta^{15}N$ =-16.61‰, δ13C =-34.46‰). Those internal standards were previously calibrated against international standards IAEA-N1 (+0.4±0.07‰; IAEA, 2022a), IAEA-N2 (+20.3±0.12‰; IAEA, 2022b), USGS-40 (-4.52‰±0.06‰; USGS, 2019b) and USGS-41 (47.57±0.11‰; USGS, 2011) for nitrogen, and IAEA-CH-6 (-10.4±0.033‰; IAEA, 2024), NBS-22 (-29.91±0.04‰; NIST, 2022), USGS-40 (-26.24±0.04‰; USGS, 2019b) and USGS-41 (37.76±0.05‰; USGS, 2011) for carbon. Each run calibration was verified against a blind internal standard C-55 L-glutamic acid (Merck, Germany) $\delta^{15}N$=-3.9 ± 0.1‰, $\delta^{13}C$ =-28.5 ± 0.1‰, n=10. This standard was calibrated against the same international standards mentioned above (USGS, 2011, 2019; IAEA, 2022a, 2022b, 2024; NIST, 2022). A full set consisting of each of the calibration and blind reference materials was analyzed at the beginning and end of each run, as well as throughout the

middle of the run after every 30 samples. Calibration and blind reference materials were weighted to provide 100 µg N ± 5 µg and 300 µg C ± 15 ug for the $\delta^{15}N$ and $\delta^{13}C$ analyses, respectively to match samples. The C55 L-glutamic acid reference material was analyzed at a range of masses (0.53-2.11 µg) in the middle of each run to confirm system linearity, minor linearity corrections were applied if necessary. For each run, we verified that the $\delta^{15}N$ and $\delta^{13}C$ of the blind C-55 L-glutamic acid fell within the range of the accepted calibrated value. Analytical precision of the blind standard and calibration standards averaged 0.09‰ for the different runs (n=4). The measured values for C-55 L-glutamic among runs varied between -4.0‰ to -3.9‰ for $\delta^{15}N$ and between -28.6‰ to -28.5‰ for $\delta^{13}C$ (among run average $\delta^{15}N$ = -3.93 ± 0.05‰ and $\delta^{13}C$ = -28.52 ± 0.04 ‰, n = 5) and were within the laboratory long-term reported values.

Isotopes of sulfur were analyzed at the Jan Veizer Stable Isotope Laboratory at the University of Ottawa. We micro-weighed a target mass of 60 ± 6 mg of conifer needle powder (S%= 0.09 ± 0.03, into tin capsules (Elemental Microanalysis, United Kingdom). Samples were combusted through an Elemental Analyser Isotope Cube in S mode (Elementar, Germany) with combusted SO_2 from the sample carried to a Delta Plus XP IRMS (ThermoFinnigan, Germany) equipped with a ConFlo IV. The $^{34}S/^{32}S$ ratios were obtained from *m/z* 48, 49 and 50 of SO^+ produced from SO_2. Standards used for three-point calibration were sulfide-based IAEA-S1 (argentite, $\delta^{34}S$ = -0.3 ‰ ± 0.03; IAEA, 2020), IAEA-S2 (argentite, $\delta^{34}S$ = 22.7 ‰ ± 0.08; IAEA, 2020), and IAEA-S3 (argentite, $\delta^{34}S$ = -32.6 ‰ ± 0.08; IAEA, 2020); AG-2 (argentite, $\delta^{34}S$ = -0.6 ‰) was used as an internal blind standard. Sulfur isotope values are reported to the international scale Vienna Canyon Diablo Troilite (VCDT). A full set consisting of each of the calibration and blind reference materials was analyzed at the beginning and

end of each run, as well as throughout the middle of the run after every 30 samples. Calibration and blind reference materials were weighted to provide 50 ± 0.05 µg S and match samples. The AG-2 reference material was analyzed at a range of masses (25-100 µg) in the middle of each run to confirm system linearity, minor linearity corrections were applied if necessary. The measured values for AG-2 among runs varied between -0.4‰ and -1.1‰ (among run average = -0.8± 0.3‰, n = 9) and were within the laboratory long-term reported value of -0.6 ± 0.3‰. Duplicates were run for 22 foliar powder samples and showed a mean difference of 0.16 ‰ ± 0.15‰.

Samples were prepared for strontium isotopes at the University of Ottawa. Approximately 1g of plant was ashed at 800C for 12h using a furnace oven. The ash was redissolved in 1 mL concentrated distilled HNO_3. An aliquot of 200 µL from each sample was separated and diluted to 2 mL of 2% v/v HNO_3 and analyzed for Sr content via inductively coupled plasma mass spectrometry (ICP-MS; Agilent 8800 ICP-QQQ; Agilent Technologies Inc., CA, USA) at the Department of Earth and Environmental Science, University of Ottawa (ON, Canada). Calibration standards were prepared using single-element-certified standards purchased from SCP Science (Montreal, Canada). The remaining aliquot of sample digest was dried down and re-dissolved in 0.5 mL of distilled 6M HNO_3. The separation of Sr was processed in a 100-µL microcolumn loaded with Sr-spec Resin (100–150 µm; Eichrom Technologies, LLC). The matrix was rinsed out using 6M HNO_3, and Sr was collected with 0.05M HNO_3. After separation, eluates were dried. All isotope analyses performed on a NuPlasma HR MC-ICP-MS housed in the Department of Geological Sciences, University of Cape Town, Rondebosch, South Africa. Purified Sr were analyzed for $^{87}Sr/^{86}Sr$ in solution of 200 ppb in 0.2% distilled HNO_3. The isotopes ^{84}Sr, ^{86}Sr, and ^{87}Sr have isobaric interferences from ^{84}Kr, ^{86}Kr, and ^{87}Rb

respectively, and were corrected for using the ^{85}Rb and ^{83}Kr signals. Instrumental mass fractionation was corrected by normalizing $^{86}Sr/^{88}Sr$ to 0.1194 using the exponential law. Procedural blanks were negligible.

3.3.3 Isoscape development

We built foliar isoscape using a similar framework for each isotope. We used random forest regression following the methods of Bataille et al., (2020) and the code of Paris et al. (2026). The model integrates the foliar isotope data from eastern Canada with continuous geospatial variables representing geological, atmospheric, climatic or environmental controls of isotope variations in the environment (Table 3-2). For $^{87}Sr/^{86}Sr$, we augmented the training dataset to train a more generalizable model by integrating plant samples from across North America using a recent compilation (Stantis et al., 2026). The tuning and optimization of the random forest model has been described in previous work (Bataille et al., 2020). Briefly we used the "tuneRF" function of the *caret* package (Kuhn, 2008) using RMSE (root mean square error) through a 10-fold cross-validation approach with five repetitions where 80% of the data was used for training at each iteration. We used the *VSURF* package (Genuer et al., 2015) to maximize model performance while minimizing the number of predictors. Partial dependence plots were also used to evaluate the relationship between foliar isotope values and the selected predictors. We estimated model uncertainty using quantile random forest to calculate a 68.27% prediction interval which we used to then estimate the standard deviation (σ) of predictions at each pixel with: $\sigma \approx q(0.841) - q(0.159)$. Isoscapes were then trimmed to remove areas beyond the range of the predictor values used in the training set to ensure the model only extrapolate to areas for which it was properly trained.

Table 3-2 - Auxiliary variables tested for developing the random forest regression for each isotope system.

No.	Variables	Description	Resolution	Type	Reference
1	r.m1	Median bedrock model	1 km	D	(Bataille et al., 2021; Le Corre et al., 2025)
2	r.srsrq1	1st quartile bedrock model	1 km	D	(Bataille et al., 2021; Le Corre et al., 2025)
3	r.srsrq3	3rd quartile bedrock model	1 km	D	(Bataille et al., 2021; Le Corre et al., 2025)
4	r.meanage_geol	Mean geological age (Ma) from the GLiM	1 km	D	(Hartmann and Moosdorf, 2012; Bataille et al., 2021; Le Corre et al., 2025)
5	r.minage_geol	Minimum geological age (Ma) from the GLiM	1 km	D	(Hartmann and Moosdorf, 2012; Bataille et al., 2021; Le Corre et al., 2025).
6	r.maxage_geol	Maximum geological age (Ma) from the GLiM	1 km	D	(Hartmann and Moosdorf, 2012; Bataille et al., 2021; Le Corre et al., 2025)
7	r.age	Global mean terrane (basement) age, in millions of years (Ma)	1 km	D	(Mooney et al., 1998)
8	r.GUM	Global Unconsolidated Material (GUM) type	1 km	C	(Börker et al., 2018)
9	r.bouger	Bouguer anomaly (mGal)	2 arc-min	C	(Balmino et al., 2012)
10	r.elevation	SRTM elevation (m)	90 m	C	(Jarvis et al., 2008)
11	r.mat	Mean annual temperature (°C)	30-arc sec	C	(Harris et al., 2020)
12	r.map	Mean annual precipitation (mm/year)	30-arc sec	C	(Harris et al., 2020)
13	r.ai	Global aridity index	30-arc sec	C	(Trabucco and Zomer, 2019)
14	r.pet	Global potential evapotranspiration (mm/year)	30-arc sec	C	(Trabucco and Zomer, 2019)
15	r.dust	Global dust deposition rate ($g/m^2/year$)	1° × 1°	C	(Chien et al., 2016)
16	r.salt	Global sea salt aerosol deposition ($g/m^2/year$)	1° × 1°	C	(Chien et al., 2016)
17	r.distance	Distance to the coast (km)	30-arc sec	C	(Bataille et al., 2021)
18	r.volc	Volcanic deposition rate ($kg/m^2/s$)	0.5°	C	(Brahney et al., 2015)
19	r.fire*	Black carbon deposition from wildfires ($kg/m^2/s$)	1° × 1°	C	(Chien et al., 2016)
20	r.foss	Fossil fuel black carbon deposition ($kg/m^2/s$)	1° × 1°	C	(Chien et al., 2016)
21	r.clay	Soil clay fraction (%) in the topsoil (5–15 cm depth)	250 m	C	(Poggio et al., 2021; Le Corre et al., 2025)
22	r.ph	Soil pH (H_2O, 5–15 cm depth, decimal scale)	250 m	C	(Poggio et al., 2021; Le Corre et al., 2025)
23	r.cec	Cation exchange capacity ($cmol^+/kg$, 5–15 cm depth)	250 m	C	(Poggio et al., 2021; Le Corre et al., 2025)
24	r.bulk	Soil bulk density (g/cm^3, 5–15 cm depth)	250 m	C	(Poggio et al., 2021; Le Corre et al., 2025)
25	r.ocs	Soil organic carbon stock (kg/m^2, 0–30 cm depth)	250 m	C	(Poggio et al., 2021; Le Corre et al., 2025)

26	r.phkcl	Soil pH (KCl, 5–15 cm depth, decimal scale)	250 m	C	(Poggio et al., 2021; Le Corre et al., 2025)
27	r.sw	Soil moisture (m^3/m^3, 0–5 cm depth)	15 km	C	(Llamas et al., 2020)
28	r.w0010	Soil water content at −10 kPa (available water, 5–15 cm depth)	250 m	C	(Poggio et al., 2021)
29	r.w1500	Soil water content at −1500 kPa (wilting point, 5–15 cm depth)	250 m	C	(Poggio et al., 2021)
30	r.w0033	Soil water content at −33 kPa (field capacity, 5–15 cm depth)	250 m	C	(Poggio et al., 2021)
31	r.w0010_30	Available water capacity at −10 kPa integrated to 30 cm depth	250 m	C	(Poggio et al., 2021)
32	r.wetland	Global wetland/inundation extent (fractional cover, 0–1)	15-arc sec	C	(Lehner et al., 2025)
33	r.soc	Soil organic carbon content (g/kg weight, 5–15 cm depth)	250 m	C	(Poggio et al., 2021)
34	r.ocd	Soil organic carbon density (kg/m^3, 5–15 cm depth)	250 m	C	(Poggio et al., 2021)
35	r.nitrogen	Soil nitrogen content (g/kg, 5–15 cm depth)	250 m	C	(Poggio et al., 2021)
36	r.vapor	Water vapor pressure (kPa, 1970-2000)	30-arc sec	C	Fick et al., 2017(Fick and Hijmans, 2017)
37	r.solar	Solar radiation (kJ/m^2/day, 1970-2000)	30-arc sec	C	(Fick and Hijmans, 2017)
38	r.tmin	Mean annual minimum temperature (°C, 1970-2000)	30-arc sec	C	(Fick and Hijmans, 2017)
39	r.tmax	Mean annual maximum temperature (°C, 1970-2000)	30-arc sec	C	(Fick and Hijmans, 2017)
40	r.wind	Mean wind speed (m/s, 1970-2000)	30-arc sec	C	(Fick and Hijmans, 2017)
41	r.frfire	Wildfire change magnitude (differenced Normalized Burn Ratio; 1985-2022)	30 m	C	(Hermosilla et al., 2016)
42	r.frharv	Harvest Disturbance (1985-2022)	30 m	C	(Hermosilla et al., 2016)
43	r.frage	Forest Age (2022)	30 m	C	(Maltman et al., 2023)
44	r.frreturn	Forest percentage of first return above 2m	30 m	C	(Matasci et al., 2018)
45	r.frheight	Canopy height (m)	30 m	C	(Matasci et al., 2018)
46	r.frbasal	Basal Area (m^2/ha)	30 m	C	(Matasci et al., 2018)
47	r.frlorey	Lorey's tree height (m)	30 m	C	(Matasci et al., 2018)
48	r.frgsv	Gross stem volume (m^3/ha)	30 m	C	(Matasci et al., 2018)
49	r.evi	Mean annual Enhanced Vegetation Index (2017-2024)	1 km	C	(Didan, 2015)
50	r.ndvi	Mean annual Normalized Difference Vegetation Index (2017-2024)	1 km	C	(Didan, 2015)
51	r.evi2017	Mean annual Enhanced Vegetation Index (2017)	1 km	C	(Didan, 2015)
52	r.evi2018	Mean annual Enhanced Vegetation Index (2018)	1 km	C	(Didan, 2015)
53	r.evi2019	Mean annual Enhanced Vegetation Index (2019)	1 km	C	(Didan, 2015)

54	r.evi2020	Mean annual Enhanced Vegetation Index (2020)	1 km	C	(Didan, 2015)
55	r.evi2021	Mean annual Enhanced Vegetation Index (2011)	1 km	C	(Didan, 2015)
56	r.evi2022	Mean annual Enhanced Vegetation Index (2012)	1 km	C	(Didan, 2015)
57	r.evi2023	Mean annual Enhanced Vegetation Index (2013)	1 km	C	(Didan, 2015)
58	r.evi2024	Mean annual Enhanced Vegetation Index (2014)	1 km	C	(Didan, 2015)
59	r.ndvi2017	Mean annual Normalized Difference Vegetation Index (2017)	1 km	C	(Didan, 2015)
60	r.ndvi2018	Mean annual Normalized Difference Vegetation Index (2018)	1 km	C	(Didan, 2015)
61	r.ndvi2019	Mean annual Normalized Difference Vegetation Index (2019)	1 km	C	(Didan, 2015)
62	r.ndvi2020	Mean annual Normalized Difference Vegetation Index (2020)	1 km	C	(Didan, 2015)
63	r.ndvi2021	Mean annual Normalized Difference Vegetation Index (2021)	1 km	C	(Didan, 2015)
64	r.ndvi2022	Mean annual Normalized Difference Vegetation Index (2022)	1 km	C	(Didan, 2015)
65	r.ndvi2023	Mean annual Normalized Difference Vegetation Index (2023)	1 km	C	(Didan, 2015)
66	r.ndvi2024	Mean annual Normalized Difference Vegetation Index (2024)	1 km	C	(Didan, 2015)
67	r.et	Total annual evapotranspiration (mm $year^{-1}$)	500 m	C	(Running et al., 2017)
68	r.insol	Average daily Insolation(kWh/m^2)	0.1°x0.1°	D	(Natural Resources Canada, 2023)
69	r.gpp2018	Gross primary production (2018)	500 m	C	(Running et al., 2015)
70	r.etam	Annual evapotranspiration (mm $year^{-1}$)	500 m	C	(Running et al., 2017)
71	r.blspruce	Percentage of black spruce	30 m	D	(Guindon et al., 2023)
72	r.bfir	Percentage of balsam fir	30 m	D	(Guindon et al., 2023)
73	r.lancov	Land cover class	30 m	D	(Guindon et al., 2023)
74	r.closure	Percent canopy cover	30 m	C	(Guindon et al., 2023)
75	r.biomass	Vegetation biomass (ton/ha)	30 m	C	(Guindon et al., 2023)
76	r.conif	Percentage of other conifer species	30 m	C	(Guindon et al., 2023)
77	r.d2H_precip	δ^2H of precipitation	0.33°×0.33°	C	(Bowen et al., 2005)
78	r.d2H_leaf	δ^2H of leaf water	0.5° × 0.5°	C	(West et al., 2008)

D: Discrete; C: Continuous; GLiM: Global Lithological Map; SRTM: Shuttle Radar Topography Mission.

3.3.4 Selecting the most discriminatory isotope for a given area

Isotope analyses differ in analytical cost, sample mass requirements, and ecological interpretability; therefore, a transparent and quantitative criterion is needed to prioritize isotopes that are most likely to yield precise geolocation. The isotope geolocation potential is controlled by the balance between the amplitude of the spatial signal over a given area and the underlying predictive uncertainty across that area. In other words, the geolocation potential depends upon: 1) the spatial contrast at the scale of organismal movement, with higher difference in isotope values between distant locations leading to increased geolocation potential, 2) the precision of the isoscape, with lower pixel level uncertainty translating into higher geolocation resolution, 2) and 3) the redundancy of isotope values across the landscape, with more redundant values having lower geolocation potential. For each isotope k, we define a regional separability index that captures how strongly the isotope varies across space relative to its predictive uncertainty, evaluated at a biologically relevant scale. This separability metrics constrain how informative is isotope *k* on its own, relative to its own uncertainty, at this location and spatial scale. The separability index at cell i is then defined as:

$$\text{Separability}_{k,i} = \frac{\text{SD}(\mu_k)_i}{\bar{\sigma_{k}}_i}$$

with $\mu_k(x)$ the mean predicted isoscape pixel value and $\sigma_k(x)$ the corresponding pixel predictive uncertainty.

High separability values indicate regions where spatial variation in isotope values substantially exceed predictive uncertainty and therefore where the isotope is expected to provide strong geolocation potential. This formulation implicitly accounts for landscape

redundancy: isotopes with flat or repetitive spatial patterns yield low spatial variance and therefore low separability, even if predictive uncertainty is small. Conversely, isotopes with strong, unique spatial structure but high uncertainty are penalized by the denominator.

To enable direct comparison among isotopes, in a combined multi-isotope framework, we also calculated the contribution of each isotope to separability within each grid cell relative to the sum of separability across isotopes:

$$\text{Fraction}_{k,i} = \frac{\text{Separability}_{k,i}}{\sum_j \text{Separability}_{j,i}}$$

This fraction expresses the relative contribution of each isotope to total geolocation potential at a given location. The isotope with the highest fractional separability is defined as the dominant isotope, i.e., the geolocator expected to provide the greatest discriminatory power at that site and spatial scale. The magnitude of the maximum fractional value provides a quantitative measure of dominance strength, distinguishing areas where a single isotope strongly outperforms others from areas where multiple geolocators contribute similarly.

3.4 Results

3.4.1 Carbon isotopes

To assess intra-site variability, we measured $\delta^{13}C$ in at least two different trees at 24 sites randomly selected across the sampled sites of eastern Canada. We found that the intra-site variability was high with a median of 0.4‰ (min=0.1‰ and max=1.6‰) which represent 36% of the total variance across the dataset. At 8 sites, old needles were on average 1.4‰ lower $\delta^{13}C$ than young needles (t-test, p-value=0.011) and balsam fir were on average 1‰ lower than spruce (test, p-value=0.0054). The random forest regression model for $\delta^{13}C$ produced moderate predictive power with an average RMSE of 0.98‰, MAE of 0.78‰, and R^2 of 0.34 on the 10-fold cross validation (Figure 3.2A). Solar radiation and forest structure variables emerged as the dominant drivers of $\delta^{13}C$ variation with soil moisture proxy and soil nitrogen content also influencing the model significantly (Figure 3.2B). $\delta^{13}C$ values increased with increasing insolation, stand age, decreasing moisture conditions and increasing N availability (Figure 3.2B).

3.4.2 Nitrogen isotopes

To assess intra-site variability, we measured $\delta^{15}N$ in at least two different trees at 21 sites randomly selected across the sampled sites of eastern Canada. We found that the intra-site variability was moderate with a median of 0.4‰ (min=0.1‰ and max=3.4‰) which represent 21% of the total variance across the dataset. At 8 sites, needle ages or needles from different species show no significant difference in $\delta^{15}N$ (t-test, p-value=0.61 and 0.14, respectively). The random forest regression model for $\delta^{15}N$ produced moderate predictive power, with an average RMSE of 1.67‰, MAE of 1.33‰, and R^2 of 0.33 on the 10-fold cross

validation (Figure 3.3A). Predictors are dominated by climatic variables including evapotranspiration, soil moisture content, maximum temperature, geomorphological variables including minimum geological unit age, and bouger anomaly, atmospheric deposition (i.e., distance from the coast), and edaphic variables including soil organic content and pH (Figure 3.3B). $\delta^{15}N$ values increased under higher vapor pressure, soil moisture content and evapotranspiration. $\delta^{15}N$ decreased with geological age and bouger anomaly. $\delta^{15}N$ also increased with increasing pH, soil organic carbon and decreased with biomass (Figure 3.3B).

3.4.3 Sulfur isotopes

To assess intra-site variability, we measured $\delta^{34}S$ in at least two different trees at 26 sites randomly selected across the sampled sites of eastern Canada. We found that the intra-site variability was low with a median of 0.8‰ (min=0.1‰ and max=5.2‰) which represent 17% of the total variance across the dataset. At 8 sites, old needles showed lower $\delta^{34}S$ values than young needles (t-test: t = 3.70, p-value = 0.02) and balsam fir did not significantly differ from spruce (t-test: t = -2.15, p-value=0.06). The random forest regression model for $\delta^{34}S$ showed very strong predictive power with an average RMSE of 1.49‰, MAE of 1.11‰, and R^2 of 0.90 on the 10-fold cross validation (Figure 3.4A). Predictor importance was dominated by variables related to marine and sea-salt deposition including distance to the coast, and modeled atmospheric marine sulfate inputs, followed by climatic factors such as minimum temperature, precipitation, and evapotranspiration. Additional contributions came from atmospheric deposition and disturbance indicators including dust deposition, global aridity index, as well as vegetation and soil attributes including black spruce cover, lorey height, clay content, and soil water availability (Figure 3.4B). $\delta^{34}S$ values increased sharply with higher

sea-salt inputs and proximity to coastal sources, decreased with greater distance inland, and exhibited distinct nonlinear responses to minimum temperature, precipitation, and dust deposition (Figure 3.4B).

3.4.4 Hydrogen isotopes

To assess intra-site variability, we measured δ^2H in at least two different trees at 25 sites randomly selected across our sampled sites of eastern Canada. We found that the intra-site variability was moderate with a median of 2.4‰ (min=0.1‰ and max=12.8‰) which represent 4% of the total variance across the dataset. At 8 sites, old needles had δ^2H values 15‰ lower than young needles (t-test, p-value=0.03) while species did not show significant differences. The random forest regression model for δ^2H showed very strong predictive power with an average RMSE of 9.4‰, MAE of 7.4‰, and R^2 of 0.59 on the 10-fold cross validation (Figure 3.5A). Predictor importance was dominated by variables related to climatic factors such as mean minimum temperature, vapour pressure, atmospheric deposition (i.e., sea salt deposition), forest condition (i.e., forest fire), as well as mean solar insolation, and mean annual evapotranspiration (Figure 3.5B). δ^2H values in plant are also correlated with modeled δ^2H values in plant water. δ^2H values increased gradually going northward and westward with higher values in coastal areas (Figure 3.5B).

3.4.5 Strontium isotopes

To assess intra-site variability, we measured $^{87}Sr/^{86}Sr$ in at least two different trees at 34 sites randomly selected across our samples of eastern Canada. We found that the intra-site variability was low with a median of 0.00011 (min=0.0000014 and max=0.0083) which represent 2% of the entire variance across the dataset. Intra-site was generally higher in areas of higher geological complexity. The random forest regression model for $^{87}Sr/^{86}Sr$

showed strong predictive power with an average RMSE of 0.0045, MAE of 0.00230, and R^2 of 0.59 on the 10-fold cross validation (Figure 3.6A). Predictor importance was dominated by geology (mean geological age), sea salt deposition and temperature (Figure 3.6B). $^{87}Sr/^{86}Sr$ ratios decreased sharply with lower temperature, increase progressively with mean geological age and decrease towards 0.709 with increasing sea salt deposition (Figure 3.6B).

3.4.6 Isotope separability

Using the models trained for each isotope, we mapped the mean and standard deviation of isotope variations in trees across easter Canada (Figure 3.7 and Figure S1We then used these isoscapes to calculate the raw separability between isotopes at two distinct scales (10 km and 100 km) and produce spatially explicit maps identifying, for every pixel across the eastern Canadian boreal forest, the isotope with the highest relative geolocation potential (Figure 3.8, Figure S2). At the 10 km scale (Figure 3.8A,Figure S3), the relative geolocation potential is characterized by highly heterogeneous and fine-grained spatial patterns with strontium, sulfur and carbon isotopes dominating. Strontium isotopes dominate large portions of the landscape, particularly across regions with complex or heterogeneous bedrock where strong local lithological contrasts occur. Sulfur isotopes remain frequently dominant across many regions, even in the interior where $\delta^{34}S$ can vary very little. Carbon isotopes dominate in large portions of interior Ontario, primarily within poorly sampled continental interior regions. Hydrogen and nitrogen isotopes rarely emerge as dominant at the 10 km scale. At the 100 km scale (Figure 3.8B,Figure S4), sulfur isotopes emerge as the dominant geolocator across extensive coastal regions, forming a continuous band along the Atlantic coast and around the Gulf of St. Lawrence. Inland from these coastal zones, dominance transitions sharply, and strontium isotopes remain the most dominant geolocator

across large portions of interior Québec, Labrador, and Ontario. Hydrogen isotopes dominate in some interior transition zones, forming localized belts where they outperform other geolocators at this coarser spatial scale. Carbon and nitrogen isotopes continue to dominate in poorly sampled and spatially isolated areas of the continental interior of Quebec and Ontario.

3.5 Discussion

3.5.1 Carbon isotopes

The $\delta^{13}C$ isoscape generated for the eastern Canadian boreal forest highlights the central role of stand structure, light environment, moisture, and edaphic properties in shaping foliar carbon isotope composition (Figure 3.7). This pattern aligns with established physiological principles: $\delta^{13}C$ reflects the balance between photosynthetic demand and stomatal conductance, which is strongly modulated by irradiance, canopy architecture, and successional stage (Farquhar et al., 1989; Handley et al., 1994; Heaton, 1999; Diefendorf et al., 2010; Kohn, 2010; Codron et al., 2013; Rumman et al., 2018). The dominance of insolation and stand age among predictors suggests that $\delta^{13}C$ spatial variability is tightly linked to forest development and the distribution of available light across the landscape, consistent with previous observations of higher $\delta^{13}C$ values mature, well-lit canopies in northern and temperate forests (Chevillat et al., 2005; Duursma and Marshall, 2006). The observed increase in $\delta^{13}C$ values with increasing stand age likely reflects shifts in canopy complexity, higher photosynthetic capacity, and reduced stomatal conductance in older forests (Whitehead, 1998; Fessenden and Ehleringer, 2002; Ewers et al., 2005), whereas young or recently disturbed stands tend to show lower $\delta^{13}C$ values due to rapid growth, high stomatal conductance, and reduced water-use efficiency (Ewers et al., 2005; Giammarchi et al., 2017; Cernusak, 2020). Relationships with soil moisture and nitrogen availability indicate that localized shifts in water or nutrient limitation modulate carbon isotope fractionation, mirroring known controls in boreal and temperate ecosystems (Panek and Waring, 1997; Brüggemann et al., 2011; Du et al., 2023). The resulting $\delta^{13}C$ isoscape displays complex

continental-scale patterns, with lower values in the less-insolated, wetter and older forest of high-latitude regions, Newfoundland and interior Ontario and higher values in the south, along the Saint Lawrence river valley, in New Brunswick or in interior areas dominated by drier and more nitrogen-rich conditions with mature forests. However, intra-site variability was high, with a median within-site spread representing a dominant portion of the total dataset variance. Many factors can explain the dominance of intra-site variance including microclimatic differences, leaf phenology, and species-specific physiology (Farquhar et al., 1989; Duursma and Marshall, 2006). We show, for example, that needle chemical composition likely contribute to the intra-site variance with older needles having more carbohydrates with lower $\delta^{13}C$ whereas younger needles have more sugar with higher $\delta^{13}C$ values (Jäggi et al., 2002). Similarly, species-specific physiology with fir showing systematically lower $\delta^{13}C$ values. Although $\delta^{13}C$ alone cannot resolve fine-scale origin due to the dominance of intra-site variability, its patterns provide an independent, complementary constraint when integrated into multi-isotope frameworks. Thus, despite moderate model performance ($R^2 = 0.34$), the $\delta^{13}C$ isoscape offers meaningful geolocation potential within an integrated, multi-isotope approach for tracking the origins of insect pests across the boreal forest.

3.5.2 Nitrogen isoscape

The $\delta^{15}N$ isoscape reflects the strong influence of nitrogen cycling processes that vary predictably across boreal landscapes (Figure 3.7). The dominance of vapor pressure, evapotranspiration, and soil moisture as key predictors is consistent with the sensitivity of microbial mineralization and nitrification rates to warmer and wetter conditions, which generally produce higher $\delta^{15}N$ values. In contrast, the sharp decline of $\delta^{15}N$ with increasing

geological age points to tighter nitrogen retention and reduced mineralization on older cratonic substrates of the Canadian interior, a pattern well documented in nitrogen-limited boreal soils (Peltzer et al., 2010; Blaško et al., 2015). Positive relationships with soil pH and SOC, and the negative association with biomass, further highlight how substrate fertility and stand productivity modulate nitrogen availability and isotopic fractionation pathways (Högberg, 1997; Robinson, 2001). These interlinked drivers generate the broad spatial gradients in the $\delta^{15}N$ isoscape, with higher values in warmer, humid eastern and coastal regions and lower values across the cooler, older, nutrient-poor cratonic interiors. However, high intra-site variance likely driven by microclimatic conditions affecting the nitrogen locally (Amundson et al., 2003; Schimel and Bennett, 2004; Grandpré et al., 2022). Although model performance was moderate ($R^2 = 0.32$), the regional gradients captured here still offer meaningful geolocation potential.

3.5.3 Sulfur isoscape

The $\delta^{34}S$ isoscape reveals the dominant influence of marine sulfate deposition and coastal proximity on sulfur cycling across the eastern Canadian boreal forest (Figure 3.7). As expected for terrestrial ecosystems and from previous work using part of this sample set(Dargent et al., 2026), $\delta^{34}S$ is influenced by maritime aerosols. Model performance was similarly strong between studies, although the present eastern Canada model showed slightly improved predictive performance relative to the continental-scale model of Dargent et al. (2026), likely reflecting the increased number of foliar training samples and a more regionally focused calibration extent of the present study. Similar to Dargent et al. (2026), $\delta^{34}S$ values increased strongly with indicators of sea-salt deposition and decreased with greater distance from the coast, reflecting the steep decrease in atmospheric deposition of

ocean-derived sulfates (Thode, 1991; Bataille et al., 2021). Within a few dozens of kilometers from the coast, wet sulfate deposition from sea spray is high and dominate sulfur cycle near the shoreline (Thode, 1991; Bataille et al., 2021) as reflected by the sharp 100 km band of high $\delta^{34}S$ along coastal areas. Further away from the coast, the majority of marine sulfur originate from dry deposition from sulfates or Dimethylsulfates (Chukhrov et al., 1980; Bataille et al., 2021) with $\delta^{34}S$ values showing a progressive decreasing gradient away from the coast as wet marine sulfur deposition decreases. Climatic variables such as minimum temperature, precipitation, evapotranspiration and soil moisture contributed additional structure, indicating that atmospheric transport efficiency and moisture regimes modulate the $\delta^{34}S$ patterns through change in soil redox conditions and the source of sulfur to ecosystems (Humphries, 2003; Schiff et al., 2005; Bataille et al., 2021). Other atmospheric deposition sources and forest disturbance including dust load, fossil sulfur emissions, forest height and fire history further shaped $\delta^{34}S$ variability, reflecting contribution of isotopically-distinct sources of sulfur (Mitchell and Lindberg, 1992; Mitchell et al., 1998; Tarrant and Richards, 2024). Together, these drivers generate the pronounced coastal-interior $\delta^{34}S$ gradient evident in the isoscape, with the highest values along the Atlantic coastal zone and progressively lower values moving inland across Québec, Labrador, and Ontario, and reaching the lowest $\delta^{34}S$ in the far continental interior. The high predictive performance of the model (R^2 = 0.90) further underscores the robustness of $\delta^{34}S$ as a geolocator, with minimal influence from intra-site variability. As a result, the $\delta^{34}S$ isoscape represents a strongest and most spatially coherent geolocator across the boreal forest (Dargent et al., 2025).

3.5.4 Hydrogen isotopes

The δ^2H isoscape generated for the eastern Canadian boreal forest highlights the central role of large-scale hydrological and climatic processes in structuring foliar hydrogen isotope composition. Predictor importance in the random forest model was led by climatic variables, particularly mean minimum temperature, vapor pressure and mean annual evapotranspiration followed by sea salt deposition and mean solar insolation, with some influence of forest fire history. These predictors align with known controls on foliar δ^2H across northern forest systems: precipitation influences δ^2H through rainout fractionation, temperature and vapor pressure regulate isotopic fractionation during evaporation and transpiration, and stand-level processes influence leaf water turnover and evaporative fractionation (Ingraham and Taylor, 1991; Bowen, 2008; Hobson and Wassenaar, 2019). The influence of sea-salt deposition likely reflects coastal precipitation sourcing, while mean solar insolation modulates canopy-scale evaporative demand (Rozanski et al., 1993; Hobson et al., 1999b; Cernusak et al., 2016). The influence of forest fire history suggests that canopy openness and changes in stand structure can modulate evaporative fractionation in leaf water, consistent with observations in other boreal and temperate ecosystems (Aron et al., 2019). The resulting δ^2H isoscape displays broad, continent-scale gradients (Figure 3.7). δ^2H values become progressively more depleted moving northward and westward, with high values along portions of the Atlantic and Great Lakes coasts and low values across interior Québec, Labrador, and northern Ontario. These patterns reflect regional to continental precipitation gradients superimposed on local evaporative effects. Previously developed δ^2H isoscapes were incorporated as predictors in our random forest model (Bowen et al., 2005), yet precipitation δ^2H was not retained among the strongest predictors. The broad spatial

structure of the foliar δ^2H isoscape resembles previously documented precipitation δ^2H gradients across eastern Canada (Bowen and Revenaugh, 2003; Bowen et al., 2005; Terzer et al., 2013). This suggests that foliar δ^2H is partially decoupled from precipitation inputs by local hydrological and physiological processes (Roden et al., 2000; Cernusak et al., 2016; Hobson and Wassenaar, 2019). Compared with interpolation-based precipitation isoscapes (Bowen and Revenaugh, 2003; Bowen et al., 2005), the random forest model captures additional nonlinear effects of forest structure, disturbance, and local climate on foliar δ^2H variability. As a result, the isoscape reflects an integrated ecological signal rather than a direct proxy of precipitation δ^2H. Intra-site variability was moderate, with a median within-site spread representing a measurable portion of the total dataset variance. Differences between young and old needles like carbon likely indicate that the chemical composition of the needle affect δ^2H values (Shu et al., 2008; Angove et al., 2025). Despite this local variability, δ^2H exhibited strong predictive performance (R^2 = 0.59), and the large-scale gradients evident in the isoscape provide substantial discriminatory structure across the region. These broad spatial patterns make δ^2H particularly informative for geolocation applications operating at regional to continental scales, where precipitation-driven isotopic gradients exceed within-site variance. However, at finer scales such as those relevant to short-range dispersal, local processes and microclimatic variation can limit the precision of δ^2H-based assignments, making δ^2H most effective when integrated with complementary isotope systems that capture finer spatial heterogeneity.

3.5.5 Strontium isotopes

The small within-site variance indicates that most of the variability in $^{87}Sr/^{86}Sr$ is expressed at broader spatial scales rather than within individual locations. As expected, slightly higher

intra-site variability occurred in regions with more complex geological substrates, but these deviations remained minor compared to the strong geographic structuring of the isoscape. These results confirm that bioavailable $^{87}Sr/^{86}Sr$ is relatively homogeneous at the site level and that the dominant controls of $^{87}Sr/^{86}Sr$ variations are local geological and atmospheric deposition conditions (Stewart, 1975; Bataille et al., 2020). The $^{87}Sr/^{86}Sr$ isoscape generated in this study is similar to that generated by Le Corre et al. (2025) using part of this dataset, despite differences in model structure and spatial extent. All approaches identified strong radiogenic compositions across the Canadian shield and lower $^{87}Sr/^{86}Sr$ values in younger sedimentary and coastal regions. Spatial uncertainty patterns were broadly consistent among models, with higher prediction errors occurring in geologically heterogenous regions and lower uncertainties in more uniform sedimentary landscapes. Despite these differences the overall concordance between these independent modeling approaches highlights the dominant influence of geological and atmospheric processes on bioavailable strontium, consistent with long-established principles in isotope geochemistry and previous observations of plant-derived $^{87}Sr/^{86}Sr$ variability. As expected, $^{87}Sr/^{86}Sr$ ratios primarily reflect the age and composition of underlying bedrock, as indicated by the high predictive importance of mean geological age. The positive association between $^{87}Sr/^{86}Sr$ and geological age captured by our random forest model mirrors a well-known mechanism whereby older rocks accumulate more radiogenic ^{87}Sr through the decay of ^{87}Rb relative to younger substrates (Bataille and Bowen, 2012). The model also captured the strong dampening effect of marine aerosol inputs: $^{87}Sr/^{86}Sr$ values trend toward the global marine composition of 0.7092 in regions experiencing high sea-salt deposition, which can override local geological signals in coastal or high-precipitation environments (Capo and DePaolo,

1992; Erban Kochergina et al., 2021). Temperature emerged as an unexpectedly influential predictor in the Canadian context, likely due to its strong correlation with geological age. In eastern Canada, the oldest cratonic rocks are concentrated in northern Quebec, with a southward transition toward younger marine sediments, producing a temperature-age gradient that mimics that of $^{87}Sr/^{86}Sr$ variability (Shilts et al., 1987; Thériault and Beauséjour, 2012). The resulting isoscape reveals coherent regional patterns shaped by the interplay of bedrock age and marine influence. Radiogenic values dominate the older felsic terrains of northern cratonic Canada, whereas younger sedimentary landscapes along the Saint Lawrence River, the Gaspé region, and southern Ontario show markedly lower $^{87}Sr/^{86}Sr$ ratios. Model performance was strong (R^2 = 0.60; RMSE = 0.0045), comparable to recent machine-learning strontium isoscapes developed across continental systems. Nevertheless, Canada's geological complexity, particularly the presence of extremely old terrains with heterogeneous lithologies (Bataille et al., 2020), generates a wide range of $^{87}Sr/^{86}Sr$ ratios, especially across the Canadian craton (Shilts et al., 1987). The model's ability to reproduce these fine-scale geological patterns was constrained by the spatial resolution of the available geological and surficial deposit layers. When integrated with other isotopes, strontium isotopes remain among the most powerful tools for constraining geographic origin due to its uniquely heterogeneous and discrete patterns that are independent from other isotopes. Thus, despite predictable limitations in accuracy due to the limited geological maps of Canada, the developed $^{87}Sr/^{86}Sr$ isoscape represents a robust and highly informative component of a multi-isotope geolocation framework for ecological, archaeological, and forensic applications.

3.5.6 Isotope geolocation potential

The separability-based dominance maps reveal that isotope geolocation potential across the eastern Canadian boreal forest is strongly scale dependent and governed by the interaction between spatial structure, predictive uncertainty, and landscape heterogeneity. No single isotope dominates uniformly across space or scale. Instead, different isotopes emerge as the most informative geolocators depending on the spatial scale at which geographic origin is evaluated and the environmental context of each region. These results emphasize that isotope selection for geolocation cannot be generalized across regions or movement scales but must be explicitly matched to organismal dispersal distances and local environmental structure.

At the 10 km scale, isotope dominance is primarily controlled by the presence or absence of sharp local spatial contrasts. Strontium isotopes dominate many regions at this scale because even modest lithological heterogeneity can generate abrupt changes in bioavailable $^{87}Sr/^{86}Sr$ over short distances. This sensitivity to bedrock variation allows strontium to provide high separability where geological units are complex or spatially heterogeneous such as across Newfoundland and most of the Canadian craton. However, within domains characterized by more uniform bedrock composition such as carbonate platforms along the Gaspesie region or large relatively uniform geology of unit on the craton, predicted $^{87}Sr/^{86}Sr$ is less variable over tens of kilometers, reducing its local discriminatory power. Sulfur isotopes remain frequently dominant at the 10 km scale across much of the study area, including the continental interior where $\delta^{34}S$ values vary only weakly. This dominance reflects the exceptionally low predictive uncertainty of the sulfur isoscape relative to other isotope systems (Figure 3.4A). Separability is defined as the ratio of spatial variance to uncertainty,

sulfur tends to retain moderate separability even when spatial gradients are shallow, particularly when other isotopes exhibit similarly low spatial contrast but higher uncertainty. As a result, $\delta^{34}S$ often emerges as the dominant isotope by default in regions lacking strong fine-scale structure in other isotope systems. Carbon isotopes dominate within most of western Ontario, where all other isotopes (strontium, sulfur, and hydrogen) exhibit minimal spatial variability at short distances. In these settings, even weak but high-resolution spatial structure in $\delta^{13}C$ associated with variation in forest properties can produce higher relative separability. However, this separability might be variable in time as forest structure evolves which complicates the application of carbon isotopes for geolocation. However, despite their high predictive uncertainty, carbon and to a lesser extent nitrogen isotopes can occasionally represent the most informative isotopes where ecological gradients dominate, and geochemical gradients are absent. Hydrogen isotopes rarely emerge as dominant at the 10 km scale because $\delta^{2}H$ values are spatially smooth at short distances across most of the boreal forest. The resulting lack of local variance strongly limits separability, regardless of the predictive strength of the $\delta^{2}H$ isoscape.

At the 100 km scale, dominance patterns shift toward isotopes structured by broad climatic and atmospheric gradients. Sulfur isotopes emerge as the dominant geolocator across extensive coastal regions, reflecting the steep coast-to-inland gradients in $\delta^{34}S$ driven by marine sulfate and sea-salt deposition combined with low predictive uncertainty. At this scale, the spatial variance of sulfur increases markedly, while uncertainty remains low, yielding high separability across much of the Atlantic coastal zone and the Gulf of St. Lawrence. Inland of coastal regions, strontium isotopes remain dominant across large portions of interior Québec, Labrador, and Ontario. At regional scales, large lithological

transitions between terranes or sedimentary basins become prominent drivers of spatial variance in $^{87}Sr/^{86}Sr$, allowing strontium to outperform other isotopes. This pattern highlights the multiscale nature of geological controls on strontium isotopes, which have been highlighted before (Bataille et al., 2018) and can dominate both fine and coarse spatial scales depending on geological context. Hydrogen isotopes dominate only in restricted interior transition zones at the 100 km scale. These areas correspond to regions where large-scale climatic gradients in precipitation δ^2H are steepest such as around the Great Lakes. Elsewhere in the relatively flat and climatically homogeneous interior of Canada, δ^2H values remain too spatially uniform relative even at 100 km scales, limiting its discriminatory power relative to other isotopes. Carbon and nitrogen isotopes continue to dominate primarily in isolated and poorly-sampled regions of the continental interior. Their persistence reflects a lack of strong contrast in other isotopes rather than intrinsically high geolocation power but, despite their high uncertainty, they can dominate in regions with strong gradients in forest characteristics or edaphic.

3.5.7 Implications for isotope-based geolocation

These results demonstrate that isotope geolocation potential is inherently scale dependent. Isotopes that perform well at fine spatial scales may lose discriminatory power at broader scales, and vice versa. Strontium isotopes are particularly effective for resolving fine-scale heterogeneity where geological variability exists, sulfur isotopes dominate regional-scale assignments in coastal and marine-influenced regions, and hydrogen isotopes contribute meaningfully only where large-scale climatic gradients are pronounced. Carbon and nitrogen isotopes act as complementary geolocators that can provide residual discriminatory power in ecologically structured landscapes when other isotopes are spatially invariant. This scale

dependence underscores the importance of explicitly considering movement ecology when designing isotope geolocation studies. Selecting isotopes without regard to dispersal distance or regional context risks prioritizing isotopes with low effective geolocation power for the question at hand. The separability-based framework introduced here provides a practical means of identifying which isotope systems are most informative at a given location and scale, thereby enabling more efficient allocation of analytical effort and more robust inference of geographic origin across heterogeneous boreal landscapes.

3.5.8 Limitations

Several limitations of the separability-based framework should be considered when interpreting isotope dominance patterns. First, predictive uncertainty within each spatial window is summarized using the mean of standard deviation within that region, which may not fully represent the underlying uncertainty structure for isotope systems with strongly non-normal or spatially clustered uncertainty. This issue is particularly relevant for strontium isotopes, where sharp lithological boundaries, mixed substrates, and uneven sampling density can produce skewed or bimodal uncertainty distributions (Bataille et al., 2018). In such cases, averaging may downplay localized zones of high uncertainty or over-weight well-constrained areas. A second important limitation is that the isoscapes generated represent plant-level baseline isotope surfaces and do not explicitly account for uncertainty associated with trophic and tissue-specific isotope transmission in the focal organisms (Boecklen et al., 2011; Hobson, 2023). While foliar baselines are a logical and widely used starting point for terrestrial isoscape development, isotope values measured in consumer tissues reflect additional sources of variance introduced by trophic discrimination,

metabolic routing, tissue turnover, and physiological state (McCutchan et al., 2003; Spence and Rosenheim, 2005; Doi et al., 2007). Numerous studies have demonstrated that these processes can introduce substantial noise and bias relative to plant baselines, effectively increasing relative geolocation uncertainty (Hobson, 2023; Stephens et al., 2023). Strontium and sulfur isotopes are generally transmitted with high fidelity from plants to higher trophic levels, retaining strong correspondence to baseline spatial patterns (Flockhart et al., 2015; Bataille et al., 2021), whereas hydrogen, carbon, and nitrogen isotopes often exhibit additional metabolic and physiological modification that can dampen spatial signal or inflate variance(McCutchan et al., 2003; Doi et al., 2007; Magozzi et al., 2020). Because the separability framework relies on foliar isoscapes alone, it implicitly assumes equal and error-free transmission across isotopes. In practice, incorporating tissue-specific calibration functions and transmission uncertainty would likely shift isotope rankings and reduce effective geolocation potential for isotopes subject to strong metabolic noise (Wunder and Norris, 2008; Trueman et al., 2017). Extending the framework to consumer-specific isoscapes that propagate uncertainty from baseline through trophic transfer represents a necessary next step for accurately estimating realized geolocation performance in applied ecological studies. Third, isotope dominance in sparsely sampled regions should be interpreted cautiously. In portions of the continental interior, carbon or nitrogen isotopes may emerge as dominant not because they provide strong absolute geolocation power, but because other isotopes exhibit minimal spatial variance at the evaluated scale. In these situations, dominance reflects relative separability rather than high precision. Finally, the framework evaluates isotopes independently and does not account for their collinearity(Hobson et al., 2010) potentially inflating geolocation potential (Ma et al., 2020;

Courtiol, 2022). Despite these limitations, the approach remains intentionally simple, transparent, and scale-explicit, offering robust first-order guidance for isotope selection and study design while providing a clear foundation for future methodological refinement.

3.6 Conclusion

This study provides the first comprehensive, multi-isotope assessment of geolocation potential across the eastern Canadian boreal forest by developing foliar carbon, nitrogen, hydrogen, sulfur, and strontium isoscapes. By integrating extensive field sampling with machine-learning isoscape models, we show that isotopes differ markedly in their ability to resolve geographic origin across this heterogeneous landscape and that this ability is strongly scale dependent. Sulfur isotopes offer exceptional geolocation potential in coastal and marine-influenced regions due to steep sea-salt-driven gradients combined with low predictive uncertainty, while strontium isotopes dominate inland where sharp lithological transitions generate strong spatial contrast. Hydrogen isotopes become informative only at broader spatial scales associated with large-scale climatic gradients, whereas carbon and nitrogen isotopes provide context-dependent value in regions structured by moisture availability, forest age, or edaphic conditions, particularly where other isotope systems exhibit limited spatial variation. Our separability-based framework provides a simple, transparent, and scale-explicit tool for prioritizing isotopes when analytical resources and budgets are limited. By quantifying the balance between spatial variance and predictive uncertainty at biologically relevant movement scales, the approach enables researchers and managers to estimate *a priori* which isotope systems are most likely to yield the greatest geolocation potential for a given organism and dispersal distance. Important limitations remain. The framework evaluates isotope systems independently and therefore cannot quantify redundancy or complementarity among isotope combinations, nor does it directly account for tissue-specific calibration or trophic transfer between foliar baselines and consumers. Despite these constraints, our results represent an important first step toward

estimating isotope geolocation potential *a priori* and provide practical guidance for designing future isotope-based studies of dispersal, migratory connectivity, invasion dynamics, and conservation management across the eastern Canadian boreal forest.

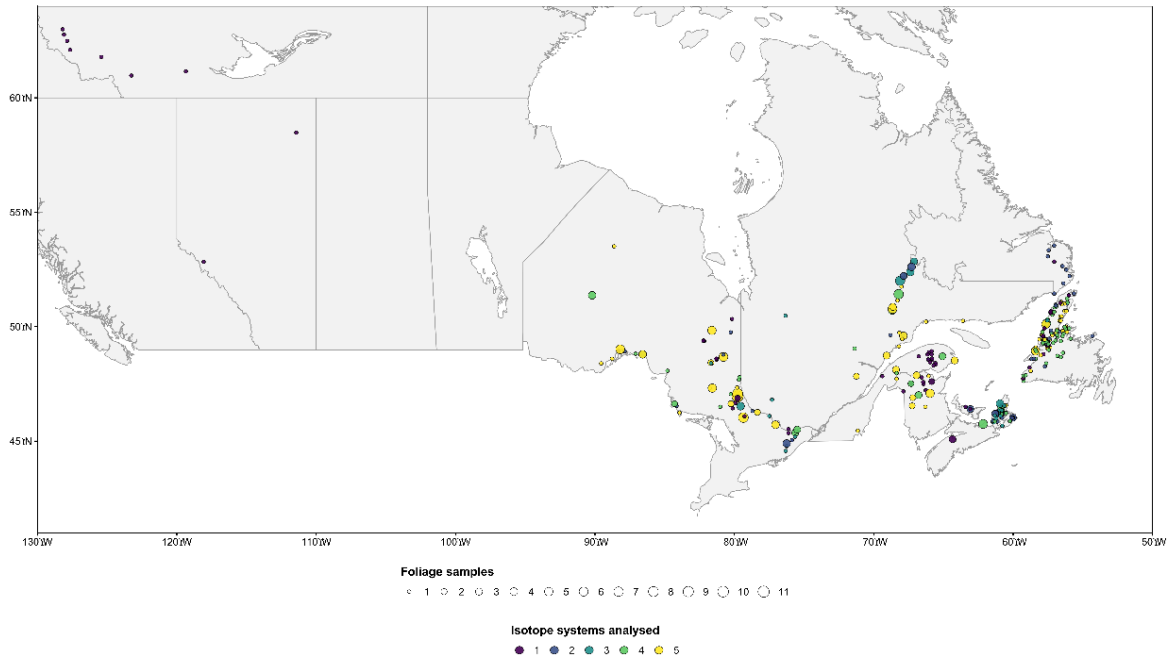

Figure 3.1 - Sampling sites across the eastern Canadian boreal forest. Distribution of sampled individuals across 339 sites in the eastern Canadian forest. Numbers correspond to site identifiers listed in Table 1. The map highlights the provinces where sampling took place, with grey lines indicating provincial boundaries. Symbols represent sampled sites, and the colour represent the number of isotope systems that was analyzed for each. Symbol size is scaled according to the number of individuals sampled per site (see legend). Provincial boundaries were obtained from Natural Earth (2023).

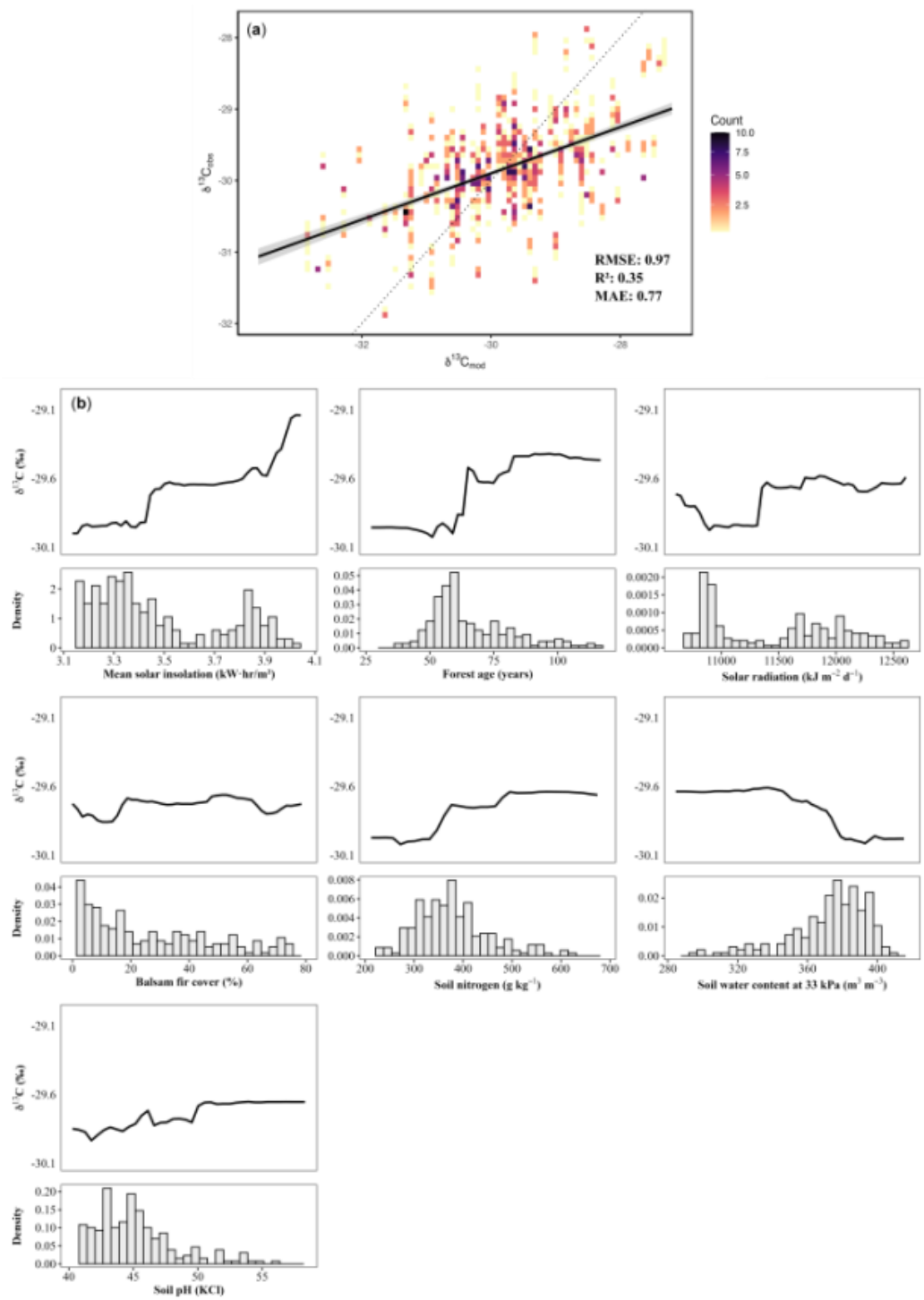

Figure 3.2 - Random Forest regression performance, partial dependence plots (PDPs) and predictions for $\delta^{13}C$ in needles. **(a)** Relationship between observed and predicted $\delta^{13}C$ values, with a fitted regression line (black) and the 1:1 reference line (dotted). **(b)** PDPs of predictors on predicted $\delta^{13}C$. Solid black lines represent the average predicted response when varying each predictor independently. Histograms below each plot indicate the

distribution of observed values for the corresponding variable, providing context on sampling density.

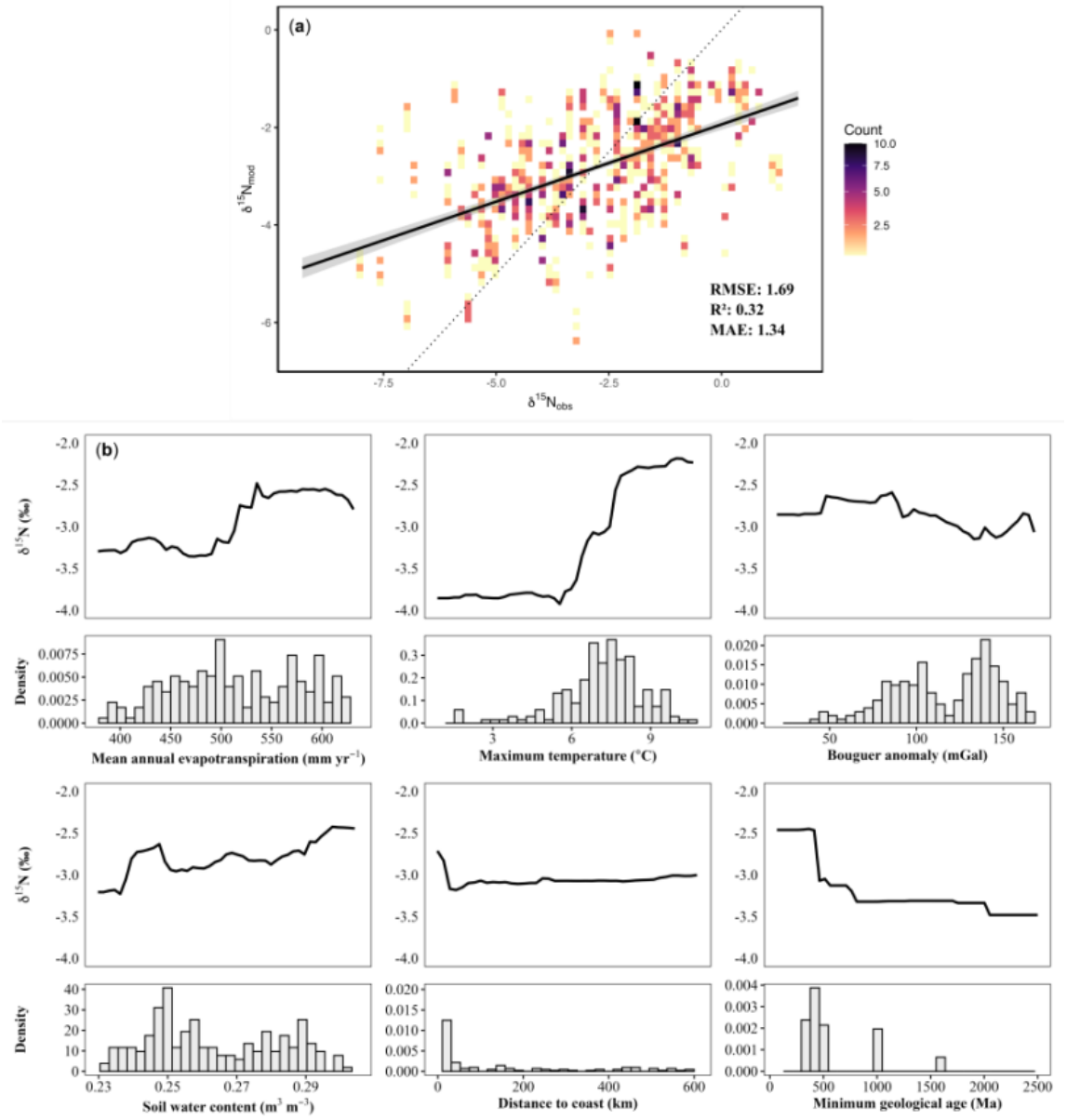

Figure 3.3 - Random Forest regression performance, partial dependence plots (PDPs) and predictions for δ^{15}N in needles. **(a)** Relationship between observed and predicted δ^{15}N values, with a fitted regression line (black) and the 1:1 reference line (dotted). **(b)** PDPs of predictors on predicted δ^{15}N. Solid black lines represent the average predicted response when varying each predictor independently. Histograms below each plot indicate the distribution of observed values for the corresponding variable, providing context on sampling density.

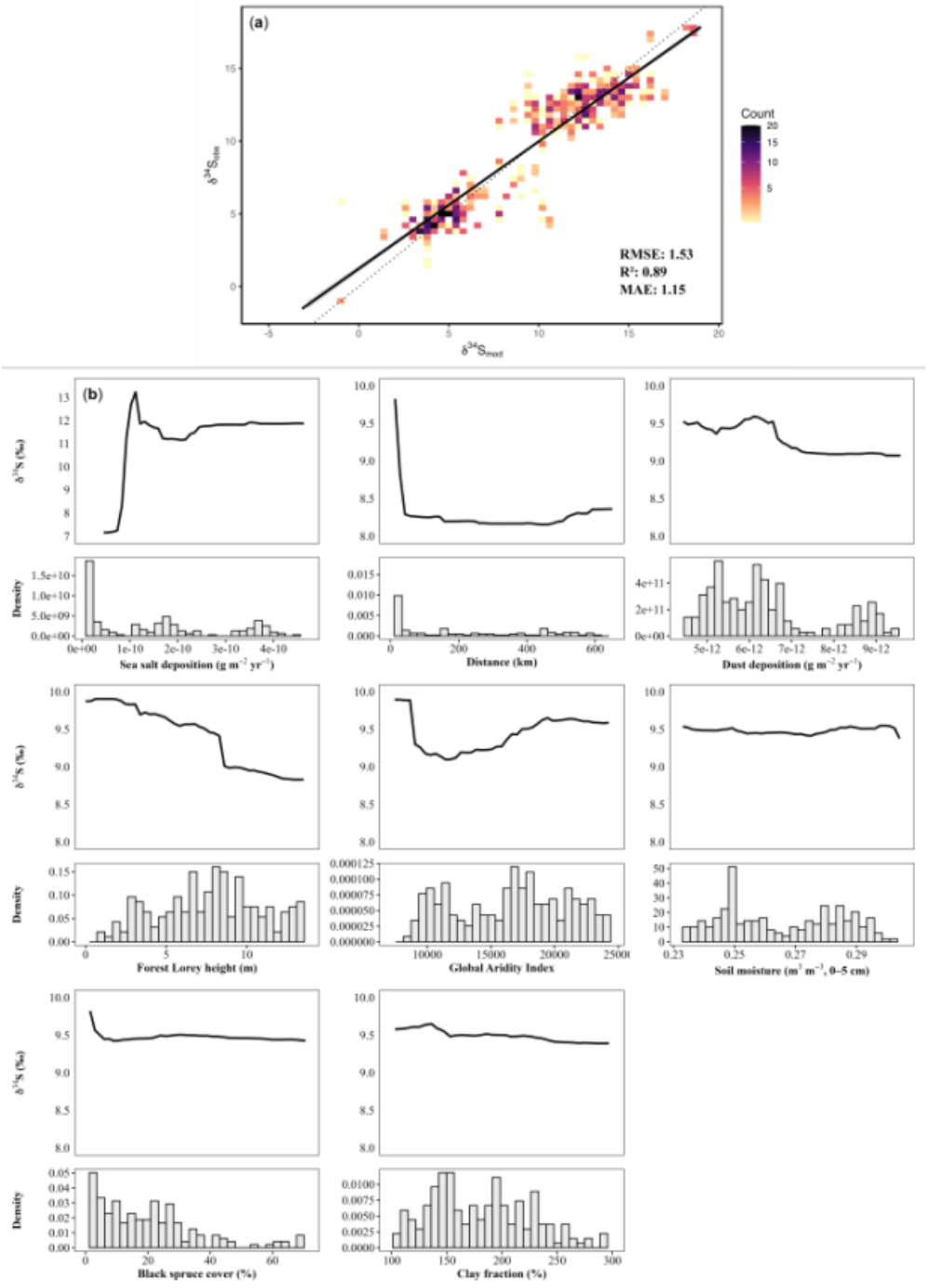

Figure 3.4 - Random Forest regression performance, partial dependence plots (PDPs) and predictions for $\delta^{34}S$ in needles. **(a)** Relationship between observed and predicted $\delta^{34}S$ values, with a fitted regression line (black) and the 1:1 reference line (dotted). **(b)** PDPs of predictors on predicted $\delta^{34}S$. Solid black lines represent the average predicted response when varying each predictor independently. Histograms below each plot indicate the distribution of observed values for the corresponding variable, providing context on sampling density.

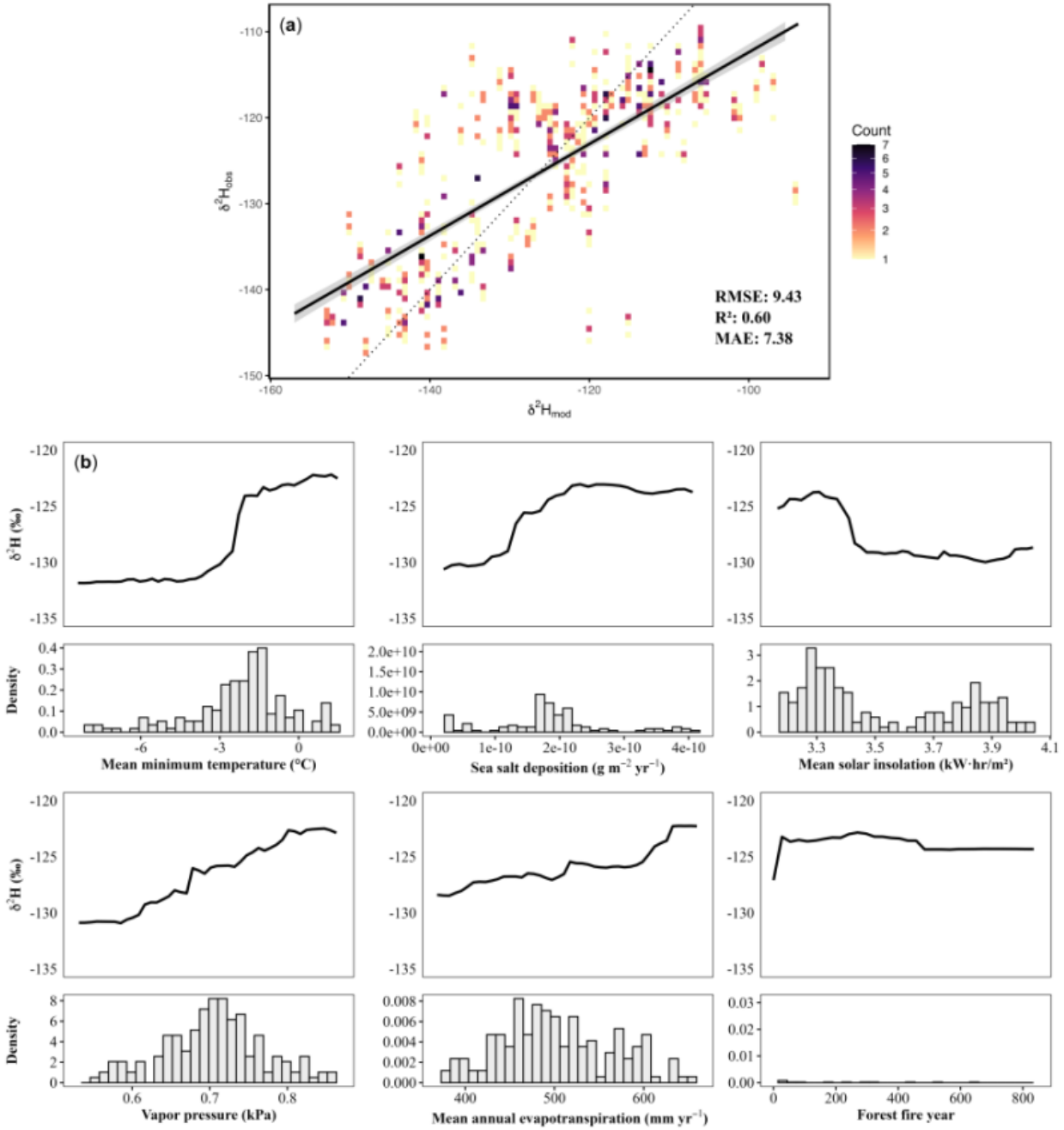

Figure 3.5 - Random Forest regression performance, partial dependence plots (PDPs) and predictions for δ^2H in needles. **(a)** Relationship between observed and predicted δ^2H values, with a fitted regression line (black) and the 1:1 reference line (dotted). **(b)** PDPs of predictors on predicted δ^2H. Solid black lines represent the average predicted response when varying each predictor independently. Histograms below each plot indicate the distribution of observed values for the corresponding variable, providing context on sampling density.

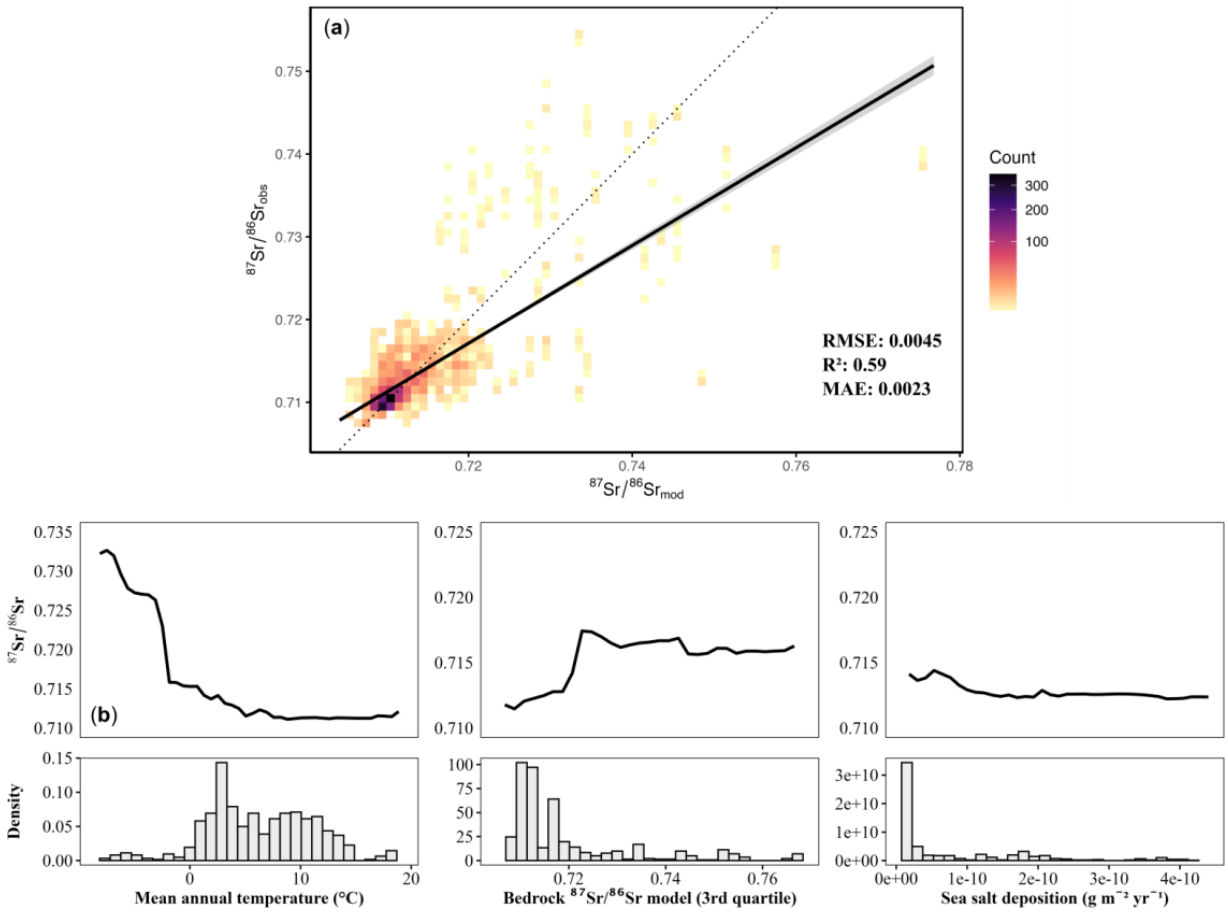

Figure 3.6 - Random Forest regression performance, partial dependence plots (PDPs) and predictions for $^{87}Sr/^{86}Sr$ in needles. **(a)** Relationship between observed and predicted $^{87}Sr/^{86}Sr$ ratios, with a fitted regression line (black) and the 1:1 reference line (dotted). **(b)** PDPs of predictors on predicted $^{87}Sr/^{86}Sr$. Solid black lines represent the average predicted response when varying each predictor independently. Histograms below each plot indicate the distribution of observed values for the corresponding variable, providing context on sampling density.

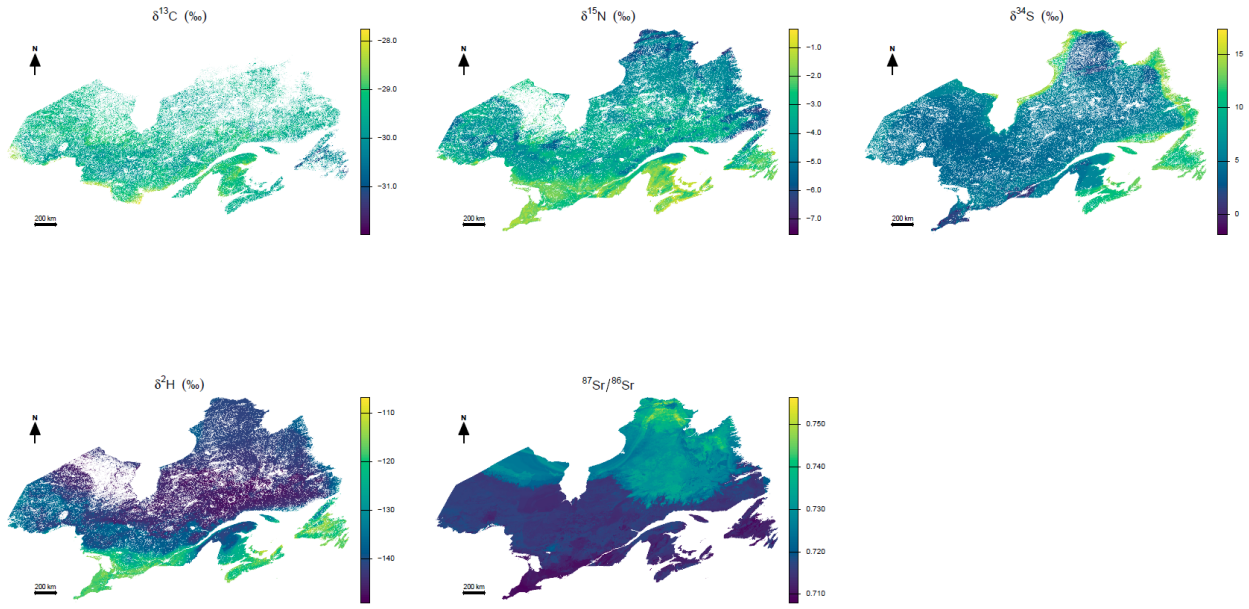

Figure 3.7 - Predicted mean foliar isoscapes for carbon ($\delta^{13}C$), nitrogen ($\delta^{15}N$), sulfur ($\delta^{34}S$), hydrogen ($\delta^{2}H$), and strontium ($^{87}Sr/^{86}Sr$) across eastern Canada.

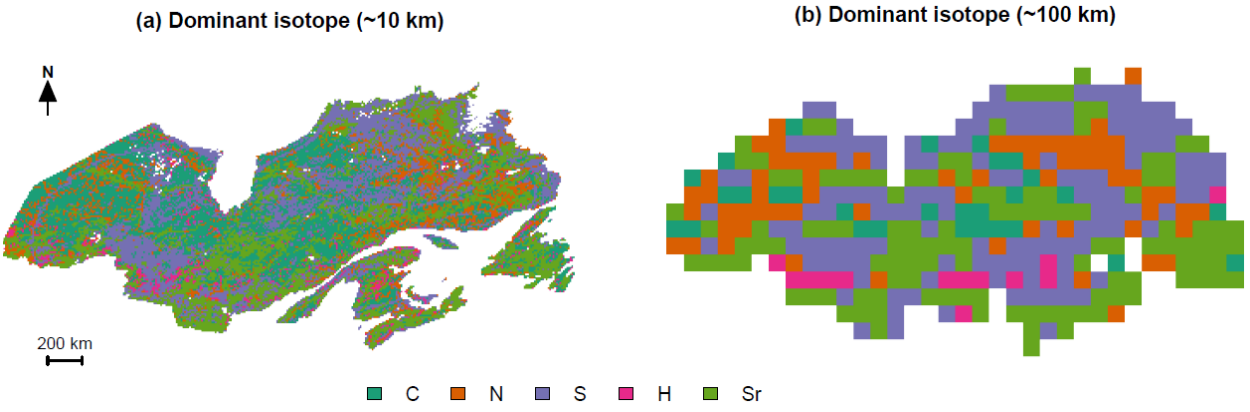

Figure 3.8 - Scale-dependent dominance of isotope geolocation potential across eastern Canada. Maps show the isotopes with the highest relative separability at each location, ranking the isotope expected to provide the strongest geolocation power at a given spatial scale. Panel (a) displays dominance evaluated at a ~10 km scale, while panel (b) shows dominance at a ~100 km scale.

CHAPTER 4: CONCLUSION

4.1 Summary of Main Findings

These findings establish the biological and environmental framework that supports the future application of stable isotope geolocation to investigate the natal origins and migratory connectivity of eastern spruce budworm (SBW) populations across Canada. By quantifying the trophic transmission of five isotope systems from host foliage into SBW tissues and developing high-resolution foliar isoscapes across eastern Canada, this work identifies which systems behave as reliable geolocators and provides the baselines against which tissue compositions can be compared.

Carbon foliar isoscapes exhibited weak spatial structure across eastern Canada, likely reflecting the influence of local physiological and microclimatic controls on δ^{13}C values, and the trophic transmission of δ^{13}C similarly indicated limited geographic discrimination relative to other systems. This is consistent with previous work showing that δ^{13}C variability in forest ecosystems is governed largely by water availability, canopy structure, photosynthetic discrimination, and metabolic routing rather than by large-scale spatial gradients (Farquhar et al., 1989; Heaton, 1999; Diefendorf et al., 2010). δ^{13}C is therefore unlikely to serve as a useful geolocator for SBW, although the patterns recovered may still provide complementary ecological information for other species and within multi-isotope frameworks.

Nitrogen isotopes exhibited strong trophic relationships and pronounced site-level clustering, indicating that environmentally structured δ^{15}N variation was effectively transferred from host foliage into SBW tissues. Spatial variability in the foliar isoscapes likely

reflected differences in nitrogen cycling, soil processes, climate, and ecosystem productivity, consistent with established controls on terrestrial δ^{15}N distributions (Amundson et al., 2003; Craine et al., 2009). The relatively strong geographic structure of δ^{15}N highlights its potential utility for specialist feeders such as SBW, whose simple diet avoids the complex mixing of isotopically distinct sources.

Hydrogen isotopes in foliage showed strong spatial structure but almost no trophic relationship with SBW tissues, owing to very large within-site variability. These results underline several constraints on using δ^{2}H as a regional geolocator: it varies primarily at large spatial scales, which complicates its use at regional scales; intra-site variability in plants and insects is high through a combination of analytical limitation and genuine biological noise; and analytical uncertainty remains large relative to the regional variance. Nevertheless, the resulting foliar isoscapes retained the broad climatic and hydrological gradients expected from established precipitation-isotope relationships across North America (Bowen and Revenaugh, 2003; Bowen et al., 2005), echoing previous studies in which the strong continental-scale gradients of δ^{2}H are offset by physiological complexity and uncertainty in trophic transfer (Hobson et al., 1999b; Vander Zanden et al., 2016).

Sulfur isotopes displayed some of the strongest regional structure of all systems, with pronounced coastal-to-inland gradients reflecting marine sulfate deposition and atmospheric transport. Strong trophic relationships and site-level clustering further demonstrated that δ^{34}S compositions were effectively retained within SBW tissues, making sulfur the most reliable geolocator for SBW at the regional scale and consistent with its

established power as a tracer of geographic origin in coastal and maritime-influenced environments (Bataille et al., 2021; Dargent et al., 2026).

Strontium isotopes exhibited strong regional heterogeneity associated primarily with underlying lithology and surficial geology across eastern Canada. The foliar isoscapes showed pronounced geographic structure and strong site-level discrimination, supporting the utility of $^{87}Sr/^{86}Sr$ as a powerful geolocation tracer. However, the low strontium concentrations in SBW tissues required sample pooling in some cases, an important methodological consideration for future isotope applications in small-bodied insects.

These trophic transmission relationships and high-resolution foliar isoscapes constitute an integrated multi-isotope framework for reconstructing migratory connectivity in SBW. By linking environmentally structured isotopic variation to species-specific trophic transfer functions for $\delta^{13}C$, $\delta^{15}N$, $\delta^{2}H$, $\delta^{34}S$, and $^{87}Sr/^{86}Sr$, this work provides the prerequisites for a robust geographic assignment framework capable of identifying source regions, reconstructing connectivity, and improving understanding of outbreak dynamics in this eruptive forest insect. Long-distance migration is recognized as a key process governing the expansion and persistence of SBW outbreaks, yet the natal origins of immigrants have remained difficult to resolve with conventional monitoring (Johns et al., 2019) the framework developed here is the necessary first step toward closing that gap.

Beyond SBW, these high-resolution multi-isotope isoscapes represent one of the first geographically explicit environmental baseline datasets for the eastern Canadian boreal forest. Foliar isotope compositions integrate atmospheric, climatic, geological, and biological processes across landscapes. These isoscape provide a long-term resource for investigating

ecological connectivity and ecosystem processes throughout one of the world's largest biomes (Bowen et al., 2005; Hobson, 2023). Once calibrated, the same isoscapes can support geolocation of migratory birds, mammals, and other wildlife, as well as food and timber provenance, wildlife forensics, archaeological and paleoecological reconstruction, nutrient and contaminant tracing, and natural resource management. As climate change, habitat alteration, and shifting disturbance regimes continue to reshape species distributions and ecological connectivity, these baselines offer a scalable foundation for investigating organismal movement and informing conservation and management across the eastern Canadian boreal forest.

4.2 Future Directions and Recommendations

Although this thesis establishes the ecological and methodological foundation necessary for isotope geolocation in eastern spruce budworm, several areas warrant further work to improve its precision, efficiency, and operational implementation. Expanding sampling across underrepresented regions of eastern Canada would improve spatial coverage and reduce uncertainty within the foliar isoscapes, particularly in areas of strong environmental heterogeneity. Future work should also evaluate temporal variability in foliar and SBW isotopic compositions, as interannual variation in climate, atmospheric circulation, and ecosystem processes may influence baselines and geolocation reliability across outbreak cycles.

Further research is needed to refine the trophic relationships between environmental baselines and SBW tissues. Although trophic transmission was observed across all isotope systems, its strength and consistency varied substantially, indicating that additional

controlled and field-based studies of physiological routing, tissue-specific incorporation, and isotopic turnover would improve understanding of isotope dynamics in SBW. Extending these analyses across additional life stages, host species, and environmental conditions would further strengthen the application of isotope geolocation in this system. For $^{87}Sr/^{86}Sr$ in particular, future studies on small-bodied insects should consider pooling individuals where strontium concentrations are low, to obtain sufficient mass for precise isotopic measurement.

A promising direction for advancing isotope geolocation is the development of statistical tools that optimize sampling design and isotope selection. Such tools could identify regions where additional sampling would most effectively reduce assignment uncertainty, quantify the relative contribution of each isotope system to geolocation accuracy, and guide the selection of the most informative geolocators for a given region, maximizing analytical efficiency while supporting the continued refinement of isotope geolocation across eastern Canada.

Finally, an important next step is the implementation of isotope geolocation as an operational tool for SBW monitoring and management. Integrating it with complementary approaches, atmospheric trajectory modelling, radar observation, ecological niche modelling, and automated trap networks, would improve the reconstruction of migratory pathways and the identification of source regions. Collaboration with forest managers and other stakeholders could enable annual geolocation of immigrant populations, allowing interannual variation in migration to be reconstructed and improving understanding of outbreak initiation, spread, and connectivity. Such applications have the potential to strengthen early-warning systems,

improve outbreak forecasting, help identify emerging hotspots, and support the Early Intervention Strategy through targeted, timely, and cost-effective control measures.

4.3 Use of Artificial Intelligence and Funding

Artificial intelligence tools were used solely for editing and research support during the preparation of this thesis. Their use was limited to improving language, clarity, scientific phrasing, and to identify relevant literature. All study design, data collection, data processing, statistical analyses, scientific interpretation, and conclusions were performed, evaluated, and approved by the author. The author accepts full responsibility for the accuracy, integrity, and content of the work presented in this thesis.

Funding for this research was provided by the Early Intervention Strategy of the Canadian Forest Service, Natural Resources Canada.

REFERENCES

Amundson, R., Austin, A. T., Schuur, E. a. G., Yoo, K., Matzek, V., Kendall, C., et al. (2003). Global patterns of the isotopic composition of soil and plant nitrogen. *Global Biogeochemical Cycles* 17. doi: 10.1029/2002GB001903

Anderson, D. P., and Sturtevant, B. R. (2011). Pattern analysis of eastern spruce budworm Choristoneura fumiferana dispersal. *Ecography* 34, 488–497. doi: 10.1111/j.1600-0587.2010.06326.x

Angove, C., Wiesenberg, G. L. B., Lehmann, M. M., Saurer, M., Tang, Y., Sahlstedt, E., et al. (2025). Time-integrated δ2H in n-alkanes and carbohydrates from boreal needles reveal intra-annual physiological and environmental signals. *New Phytologist* 246, 498–514. doi: 10.1111/nph.20448

Aron, P. G., Poulsen, C. J., Fiorella, R. P., and Matheny, A. M. (2019). Stable Water Isotopes Reveal Effects of Intermediate Disturbance and Canopy Structure on Forest Water Cycling. *Journal of Geophysical Research: Biogeosciences* 124, 2958–2975. doi: 10.1029/2019JG005118

Balmino, G., Vales, N., Bonvalot, S., and Briais, A. (2012). Spherical harmonic modelling to ultra-high degree of Bouguer and isostatic anomalies. *J Geod* 86, 499–520. doi: 10.1007/s00190-011-0533-4

Bataille, C. P., and Bowen, G. J. (2012). Mapping 87Sr/ 86Sr variations in bedrock and water for large scale provenance studies. *Chemical Geology* 304–305, 39–52. doi: 10.1016/j.chemgeo.2012.01.028

Bataille, C. P., Crowley, B. E., Wooller, M. J., and Bowen, G. J. (2020). Advances in global bioavailable strontium isoscapes. *Palaeogeography, Palaeoclimatology, Palaeoecology* 555, 109849. doi: 10.1016/j.palaeo.2020.109849

Bataille, C. P., Holstein, I. C. C. von, Laffoon, J. E., Willmes, M., Liu, X.-M., and Davies, G. R. (2018). A bioavailable strontium isoscape for Western Europe: A machine learning approach. *PLOS ONE* 13, e0197386. doi: 10.1371/journal.pone.0197386

Bataille, C. P., Jaouen, K., Milano, S., Trost, M., Steinbrenner, S., Crubézy, É., et al. (2021). Triple sulfur-oxygen-strontium isotopes probabilistic geographic assignment of archaeological remains using a novel sulfur isoscape of western Europe. *PLoS ONE* 16. doi: 10.1371/journal.pone.0250383

Bataille, C. P., and Skierszkan, E. K. (2025). Sulfur cycling in thawing permafrost landscapes. *Nat. Geosci.* 18, 936–937. doi: 10.1038/s41561-025-01804-2

Bates, D., Mächler, M., Bolker, B., and Walker, S. (2015). Fitting Linear Mixed-Effects Models Using lme4. *Journal of Statistical Software* 67, 1–48. doi: 10.18637/jss.v067.i01

Bauce, É., Carisey, N., Dupont, A., and van Frankenhuyzen, K. (2004). Bacillus thuringiensis subsp. kurstaki Aerial Spray Prescriptions for Balsam Fir Stand Protection Against Spruce Budworm (Lepidoptera: Tortricidae). *J Econ Entomol* 97, 1624–1634. doi: 10.1603/0022-0493-97.5.1624

Blaško, R., Holm Bach, L., Yarwood, S. A., Trumbore, S. E., Högberg, P., and Högberg, M. N. (2015). Shifts in soil microbial community structure, nitrogen cycling and the concomitant declining N availability in ageing primary boreal forest ecosystems. *Soil Biology and Biochemistry* 91, 200–211. doi: 10.1016/j.soilbio.2015.08.041

Boecklen, W. J., Yarnes, C. T., Cook, B. A., and James, A. C. (2011). On the Use of Stable Isotopes in Trophic Ecology. *Annual Review of Ecology, Evolution, and Systematics* 42, 411–440. doi: 10.1146/annurev-ecolsys-102209-144726

Börker, J., Hartmann, J., Amann, T., and Romero-Mujalli, G. (2018). Global Unconsolidated Sediments Map Database v1.0 (shapefile and gridded to 0.5° spatial resolution). *Supplement to: Börker, J et al. (2018): Terrestrial Sediments of the Earth: Development of a Global Unconsolidated Sediments Map Database (GUM). Geochemistry, Geophysics, Geosystems, 19(4), 997-1024, https://doi.org/10.1002/2017GC007273*. doi: 10.1594/PANGAEA.884822

Boulanger, Y., Fabry, F., Kilambi, A., Pureswaran, D. S., Sturtevant, B. R., and Saint-Amant, R. (2017). The use of weather surveillance radar and high-resolution three dimensional weather data to monitor a spruce budworm mass exodus flight. *Agricultural and Forest Meteorology* 234–235, 127–135. doi: 10.1016/j.agrformet.2016.12.018

Bowen, G. J. (2008). Spatial analysis of the intra-annual variation of precipitation isotope ratios and its climatological corollaries. *Journal of Geophysical Research: Atmospheres* 113. doi: 10.1029/2007JD009295

Bowen, G. J. (2010). Isoscapes: Spatial Pattern in Isotopic Biogeochemistry. *Annual Review of Earth and Planetary Sciences* 38, 161–187. doi: 10.1146/annurev-earth-040809-152429

Bowen, G. J., and Revenaugh, J. (2003). Interpolating the isotopic composition of modern meteoric precipitation. *Water Resources Research* 39. doi: 10.1029/2003WR002086

Bowen, G. J., Wassenaar, L. I., and Hobson, K. A. (2005). Global application of stable hydrogen and oxygen isotopes to wildlife forensics. *Oecologia* 143, 337–348. doi: 10.1007/s00442-004-1813-y

Bowen, G. J., and West, J. B. (2019). "Chapter 03 - Isoscapes for Terrestrial Migration Research," in *Tracking Animal Migration with Stable Isotopes*, (Elsevier), 53–84. doi: 10.1016/B978-0-12-814723-8.00003-9

Brahney, J., Mahowald, N., Ward, D. S., Ballantyne, A. P., and Neff, J. C. (2015). Is atmospheric phosphorus pollution altering global alpine Lake stoichiometry? *Global Biogeochemical Cycles* 29, 1369–1383. doi: 10.1002/2015GB005137

Brandt, J. P., Flannigan, M. D., Maynard, D. G., Thompson, I. D., and Volney, W. J. A. (2013). An introduction to Canada's boreal zone: ecosystem processes, health, sustainability, and environmental issues. *Environ. Rev.* 21, 207–226. doi: 10.1139/er-2013-0040

Brennan, S. R., Schindler, D. E., Cline, T. J., Walsworth, T. E., Buck, G., and Fernandez, D. P. (2019). Shifting habitat mosaics and fish production across river basins. *Science* 364, 783–786. doi: 10.1126/science.aav4313

Britton, K. H. (2010). Multi-isotope analysis and the reconstruction of prey species palaeomigrations and palaeoecology. Durham University.

Brüggemann, N., Gessler, A., Kayler, Z., Keel, S. G., Badeck, F., Barthel, M., et al. (2011). Carbon allocation and carbon isotope fluxes in the plant-soil-atmosphere continuum: a review. *Biogeosciences* 8, 3457–3489. doi: 10.5194/bg-8-3457-2011

Canada, N. R. (2013). Spruce budworm. Available at: https://natural-resources.canada.ca/forests-forestry/insects-disturbances/spruce-budworm (Accessed July 4, 2026).

Capo, R. C., and DePaolo, D. J. (1992). Homogeneity of Sr isotopes in the oceans. *EOS, Transactions of the American Geophysical Union* 272.

Capo, R. C., Stewart, B. W., and Chadwick, O. A. (1998). Strontium isotopes as tracers of ecosystem processes: theory and methods. *Geoderma* 82, 197–225. doi: 10.1016/S0016-7061(97)00102-X

Cardim Ferreira Lima, M., Damascena De Almeida Leandro, M. E., Valero, C., Pereira Coronel, L. C., and Gonçalves Bazzo, C. O. (2020). Automatic Detection and Monitoring of Insect Pests—A Review. *Agriculture* 10, 161. doi: 10.3390/agriculture10050161

Cernusak, L. A. (2020). Gas exchange and water-use efficiency in plant canopies. *Plant Biology* 22, 52–67. doi: 10.1111/plb.12939

Cernusak, L. A., Barbour, M. M., Arndt, S. K., Cheesman, A. W., English, N. B., Feild, T. S., et al. (2016). Stable isotopes in leaf water of terrestrial plants. *Plant, Cell & Environment* 39, 1087–1102. doi: 10.1111/pce.12703

Chang, W.-Y., Lantz, V. A., Hennigar, C. R., and MacLean, D. A. (2012). Economic impacts of forest pests: a case study of spruce budworm outbreaks and control in New Brunswick, Canada. *Can. J. For. Res.* 42, 490–505. doi: 10.1139/x11-190

Chapman, J. W., Drake, V. A., and Reynolds, D. R. (2011). Recent Insights from Radar Studies of Insect Flight. *Annu. Rev. Entomol.* 56, 337–356. doi: 10.1146/annurev-ento-120709-144820

Chapman, J. W., Reynolds, D. R., and Wilson, K. (2015). Long-range seasonal migration in insects: mechanisms, evolutionary drivers and ecological consequences. *Ecology Letters* 18, 287–302. doi: 10.1111/ele.12407

Charberet, S. M., Maria, A., Siaussat, D., Gounand, I., and Mathieu, J. (2023). Feeding and growth variations affect δ13C and δ15N budgets during ontogeny in a lepidopteran larva. *Peer Community Journal* 3. doi: 10.24072/pcjournal.265

Chevillat, V. S., Siegwolf, R. T. W., Pepin, S., and Körner, C. (2005). Tissue-specific variation of *δ*13C in mature canopy trees in a temperate forest in central Europe. *Basic and Applied Ecology* 6, 519–534. doi: 10.1016/j.baae.2005.04.008

Chien, C.-T., Mackey, K. R. M., Dutkiewicz, S., Mahowald, N. M., Prospero, J. M., and Paytan, A. (2016). Effects of African dust deposition on phytoplankton in the western tropical Atlantic Ocean off Barbados. *Global Biogeochemical Cycles* 30, 716–734. doi: 10.1002/2015GB005334

Christenson, L. M., Lovett, G. M., Mitchell, M. J., and Groffman, P. M. (2002). The fate of nitrogen in gypsy moth frass deposited to an oak forest floor. *Oecologia* 131, 444–452. doi: 10.1007/s00442-002-0887-7

Chukhrov, F. V., Ermilova, L. P., Churikov, V. S., and Nosik, L. P. (1980). The isotopic composition of plant sulfur. *Organic Geochemistry* 2, 69–75. doi: 10.1016/0146-6380(80)90022-4

Codron, J., Lee-Thorp, J. A., Sponheimer, M., and Codron, D. (2013). Plant stable isotope composition across habitat gradients in a semi-arid savanna: implications for environmental reconstruction. *Journal of Quaternary Science* 28, 301–310. doi: 10.1002/jqs.2614

Contina, A., Magozzi, S., Vander Zanden, H. B., Bowen, G. J., and Wunder, M. B. (2022). Optimizing stable isotope sampling design in terrestrial movement ecology research. *Methods in Ecology and Evolution* 13, 1237–1249. doi: 10.1111/2041-210X.13840

Cooke, B. J., and Régnière, J. (2025). The unpredictably eruptive dynamics of spruce budworm populations in eastern Canada. *Population Ecology* 67, 363–378. doi: 10.1002/1438-390X.12216

Cooke, S. J., Piczak, M. L., Singh, N. J., Åkesson, S., Ford, A. T., Chowdhury, S., et al. (2024). Animal migration in the Anthropocene: threats and mitigation options. *Biological Reviews* 99, 1242–1260. doi: 10.1111/brv.13066

Courtiol (2022). Ecological Dynamics: Isorix. Available at: https://ecodynizw.github.io/posts/isorix/

Courtiol, A., Rohwäder, M. S., Lehnert, L. S., Voigt, C. C., Kramer-Schadt, S., Rousset, F., et al. (2019). "Chapter 09 - Isoscape Computation and Inference of Spatial Origins With Mixed Models Using the R package IsoriX," in *Tracking Animal Migration with Stable Isotopes*, (Elsevier), 207–236. doi: 10.1016/B978-0-12-814723-8.00009-X

Craine, J. M., Elmore, A. J., Aidar, M. P. M., Bustamante, M., Dawson, T. E., Hobbie, E. A., et al. (2009). Global patterns of foliar nitrogen isotopes and their relationships with climate,

mycorrhizal fungi, foliar nutrient concentrations, and nitrogen availability. *New Phytologist* 183, 980–992. doi: 10.1111/j.1469-8137.2009.02917.x

Crowley, B. E., Bataille, C. P., Haak, B. A., and Sommer, K. M. (2021). Identifying nesting grounds for juvenile migratory birds with dual isotope: an initial test using North American raptors. *Ecosphere* 12, e03765. doi: 10.1002/ecs2.3765

Crowley, B. E., Miller, J. H., and Bataille, C. P. (2017). Strontium isotopes (87Sr/86Sr) in terrestrial ecological and palaeoecological research: empirical efforts and recent advances in continental-scale models. *Biological Reviews* 92, 43–59. doi: 10.1111/brv.12217

Dargent, F., Candau, J.-N., Studens, K., Perrault, K. H., Reich, M. S., and Bataille, C. P. (2023). Characterizing eastern spruce budworm's large-scale dispersal events through flight behavior and stable isotope analyses. *Frontiers in Ecology and Evolution* 11. doi: 10.3389/fevo.2023.1060982

Dargent, F., Reich, M. S., Miller, M., Studens, K., Benvidi, N., Perrault, K., et al. (2025). A novel integrated framework to identify and characterize regional-scale pest insect dispersal. 2025.02.26.640127. doi: 10.1101/2025.02.26.640127

Dargent, F., Reich, M. S., Miller, M., Studens, K., Benvidi, N., Perrault, K., et al. (2026). An integrated framework to identify and characterize regional-scale insect dispersal. *Ecological Applications* 36, e70230. doi: 10.1002/eap.70230

Deniro, M. J., and Epstein, S. (1978). Influence of diet on the distribution of carbon isotopes in animals. *Geochimica et Cosmochimica Acta* 42, 495–506. doi: 10.1016/0016-7037(78)90199-0

Deniro, M. J., and Epstein, S. (1981). Influence of diet on the distribution of nitrogen isotopes in animals. *Geochimica et Cosmochimica Acta* 45, 341–351. doi: 10.1016/0016-7037(81)90244-1

Didan, K. (2015). MOD13A3 MODIS/Terra vegetation Indices Monthly L3 Global 1km SIN Grid V006. doi: https://doi.org/10.5067/MODIS/MOD13A3.006

Diefendorf, A. F., Mueller, K. E., Wing, S. L., Koch, P. L., and Freeman, K. H. (2010). Global patterns in leaf 13C discrimination and implications for studies of past and future climate. *PNAS* 107, 5738–5743. doi: 10.1073/pnas.0910513107

Doi, H., Kikuchi, E., Takagi, S., and Shikano, S. (2007). Changes in carbon and nitrogen stable isotopes of chironomid larvae during growth, starvation and metamorphosis. *Rapid Communications in Mass Spectrometry* 21, 997–1002. doi: 10.1002/rcm.2925

Du, L., Li, Y., and Zheng, X. (2023). Climate Seasonality Mediates Global Patterns of Foliar Carbon and Nitrogen Isotopes. *Forests* 14, 461. doi: 10.3390/f14030461

Duursma, R. A., and Marshall, J. D. (2006). Vertical canopy gradients in δ13C correspond with leaf nitrogen content in a mixed-species conifer forest. *Trees* 20, 496–506. doi: 10.1007/s00468-006-0065-3

Dymond, C. C., Neilson, E. T., Stinson, G., Porter, K., MacLean, D. A., Gray, D. R., et al. (2010). Future Spruce Budworm Outbreak May Create a Carbon Source in Eastern Canadian Forests. *Ecosystems* 13, 917–931. doi: 10.1007/s10021-010-9364-z

Erban Kochergina, Y. V., Novak, M., Erban, V., and Stepanova, M. (2021). 87Sr/86Sr isotope ratios in trees as an archaeological tracer: Limitations of linking plant-biomass and bedrock Sr isotope signatures. *Journal of Archaeological Science* 133, 105438. doi: 10.1016/j.jas.2021.105438

Ewers, B. E., Gower, S. T., Bond-Lamberty, B., and Wang, C. K. (2005). Effects of stand age and tree species on canopy transpiration and average stomatal conductance of boreal forests. 28. Available at: https://onlinelibrary.wiley.com/doi/10.1111/j.1365-3040.2005.01312.x (Accessed May 7, 2026).

FAO (2020). Desert Locust Component: Strengthening Desert Locust Management FAO's Response to the Desert Locust Problem. Available at: https://www.fao.org/ag/locusts/common/ecg/1344/en/EMPRESbrochureE.pdf (Accessed November 8, 2024).

Farquhar, G. D., Ehleringer, J. R., and Hubick, K. T. (1989). Carbon Isotope Discrimination and Photosynthesis. *Annual Review of Plant Biology* 40, 503–537. doi: 10.1146/annurev.pp.40.060189.002443

Faure, G., and Powell, J. L. (1972). *Strontium Isotope Geology*. Berlin: Springer-Verlag. Available at: https://linkinghub.elsevier.com/retrieve/pii/0016703771901335 (Accessed January 24, 2025).

Fessenden, J. E., and Ehleringer, J. R. (2002). Age-related variations in δ13C of ecosystem respiration across a coniferous forest chronosequence in the Pacific Northwest. *Tree Physiol* 22, 159–167. doi: 10.1093/treephys/22.2-3.159

Fick, S. E., and Hijmans, R. J. (2017). WorldClim 2: new 1-km spatial resolution climate surfaces for global land areas. *International Journal of Climatology* 37, 4302–4315. doi: 10.1002/joc.5086

Flockhart, D. T. T., Kyser, T. K., Chipley, D., Miller, N. G., and Norris, D. R. (2015). Experimental evidence shows no fractionation of strontium isotopes (87Sr/86Sr) among soil, plants, and herbivores: implications for tracking wildlife and forensic science. *Isotopes in Environmental and Health Studies* 51, 372–381. doi: 10.1080/10256016.2015.1021345

Foster, A. C., Wang, J. A., Frost, G. V., Davidson, S. J., Hoy, E., Turner, K. W., et al. (2022). Disturbances in North American boreal forest and Arctic tundra: impacts, interactions, and responses. *Environ. Res. Lett.* 17, 113001. doi: 10.1088/1748-9326/ac98d7

Fuentealba, A., Dupont, A., Hébert, C., Berthiaume, R., Quezada-García, R., and Bauce, É. (2019). Comparing the efficacy of various aerial spraying scenarios using *Bacillus thuringiensis* to protect trees from spruce budworm defoliation. *Forest Ecology and Management* 432, 1013–1021. doi: 10.1016/j.foreco.2018.10.034

Gannes, L. Z., O'Brien, D. M., and Del Rio, C. M. (1997). Stable isotopes in animal ecology: assumptions, caveats, and a call for more laboratory experiments. *Ecology* 78, 1271-.

Gauthier, S., Bernier, P., Kuuluvainen, T., Shvidenko, A. Z., and Schepaschenko, D. G. (2015). Boreal forest health and global change. *Science* 349, 819–822. doi: 10.1126/science.aaa9092

Gauthier, S., Kuuluvainen, T., Macdonald, S. E., Shorohova, E., Shvidenko, A., Bélisle, A.-C., et al. (2023). "Ecosystem Management of the Boreal Forest in the Era of Global Change," in *Boreal Forests in the Face of Climate Change: Sustainable Management*, eds. M. M. Girona, H. Morin, S. Gauthier, and Y. Bergeron (Cham: Springer International Publishing), 3–49. doi: 10.1007/978-3-031-15988-6_1

Genuer, R., Poggi, J.-M., and Tuleau-Malot, C. (2015). VSURF: An R Package for Variable Selection Using Random Forests. *The R Journal* 7, 19–33. doi: 10.32614/RJ-2015-018

Giammarchi, F., Cherubini, P., Pretzsch, H., and Tonon, G. (2017). The increase of atmospheric CO2 affects growth potential and intrinsic water-use efficiency of Norway spruce forests: insights from a multi-stable isotope analysis in tree rings of two Alpine chronosequences. *Trees* 31, 503–515. doi: 10.1007/s00468-016-1478-2

Gigleux, C., Grimes, V., Tütken, T., Knecht, R., and Britton, K. (2019). Reconstructing caribou seasonal biogeography in Little Ice Age (late Holocene) Western Alaska using intra-tooth strontium and oxygen isotope analysis. *Journal of Archaeological Science: Reports* 23, 1043–1054. doi: 10.1016/j.jasrep.2017.10.043

Gilbert, F. (2019). Migration: Ecosystem Services Helicoptered In. *Current Biology* 29, R697–R699. doi: 10.1016/j.cub.2019.06.013

Grandpré, L. D., Marchand, M., Kneeshaw, D. D., Paré, D., Boucher, D., Bourassa, S., et al. (2022). Defoliation-induced changes in foliage quality may trigger broad-scale insect outbreaks. *Communications Biology* 5, 1–10. doi: 10.1038/s42003-022-03407-8

Greenbank, D. O. (1963a). Host Species And The Spruce Budworm. *The Memoirs of the Entomological Society of Canada* 95, 219–223. doi: 10.4039/entm9531219-1

Greenbank, D. O. (1963b). The Development Of The Outbreak. *Mem. Entomol. Soc. Can.* 95, 19–23. doi: 10.4039/entm9531019-1

Greenbank, D. O., Schaefer, G. W., and Rainey, R. C. (1980). Spruce Budworm (Lepidoptera: Tortricidae) Moth Flight and Dispersal: New Undersanding from Canopy Observations, Radar, and Aircraft. *The Memoirs of the Entomological Society of Canada* 112, 1–49. doi: 10.4039/entm112110fv

Grondin, P., Ansseau, C., Bélanger, L., Bergeron, J., Bergeron, Y., Bouchard, A., et al. (1996). Écologie forestière. *Manuel de foresterie*, 133–279.

Guindon, L., Villemaire, P., Correia, D. L. P., Manka, F., Lacarte, S., and Smiley, B. (2023). SCANFI: Spatialized CAnadian National Forest Inventory data product. doi: https://doi.org/10.23687/18e6a919-53fd-41ce-b4e2-44a9707c52dc

Gunn, A. (2003). Voles, lemmings and caribou - population cycles revisited? *Rangifer*, 105–111. doi: 10.7557/2.23.5.1689

Handley, L. L., Odee, D., and Scrimgeour, C. M. (1994). δ15N and δ13C Patterns in Savanna Vegetation: Dependence on Water Availability and Disturbance. *Functional Ecology* 8, 306–314. doi: 10.2307/2389823

Handley, L. L., and Raven, J. A. (1992). The use of natural abundance of nitrogen isotopes in plant physiology and ecology. *Plant, Cell & Environment* 15, 965–985. doi: 10.1111/j.1365-3040.1992.tb01650.x

Harris, I., Osborn, T. J., Jones, P., and Lister, D. (2020). Version 4 of the CRU TS monthly high-resolution gridded multivariate climate dataset. *Sci Data* 7, 109. doi: 10.1038/s41597-020-0453-3

Hartmann, J., and Moosdorf, N. (2012). The new global lithological map database GLiM: A representation of rock properties at the Earth surface. *Geochemistry, Geophysics, Geosystems* 13. doi: 10.1029/2012GC004370

Healthy Forest Partnership (2019). What is spruce budworm? – Healthy Forest Partnership. Available at: https://healthyforestpartnership.ca/get-informed/what-is-spruce-budworm/?utm_source=chatgpt.com (Accessed July 4, 2026).

Heaton, T. H. E. (1999). Spatial, Species, and Temporal Variations in the13C/12C Ratios of C3Plants: Implications for Palaeodiet Studies. *Journal of Archaeological Science* 26, 637–649. doi: 10.1006/jasc.1998.0381

Hermosilla, T., Wulder, M. A., White, J. C., Coops, N. C., Hobart, G. W., and Campbell, L. B. (2016). Mass data processing of time series Landsat imagery: pixels to data products for forest monitoring. *International Journal of Digital Earth* 9, 1035–1054. doi: 10.1080/17538947.2016.1187673

Hobson, K. A. (1999). Tracing origins and migration of wildlife using stable isotopes: a review. *Oecologia* 120, 314–326. doi: 10.1007/s004420050865

Hobson, K. A. (2019). "Chapter 04 - Application of Isotopic Methods to Tracking Animal Movements," in *Tracking Animal Migration with Stable Isotopes*, (Elsevier), 85–115. doi: 10.1016/B978-0-12-814723-8.00004-0

Hobson, K. A. (2023). Stable isotopes and a changing world. *Oecologia* 203, 233–250. doi: 10.1007/s00442-023-05387-w

Hobson, K. A., Atwell, L., and Wassenaar, L. I. (1999a). Influence of drinking water and diet on the stable-hydrogen isotope ratios of animal tissues. *Proc. Natl. Acad. Sci. U.S.A.* 96, 8003–8006. doi: 10.1073/pnas.96.14.8003

Hobson, K. A., Barnett-Johnson, R., and Cerling, T. (2010). "Using Isoscapes to Track Animal Migration," in *Isoscapes: Understanding movement, pattern, and process on Earth through isotope mapping*, eds. J. B. West, G. J. Bowen, T. E. Dawson, and K. P. Tu (Dordrecht: Springer Netherlands), 273–298. doi: 10.1007/978-90-481-3354-3_13

Hobson, K. A., Kardynal, K. J., and Koehler, G. (2019a). Expanding the isotopic toolbox to track monarch butterfly (Danaus plexippus) origins and migration: On the utility of stable oxygen isotope (δ18O) measurements. *Frontiers in Ecology and Evolution* 7. doi: 10.3389/fevo.2019.00224

Hobson, K. A., Kardynal, K. J., Norris, D. R., and Yohannes, E. (2019b). "Chapter 01 - Animal Migration," in *Tracking Animal Migration with Stable Isotopes*, (Elsevier), 1–23. doi: 10.1016/B978-0-12-814723-8.00001-5

Hobson, K. A., and Wassenaar, L. I. (2019). *Tracking Animal Migration with Stable Isotopes*., 2nd Edn. Elsevier.

Hobson, K. A., Wassenaar, L. I., and Taylor, O. R. (1999b). Stable isotopes (δD and δ13C) are geographic indicators of natal origins of monarch butterflies in eastern North America. *Oecologia* 120, 397–404. doi: 10.1007/s004420050872

Hobson, K. A., Wassenaar, L. I., Taylor, O. R., Canada, E., Wassenaar, L. I., and Taylor, O. R. (1999c). Stable Isotopes (δD and δ 13C) Are Geographic Indicators of Natal Origins of Monarch Butterflies in Eastern North America Stable isotopes (6D and 13C) are geographic indicators of natal origins of monarch butterflies in eastern North America. Springer-Verlag.

Hoefs, J. (2021). *Stable Isotope Geochemistry*. Cham: Springer International Publishing. doi: 10.1007/978-3-030-77692-3

Högberg, P. (1997). Tansley Review No. 95 15N natural abundance in soil-plant systems. *New Phytologist* 137, 179–203. doi: 10.1046/j.1469-8137.1997.00808.x

Holland, R. A., Wikelski, M., and Wilcove, D. S. (2006). How and Why Do Insects Migrate? *Science* 313, 794–796.

Holmes, B., Candau, J.-N., Le Roux, P., Reich, M. S., Bataille, C. P., and Dargent, F. (2026). Not All Isotopes Make Good Geolocators: Trophic Transfer Reveals Contrasting Geolocation Potential in Eastern Spruce Budworm. *In Review*.

Hopkinson, R. F., and Soroka, J. J. (2010). Air trajectory model applied to an in-depth diagnosis of potential diamondback moth infestations on the Canadian Prairies. *Agricultural and Forest Meteorology* 150, 1–11. doi: 10.1016/j.agrformet.2009.07.015

Hu, G., Lim, K. S., Horvitz, N., Clark, S. J., Reynolds, D. R., Sapir, N., et al. (2016). Mass seasonal bioflows of high-flying insect migrants. *Science* 354, 1584–1587. doi: 10.1126/science.aah4379

Huestis, D. L., Dao, A., Diallo, M., Sanogo, Z. L., Samake, D., Yaro, A. S., et al. (2019). Windborne long-distance migration of malaria mosquitoes in the Sahel. *Nature* 574, 404–408. doi: 10.1038/s41586-019-1622-4

Humphries, S. A. (2003). Stable Isotopes of Sulphur and Oxygen in Forested Catchments: Insight from New Techniques into Sulphur Cycling and Dissolved Organic Matter Alteration. University of Waterloo.

IAEA (2020). Reference Materials for δ34S isotope values: IAEA-S-1 (NIST - RM8554), IAEA-S-2 (NIST - RM8555), IAEA-S-3 (NIST - RM8529). International Atomic Energy Agency.

IAEA (2022a). Reference Material for δ15N - Reference Sheets - IAEA-N1. International Atomic Energy Agency. Available at:

https://nucleus.iaea.org/sites/AnalyticalReferenceMaterials/Shared%20Documents/ReferenceMaterials/StableIsotopes/IAEA-N1/RS_IAEA-N-1.pdf (Accessed June 5, 2026).

IAEA (2022b). Reference Material for δ15N - Reference Sheets - IAEA-N2. International Atomic Energy Agency. Available at: https://nucleus.iaea.org/sites/AnalyticalReferenceMaterials/Shared%20Documents/ReferenceMaterials/StableIsotopes/IAEA-N2/RS_IAEA-N-2.pdf (Accessed June 5, 2026).

IAEA (2024). Reference Material for δ13C - Reference Sheet - IAEA-CH-6-rev1. International Atomic Energy Agency. Available at: https://nucleus.iaea.org/sites/AnalyticalReferenceMaterials/Shared%20Documents/ReferenceMaterials/StableIsotopes/IAEA-CH-6/RS-IAEA-CH-6-rev1.pdf (Accessed June 5, 2026).

Ingraham, N. L., and Taylor, B. E. (1991). Light stable isotope systematics of large-scale hydrologic regimes in California and Nevada. *Water Resources Research* 27, 77–90. doi: 10.1029/90WR01708

Jäggi, M., Saurer, M., Fuhrer, J., and Siegwolf, R. (2002). The relationship between the stable carbon isotope composition of needle bulk material, starch, and tree rings in Picea abies. *Oecologia* 131, 325–332. doi: 10.1007/s00442-002-0881-0

James, D. G., James, T. S., Seymour, L., Kappen, L., Russell, T., Harryman, B., et al. (2018). Citizen Scientist Tagging Reveals Destinations of Migrating Monarch Butterflies, Danaus plexippus (L.) from the Pacific Northwest. *The Journal of the Lepidopterists' Society* 72, 127–144. doi: 10.18473/lepi.v72i2.a5

James, P. M. A., Robert, L.-E., Wotton, B. M., Martell, D. L., and Fleming, R. A. (2017). Lagged cumulative spruce budworm defoliation affects the risk of fire ignition in Ontario, Canada. *Ecol Appl* 27, 532–544. doi: 10.1002/eap.1463

Jarvis, A., Reuter, H. I., Nelson, A., and Guevara, E. (2008). Hole-filled seamless SRTM data v4. *International Centre for Tropical Agriculture (CIAT)*. Available at: https://www.researchgate.net/publication/255267222_Hole-filled_seamless_SRTM_data_v4 (Accessed May 11, 2026).

Johns, R. C., Bowden, J. J., Carleton, D. R., Cooke, B. J., Edwards, S., Emilson, E. J. S., et al. (2019). A conceptual framework for the spruce budworm Early Intervention Strategy: Can outbreaks be stopped? *Forests* 10. doi: 10.3390/f10100910

Johns, R. C., Edwards, S., Amos-Binks, L., Bowden, J. J., Carleton, D., Edge, C., et al. (2026). Adaptive area-wide management for suppressing spruce budworm outbreaks: effectiveness of the early intervention strategy. *J Pest Sci* 99, 51. doi: 10.1007/s10340-025-02002-0

Johnson, C. (1969). *Migration and the dispersal of insects by flight*. London, U.K.: Chaucer Press.

Kettela, E. G. (1983). A cartographic history of spruce budworm defoliation 1967 to 1981 in eastern North America. 8 pp.

Kittel, T. G. F., Steffen, W. L., and Chapin III, F. S. (2000). Global and regional modelling of Arctic–boreal vegetation distribution and its sensitivity to altered forcing. *Global Change Biology* 6, 1–18. doi: 10.1046/j.1365-2486.2000.06011.x

Koenig, W. D., and Knops, J. M. H. (2001). Seed-crop size and eruptions of North American boreal seed-eating birds. *Journal of Animal Ecology* 70, 609–620. doi: 10.1046/j.1365-2656.2001.00516.x

Kohn, M. J. (2010). Carbon isotope compositions of terrestrial C3 plants as indicators of (paleo)ecology and (paleo)climate. *PNAS* 107, 19691–19695. doi: 10.1073/pnas.1004933107

Kubelka, V., Sandercock, B. K., Székely, T., and Freckleton, R. P. (2022). Animal migration to northern latitudes: environmental changes and increasing threats. *Trends in Ecology & Evolution* 37, 30–41. doi: 10.1016/j.tree.2021.08.010

Kuhn, M. (2008). Building Predictive Models in R Using the caret Package. *Journal of Statistical Software* 28, 1–26. doi: 10.18637/jss.v028.i05

Kuznetsova, A., Brockhoff, P. B., and Christensen, R. H. B. (2017). lmerTest Package: Tests in Linear Mixed Effects Models. *Journal of statistical software* 82, 1–26. doi: 10.18637/jss.v082.i13

Langor, D. W., Cameron, E. K., MacQuarrie, C. J. K., McBeath, A., McClay, A., Peter, B., et al. (2014). Non-native species in Canada's boreal zone: diversity, impacts, and risk. *Environ. Rev.* 22, 372–420. doi: 10.1139/er-2013-0083

Larsen, T. B. (1975). Provisional notes of migrant butterflies in Lebanon. *Atalanta* 6.

Le Corre, M., Dargent, F., Grimes, V., Wright, J., Côté, S. D., Reich, M. S., et al. (2025). An ensemble machine learning bioavailable strontium isoscape for Eastern Canada. *FACETS* 10, 1–17. doi: 10.1139/facets-2024-0180

Lehner, B., Anand, M., Fluet-Chouinard, E., Tan, F., Aires, F., Allen, G. H., et al. (2025). Mapping the world's inland surface waters: an upgrade to the Global Lakes and Wetlands Database (GLWD v2). *Earth System Science Data* 17, 2277–2329. doi: 10.5194/essd-17-2277-2025

Lindroos, E. E., Bataille, C. P., Holder, P. W., Talavera, G., and Reich, M. S. (2023). Temporal stability of δ2H in insect tissues: Implications for isotope-based geographic assignments. *Frontiers in Ecology and Evolution* 11. Available at: https://www.frontiersin.org/articles/10.3389/fevo.2023.1060836 (Accessed November 30, 2023).

Liu, Z., Peng, C., MacLean, D. A., De Grandpré, L., Candau, J.-N., and Kneeshaw, D. (2022). Evaluating and quantifying the effect of various spruce budworm intervention strategies on forest carbon dynamics in Atlantic Canada. *Forest Ecosystems* 9, 100052. doi: 10.1016/j.fecs.2022.100052

Llamas, R. M., Guevara, M., Rorabaugh, D., Taufer, M., and Vargas, R. (2020). Spatial Gap-Filling of ESA CCI Satellite-Derived Soil Moisture Based on Geostatistical Techniques and Multiple Regression. *Remote Sensing* 12, 665. doi: 10.3390/rs12040665

Ludwig, D., Jones, D. D., and Holling, C. S. (1978). Qualitative Analysis of Insect Outbreak Systems: The Spruce Budworm and Forest. *The Journal of Animal Ecology* 47, 315. doi: 10.2307/3939

Lumley, L. M., Pouliot, E., Laroche, J., Boyle, B., Brunet, B. M. T., Levesque, R. C., et al. (2020). Continent-wide population genomic structure and phylogeography of North America's most destructive conifer defoliator, the spruce budworm (*Choristoneura fumiferana*). *Ecology and Evolution* 10, 914–927. doi: 10.1002/ece3.5950

Ma, C., Vander Zanden, H. B., Wunder, M. B., and Bowen, G. J. (2020). assignR: An r package for isotope-based geographic assignment. *Methods in Ecology and Evolution* 11, 996–1001. doi: 10.1111/2041-210X.13426

MacLean, D. A. (2016). Impacts of insect outbreaks on tree mortality, productivity, and stand development. *Can Entomol* 148, S138–S159. doi: 10.4039/tce.2015.24

Magozzi, S., Bataille, C. P., Hobson, K. A., Wunder, M. B., Howa, J. D., Contina, A., et al. (2021). Calibration chain transformation improves the comparability of organic hydrogen and oxygen stable isotope data. *Methods in Ecology and Evolution* 12, 732–747. doi: 10.1111/2041-210X.13556

Magozzi, S., Vander Zanden, H. B., Wunder, M. B., and Bowen, G. J. (2019). Mechanistic model predicts tissue–environment relationships and trophic shifts in animal hydrogen and oxygen isotope ratios. *Oecologia* 191, 777–789. doi: 10.1007/s00442-019-04532-8

Magozzi, S., Vander Zanden, H. B., Wunder, M. B., Trueman, C. N., Pinney, K., Peers, D., et al. (2020). Combining Models of Environment, Behavior, and Physiology to Predict Tissue Hydrogen and Oxygen Isotope Variance Among Individual Terrestrial Animals. *Front. Ecol. Evol.* 8. doi: 10.3389/fevo.2020.536109

Maltman, J. C., Hermosilla, T., Wulder, M. A., Coops, N. C., and White, J. C. (2023). Estimating and mapping forest age across Canada's forested ecosystems. *Remote Sensing of Environment* 290. doi: 10.1016/j.rse.2023.113529

Manzello, S. L. ed. (2020). *Encyclopedia of Wildfires and Wildland-Urban Interface (WUI) Fires*. Cham: Springer International Publishing. doi: 10.1007/978-3-319-52090-2

Marini, L., Ayres, M. P., and Jactel, H. (2022). Impact of Stand and Landscape Management on Forest Pest Damage. *Annu. Rev. Entomol.* 67, 181–199. doi: 10.1146/annurev-ento-062321-065511

Martinelli, L. A., Figueiredo Almeida, R., da Silva Araújo, M. G., Amorim, D. J., Batista, A. C. G., Souza-Silva, I. M., et al. (2026). Isotope fingerprinting for traceability in the amazon bioeconomy: A Bayesian assignment approach with açaí. *Trees, Forests and People* 24, 101207. doi: 10.1016/j.tfp.2026.101207

Martínez Del Rio, C., Wolf, N., Carleton, S. A., and Gannes, L. Z. (2009). Isotopic ecology ten years after a call for more laboratory experiments. *Biological Reviews* 84, 91–111. doi: 10.1111/j.1469-185X.2008.00064.x

Martínez del Rio, C., Wolf, N., Carleton, S. A., and Gannes, L. Z. (2009). Isotopic ecology ten years after a call for more laboratory experiments. *Biological Reviews* 84, 91–111. doi: 10.1111/j.1469-185X.2008.00064.x

Matasci, G., Hermosilla, T., Wulder, M. A., White, J. C., Coops, N. C., Hobart, G. W., et al. (2018). Large-area mapping of Canadian boreal forest cover, height, biomass and other structural attributes using Landsat composites and lidar plots. *Remote Sensing of Environment* 209, 90–106. doi: 10.1016/j.rse.2017.12.020

Mattson, W. J., Simmons, G. A., and Witter, J. A. (1988). "The Spruce Budworm in Eastern North America," in *Dynamics of Forest Insect Populations*, ed. A. A. Berryman (Boston, MA: Springer US), 309–330. doi: 10.1007/978-1-4899-0789-9_16

McCutchan, J. H., Lewis, W. M., Kendall, C., and McGrath, C. C. (2003). Variation in Trophic Shift for Stable Isotope Ratios of Carbon, Nitrogen, and Sulfur. *Oikos* 102, 378–390.

Menchetti, M., Guéguen, M., and Talavera, G. (2019). Spatio-temporal ecological niche modelling of multigenerational insect migrations. *Proc Biol Sci* 286, 20191583. doi: 10.1098/rspb.2019.1583

Michener, R., and Lajtha, K. (2007). *Stable Isotopes in Ecology and Environmental Science*. Blackwell.

Miller, C. A. (1963). The Spruce Budworm. *The Memoirs of the Entomological Society of Canada* 95, 12–19. doi: 10.4039/entm9531012-1

Miller, W. E. (1987). Spruce Budworm (Lepidoptera: Tortricidae): Role of Adult Imbibing in Reproduction. *Environmental Entomology* 16, 1291–1295. doi: 10.1093/ee/16.6.1291

Minagawa, M., and Wada, E. (1984). Stepwise enrichment of 15N along food chains: Further evidence and the relation between δ15N and animal age. *Geochimica et Cosmochimica Acta* 48, 1135–1140. doi: 10.1016/0016-7037(84)90204-7

Mitchell, M. J., Krouse, H. R., Mayer, B., Stam, A. C., and Zhang, Y. (1998). "Use of Stable Isotopes in Evaluating Sulfur Biogeochemistry of Forest Ecosystems," in *Isotope Tracers in Catchment Hydrology*, (Elsevier), 489–518. doi: 10.1016/B978-0-444-81546-0.50022-7

Mitchell, M. J., and Lindberg, S. E. (1992). "Sulfur Chemistry, Deposition, and Cycling in Forests," in *Atmospheric Deposition and Forest Nutrient Cycling: A Synthesis of the Integrated Forest*

Study, eds. D. W. Johnson and S. E. Lindberg (New York, NY: Springer), 72–149. doi: 10.1007/978-1-4612-2806-6_5

Mooney, W. D., Laske, G., and Masters, T. G. (1998). CRUST 5.1: A global crustal model at 5° × 5°. *J. Geophys. Res.* 103, 727–747. doi: 10.1029/97JB02122

Nanini, F., Souza, P. G. C., Soliman, E. P., Zauza, E. A. V., Domingues, M. M., Santos, F. A., et al. (2024). Genetic diversity, population structure and ecological niche modeling of Thyrinteina arnobia (Lepidoptera: Geometridae), a native Eucalyptus pest in Brazil. *Sci Rep* 14, 20963. doi: 10.1038/s41598-024-71816-2

Natural Resources Canada (2023). Maps of solar resource potential in Canada.

Nealis, V. G. (2016). Comparative ecology of conifer-feeding spruce budworms (Lepidoptera: Tortricidae). *Can Entomol* 148, S33–S57. doi: 10.4039/tce.2015.15

Newton, J. (2021). An insect isoscape of UK and Ireland. *Rapid Communications in Mass Spectrometry* 35. doi: 10.1002/rcm.9126

NIST (2022). Reference Material 8539 - NBS22 Oil. National Institute of Standards and Technology. Available at: https://tsapps.nist.gov/srmext/certificates/8539.pdf (Accessed June 5, 2026).

O'Leary, M. H. (1981). Carbon isotope fractionation in plants. *Phytochemistry* 20, 553–567. doi: 10.1016/0031-9422(81)85134-5

Panek, J. A., and Waring, R. H. (1997). Stable Carbon Isotopes as Indicators of Limitations to Forest Growth Imposed by Climate Stress. *Ecological Applications* 7, 854–863. doi: 10.1890/1051-0761(1997)007[0854:SCIAIO]2.0.CO;2

Paris, E. H., Bataille, C. P., Stantis, C., George, M., López Bravo, R., and Lalo Jacinto, G. (2026). Distant provenance of archaeological dogs in Chiapas confirms complex trade networks within Mayan societies. *Journal of Archaeological Science* 187, 106482. doi: 10.1016/j.jas.2026.106482

Pedgley, D. E. (1993). Managing migratory insect pests—a review. *International Journal of Pest Management* 39, 3–12. doi: 10.1080/09670879309371751

Peltzer, D. A., Wardle, D. A., Allison, V. J., Baisden, W. T., Bardgett, R. D., Chadwick, O. A., et al. (2010). Understanding ecosystem retrogression. *Ecological Monographs* 80, 509–529. doi: 10.1890/09-1552.1

Peterson, B. J., and Fry, B. (1987). Stable Isotopes in Ecosystem Studies. *Annual Review of Ecology and Systematics* 18, 293–320.

Poggio, L., de Sousa, L. M., Batjes, N. H., Heuvelink, G. B. M., Kempen, B., Ribeiro, E., et al. (2021). SoilGrids 2.0: producing soil information for the globe with quantified spatial uncertainty. *SOIL* 7, 217–240. doi: 10.5194/soil-7-217-2021

Pureswaran, D. S., Johns, R., Heard, S. B., and Quiring, D. (2016). Paradigms in Eastern Spruce Budworm (Lepidoptera: Tortricidae) Population Ecology: A Century of Debate. *Environ Entomol* 45, 1333–1342. doi: 10.1093/ee/nvw103

Quinby, B. M., Creighton, J. C., and Flaherty, E. A. (2020). Stable isotope ecology in insects: a review. *Ecological Entomology* 45, 1231–1246. doi: 10.1111/een.12934

Raoult, V., Phillips, A. A., Nelson, J., Niella, Y., Skinner, C., Tilcock, M. B., et al. (2024). Why aquatic scientists should use sulfur stable isotope ratios (*δ*34S) more often. *Chemosphere* 355, 141816. doi: 10.1016/j.chemosphere.2024.141816

Régnière, J., Cooke, B., Béchard, A., Dupont, A., and Therrien, P. (2019). Dynamics and Management of Rising Outbreak Spruce Budworm Populations. *Forests* 10, 748. doi: 10.3390/f10090748

Régnière, J., and Nealis, V. G. (2007). Ecological mechanisms of population change during outbreaks of the spruce budworm. *Ecological Entomology* 32, 461–477. doi: 10.1111/j.1365-2311.2007.00888.x

Régnière, J., and Nealis, V. G. (2019). Density Dependence of Egg Recruitment and Moth Dispersal in Spruce Budworms. *Forests* 10, 706. doi: 10.3390/f10080706

Reich, M. S., Flockhart, D. T. T., Norris, D. R., Hu, L., and Bataille, C. P. (2021). Continuous-surface geographic assignment of migratory animals using strontium isotopes: A case study with monarch butterflies. *Methods in Ecology and Evolution* 12, 2445–2457. doi: 10.1111/2041-210X.13707

Reich, M. S., Ghouri, S., Zabudsky, S., Hu, L., Le Corre, M., Ng'iru, I., et al. (2024). Trans-Saharan migratory patterns in *Vanessa cardui* and evidence for a southward leapfrog migration. *iScience* 27, 111342. doi: 10.1016/j.isci.2024.111342

Reich, M. S., Shipilina, D., Talla, V., Bahleman, F., Kébé, K., Berger, J. L., et al. (2025). Isotope geolocation and population genomics in Vanessa cardui: Short- and long-distance migrants are genetically undifferentiated. *PNAS Nexus* 4, pgae586. doi: 10.1093/pnasnexus/pgae586

Robinson, D. (2001). δ15N as an integrator of the nitrogen cycle. *Trends in Ecology & Evolution* 16, 153–162. doi: 10.1016/S0169-5347(00)02098-X

Roden, J. S., Lin, G., and Ehleringer, J. R. (2000). A mechanistic model for interpretation of hydrogen and oxygen isotope ratios in tree-ring cellulose. *Geochimica et Cosmochimica Acta* 64, 21–35. doi: 10.1016/S0016-7037(99)00195-7

Rowe, A. G., Bataille, C. P., Baleka, S., Combs, E. A., Crass, B. A., Fisher, D. C., et al. (2024). A female woolly mammoth's lifetime movements end in an ancient Alaskan hunter-gatherer camp. *Science Advances* 10, eadk0818. doi: 10.1126/sciadv.adk0818

Royama, T. (1984). Population Dynamics of the Spruce Budworm Choristoneura Fumiferana. *Ecological Monographs* 54, 429–462. doi: 10.2307/1942595

Royama, T., Eveleigh, E. S., Morin, J. R. B., Pollock, S. J., McCarthy, P. C., McDougall, G. A., et al. (2017). Mechanisms underlying spruce budworm outbreak processes as elucidated by a 14-year study in New Brunswick, Canada. *Ecological Monographs* 87, 600–631. doi: 10.1002/ecm.1270

Rozanski, K., Araguás-Araguás, L., and Gonfiantini, R. (1993). "Isotopic Patterns in Modern Global Precipitation," in *Climate Change in Continental Isotopic Records*, (American Geophysical Union (AGU)), 1–36. doi: 10.1029/GM078p0001

Rubenstein, D. R., and Hobson, K. A. (2004). From birds to butterflies: animal movement patterns and stable isotopes. *Trends in Ecology & Evolution* 19, 256–263. doi: 10.1016/j.tree.2004.03.017

Ruckstuhl, K. E., Johnson, E. A., and Miyanishi, K. (2008). Introduction. The boreal forest and global change. *Philos Trans R Soc Lond B Biol Sci* 363, 2245–2249. doi: 10.1098/rstb.2007.2196

Rumman, R., Atkin, O. K., Bloomfield, K. J., and Eamus, D. (2018). Variation in bulk-leaf 13C discrimination, leaf traits and water-use efficiency–trait relationships along a continental-scale climate gradient in Australia. *Global Change Biology* 24, 1186–1200. doi: 10.1111/gcb.13911

Running, S., Mu, Q., and Zhao, M. (2015). MOD17A3H MODIS/Terra Net Primary Production Yearly L4 Global 500m SIN Grid V006. doi: https://doi.org/10.5067/MODIS/MOD17A3H.006 Date

Running, S., Mu, Q., and Zhao, M. (2017). MOD16A3 MODIS/Terra Net Evapotranspiration Yearly L4 Global 500m SIN Grid V006. doi: https://doi.org/10.5067/MODIS/MOD16A3.006

Sanders, C. J. (1983). Local Dispersal of Male Spruce Budworm (Lepidoptera: Tortricidae) Moth Determined by Mark, Release, and Recapture. *Can Entomol* 115, 1065–1070. doi: 10.4039/Ent1151065-9

Saskatechewan Ministry of Environment (2018). Forest Pest Fact Sheet. Available at: https://web.archive.org/web/20180428134459/http://web.forestry.ubc.ca/fetch21/Z-PDF-pest-info-folder/Eastern%20spruce%20budworm.pdf (Accessed May 30, 2026).

Sato, N., and Azuma, N. (2016). Isotopic fractionation with morphological change and sexual specificity in the lappet moth Euthrix potatoria. *Entomologia Experimentalis et Applicata* 161, 181–186. doi: 10.1111/eea.12509

Schiff, S. L., Spoelstra, J., Semkin, R. G., and Jeffries, D. S. (2005). Drought induced pulses of SO42-from a Canadian shield wetland: use of δ34S and δ18O in SO42- to determine sources of sulfur. *Applied Geochemistry* 20, 691–700. doi: 10.1016/j.apgeochem.2004.11.011

Schimel, J. P., and Bennett, J. (2004). Nitrogen Mineralization: Challenges of a Changing Paradigm. *Ecology* 85, 591–602. doi: 10.1890/03-8002

Schuur, E. A. G., and Mack, M. C. (2018). Ecological Response to Permafrost Thaw and Consequences for Local and Global Ecosystem Services. *Annual Review of Ecology, Evolution, and Systematics* 49, 279–301. doi: 10.1146/annurev-ecolsys-121415-032349

Sharp, Z. (2007). *Principles of stable isotope geochemistry*. Upper Saddle River (N. J.): Pearson Prentice Hall.

Shilts, W., Aylsworth, J., Kaszycki, C., and Klassen, R. (1987). "Canadian Shield," in *Geomorphic systems in North America*, (Boulder, Colorado, USA: Geological Society of America), 119–163. doi: 10.1130/DNAG-CENT-v2.119

Shu, Y., Feng, X., Posmentier, E. S., Faiia, A. M., Ayres, M. P., Conkey, L. E., et al. (2008). Isotopic studies of leaf water. Part 2: Between-age isotopic variations in pine needles. *Geochimica et Cosmochimica Acta* 72, 5189–5200. doi: 10.1016/j.gca.2008.08.015

Simard, I., Morin, H., and Lavoie, C. (2006). A millennial-scale reconstruction of spruce budworm abundance in Saguenay, Quéebec, Canada. *The Holocene* 16, 31–37. doi: 10.1191/0959683606hl904rp

Soto, D. X., Koehler, G., Wassenaar, L. I., and Hobson, K. A. (2017). Re-evaluation of the hydrogen stable isotopic composition of keratin calibration standards for wildlife and forensic science applications. *Rapid Communications in Mass Spectrometry* 31, 1193–1203. doi: 10.1002/rcm.7893

Souza-Silva, I. M., Martinelli, L. A., Holmes, B., Batista, A. C. G., Araújo, M. G. S., Garção, A. L., et al. (2026). Machine-learning models of δ^{13}C and δ^{15}N isoscapes in Amazonian wood. *Biogeosciences* 23, 881–904. doi: 10.5194/bg-23-881-2026

Sparks, J. M., Crowley, B. E., Rutherford, M. G., and Jaggernauth, D. (2019). Coastal proximity, orientation, and precipitation amount drive spatial variability in δ34S values on the Caribbean island of Trinidad. *Applied Geochemistry* 108. doi: 10.1016/j.apgeochem.2019.104372

Spence, K. O., and Rosenheim, J. A. (2005). Isotopic Enrichment in Herbivorous Insects: A Comparative Field-Based Study of Variation. *Oecologia* 146, 89–97.

Stantis, C., Willmes, M., Le Corre, M., James, H. F., Kafino, C., Verostick, K. A., et al. (2026). Global compilation of bioavailable strontium isotope data. *Sci Data* 13, 299. doi: 10.1038/s41597-026-06643-3

Stephens, R. B., Ouimette, A. P., Hobbie, E. A., and Rowe, R. J. (2022). Reevaluating trophic discrimination factors (Δδ13C and Δδ15N) for diet reconstruction. *Ecological Monographs* 92, e1525. doi: 10.1002/ecm.1525

Stephens, R. B., Shipley, O. N., and Moll, R. J. (2023). Meta-analysis and critical review of trophic discrimination factors (Δ13C and Δ15N): Importance of tissue, trophic level and diet source. *Functional Ecology* 37, 2535–2548. doi: 10.1111/1365-2435.14403

Sterner, T. E., and Davidson, A. G. (1982). Forest insect and disease conditions in Canada, 1981.

Stevens, R. E., Reade, H., Sayle, K. L., Tripp, J. A., Frémondeau, D., Lister, A., et al. (2025). Major excursions in sulfur isotopes linked to permafrost change in Eurasia during the last 50,000 years. *Nat. Geosci.* 18, 961–965. doi: 10.1038/s41561-025-01760-x

Stewart, M. K. (1975). Stable isotope fractionation due to evaporation and isotopic exchange of falling waterdrops: Applications to atmospheric processes and evaporation of lakes. *Journal of Geophysical Research (1896-1977)* 80, 1133–1146. doi: 10.1029/JC080i009p01133

Stralberg, D., Arseneault, D., Baltzer, J. L., Barber, Q. E., Bayne, E. M., Boulanger, Y., et al. (2020). Climate-change refugia in boreal North America: what, where, and for how long? *Frontiers in Ecology and the Environment* 18, 261–270. doi: 10.1002/fee.2188

Sturtevant, B. R., Achtemeier, G. L., Charney, J. J., Anderson, D. P., Cooke, B. J., and Townsend, P. A. (2013). Long-distance dispersal of spruce budworm (Choristoneura fumiferana Clemens) in Minnesota (USA) and Ontario (Canada) via the atmospheric pathway. *Agricultural and Forest Meteorology* 168, 186–200. doi: 10.1016/j.agrformet.2012.09.008

Tarrant, D., and Richards, M. P. (2024). Modern plants and sulfur isoscapes — A review, discussion, and construction of a pilot δ34S isoscape for mobility and provenance studies. *Rapid Communications in Mass Spectrometry* 38, e9908. doi: 10.1002/rcm.9908

Terzer, S., Wassenaar, L. I., Araguás-Araguás, L. J., and Aggarwal, P. K. (2013). Global isoscapes for $\delta^{18}O$ and $\delta^{2}H$ in precipitation: improved prediction using regionalized climatic regression models. *Hydrology and Earth System Sciences* 17, 4713–4728. doi: 10.5194/hess-17-4713-2013

Thériault, R., and Beauséjour, S. (2012). Geological map of Québec, DV2012-07. *Ministère des Ressources naturelles et des Forêts, Québec*.

Thode, H. G. (1991). "Sulphur Isotopes in Nature and the Environment: An Overview," in *Stable isotopes: Natural and anthropogenic sulphur in the environment*, (John Wiley and Sons). Available at: https://scope.dge.carnegiescience.edu/SCOPE_43/SCOPE_43_1_Chp1.pdf (Accessed February 17, 2025).

Tibbets, T. M., Wheeless, L. A., and Del Rio, C. M. (2008). Isotopic enrichment without change in diet: an ontogenetic shift in δ15N during insect metamorphosis. *Functional Ecology* 22, 109–113. doi: 10.1111/j.1365-2435.2007.01342.x

Trabucco, A., and Zomer, R. J. (2019). Global Aridity Index and Potential Evapotranspiration Climate Database v2. Available at: https://csidotinfo.wordpress.com/2019/01/24/global-aridity-index-and-potential-evapotranspiration-climate-database-v2/ (Accessed May 11, 2026).

Trueman, C. N., MacKenzie, K. M., and St John Glew, K. (2017). Stable isotope-based location in a shelf sea setting: accuracy and precision are comparable to light-based location methods. *Methods in Ecology and Evolution* 8, 232–240. doi: 10.1111/2041-210X.12651

Trust, B. A., and Fry, B. (1992). Stable sulphur isotopes in plants: a review. *Plant, Cell & Environment* 15, 1105–1110. doi: 10.1111/j.1365-3040.1992.tb01661.x

Truszkowski, J., Maor, R., Yousuf, R. B., Biswas, S., Chater, C., Gasson, P., et al. (2025). A probabilistic approach to estimating timber harvest location. *Ecological Applications* 35, e3077. doi: 10.1002/eap.3077

Tucker, M. A., Böhning-Gaese, K., Fagan, W. F., Fryxell, J. M., Van Moorter, B., Alberts, S. C., et al. (2018). Moving in the Anthropocene: Global reductions in terrestrial mammalian movements. *Science* 359, 466–469. doi: 10.1126/science.aam9712

USGS (2011). Report of Stable Isotopic Composition: Reference Material USGS41. United States Geological Survey.

USGS (2019). Report of Stable Isotopic Composition: Reference Material USGS40. United States Geological Survey. Available at: https://d9-wret.s3.us-west-

2.amazonaws.com/assets/palladium/production/s3fs-public/atoms/files/USGS40_0.pdf (Accessed June 5, 2026).

Vander Zanden, H. B., Soto, D. X., Bowen, G. J., and Hobson, K. A. (2016). Expanding the Isotopic Toolbox: Applications of Hydrogen and Oxygen Stable Isotope Ratios to Food Web Studies. *Front. Ecol. Evol.* 4. doi: 10.3389/fevo.2016.00020

Vander Zanden, H. B., Wunder, M. B., Hobson, K. A., Van Wilgenburg, S. L., Wassenaar, L. I., Welker, J. M., et al. (2014). Contrasting assignment of migratory organisms to geographic origins using long-term versus year-specific precipitation isotope maps. *Methods in Ecology and Evolution* 5, 891–900. doi: 10.1111/2041-210X.12229

Waight, T., Baker, J., and Peate, D. (2002). Sr isotope ratio measurements by double-focusing MC-ICPMS: techniques, observations and pitfalls. *International Journal of Mass Spectrometry* 221, 229–244. doi: 10.1016/S1387-3806(02)01016-3

Wainwright, C. E., Stepanian, P. M., Reynolds, D. R., and Reynolds, A. M. (2017). The movement of small insects in the convective boundary layer: linking patterns to processes. *Sci Rep* 7, 5438. doi: 10.1038/s41598-017-04503-0

Wardlaw, A. A., Perrault, K., Roe, A. D., Dedes, J., Irwin, C. L., MacQuarrie, C. J. K., et al. (2022). Methods for estimating and modelling spruce budworm development rates at constant temperatures. *The Canadian Entomologist* 154, e9. doi: 10.4039/tce.2021.56

Wassenaar, L. I. (2019). "Chapter 02 - Introduction to Conducting Stable Isotope Measurements for Animal Migration Studies," in *Tracking Animal Migration with Stable Isotopes*, (Elsevier), 25–51. doi: 10.1016/B978-0-12-814723-8.00002-7

Wells, J. V. ed. (2011). *Boreal Birds of North America*. University of California Press. doi: 10.1525/9780520950580

West, J. B., Bowen, G. J., Dawson, T. E., and Tu, K. P. eds. (2010). *Isoscapes*. Dordrecht: Springer Netherlands. doi: 10.1007/978-90-481-3354-3

West, J. B., Sobek, A., and Ehleringer, J. R. (2008). A Simplified GIS Approach to Modeling Global Leaf Water Isoscapes. *PLoS ONE* 3, e2447–e2447. doi: 10.1371/journal.pone.0002447

Whitehead, D. (1998). Regulation of stomatal conductance and transpiration in forest canopies. *Tree Physiology* 18, 633–644. doi: 10.1093/treephys/18.8-9.633

Wickham, H. (2016). *ggplot2: Elegant Graphics for Data Analysis*. Springer-Verlag New York. Available at: https://ggplot2.tidyverse.org

Wickham, H., Averick, M., Bryan, J., Chang, W., McGowan, L. D., François, R., et al. (2019). Welcome to the tidyverse. *Journal of Open Source Software* 4, 1686. doi: 10.21105/joss.01686

Wolken, J. M., Hollingsworth, T. N., Rupp, T. S., Chapin III, F. S., Trainor, S. F., Barrett, T. M., et al. (2011). Evidence and implications of recent and projected climate change in Alaska's forest ecosystems. *Ecosphere* 2, art124. doi: 10.1890/ES11-00288.1

Wooller, M. J., Bataille, C., Druckenmiller, P., Erickson, G. M., Groves, P., Haubenstock, N., et al. (2021). Lifetime mobility of an Arctic woolly mammoth. *Science* 373, 806–808. doi: 10.1126/science.abg1134

Wunder, M. B. (2010). "Using Isoscapes to Model Probability Surfaces for Determining Geographic Origins," in *Isoscapes: Understanding movement, pattern, and process on Earth through isotope mapping*, eds. J. B. West, G. J. Bowen, T. E. Dawson, and K. P. Tu (Dordrecht: Springer Netherlands), 251–270. doi: 10.1007/978-90-481-3354-3_12

Wunder, M. B. (2012). Determining geographic patterns of migration and dispersal using stable isotopes in keratins. *Journal of Mammalogy* 93, 360–367. doi: 10.1644/11-MAMM-S-182.1

Wunder, M. B., Kester, C. L., Knopf, F. L., and Rye, R. O. (2005). A test of geographic assignment using isotope tracers in feathers of known origin. *Oecologia* 144, 607–617. doi: 10.1007/s00442-005-0071-y

Wunder, M. B., and Norris, D. R. (2008). Improved Estimates of Certainty in Stable-Isotope-Based Methods for Tracking Migratory Animals. *Ecological Applications* 18, 549–559. doi: 10.1890/07-0058.1

Wunder, M. B., and Norris, D. R. (2019). "Chapter 08 - Design and Analysis for Isotope-Based Studies of Migratory Animals," in *Tracking Animal Migration with Stable Isotopes*, (Elsevier), 191–206. doi: 10.1016/B978-0-12-814723-8.00008-8

SUPPLEMENTARY

Table S1 – Known-origin foliage samples

Site	Latitude	Longitude	$\delta^{2}H$ (‰)	$\delta^{13}C$ (‰)	$\delta^{15}N$ (‰)	$\delta^{34}S$ (‰)	$^{87}Sr/^{86}Sr$
Block 101e	50.87956	-56.91763	-	-	-	9.40 ± 0.22	0.710630 ± 0.000105
Block 322	49.39097	-57.66103	-131.0 ± 0.7	-	-	13.60 ± 0.22	0.711256 ± 0.000050
Block 405	48.93961	-58.40058	-127.3 ± 0.7	-	-	14.20 ± 0.22	0.713239 ± 0.000075
Control 12	50.11000	-57.66000	-124.5 ± 0.7	-	-	15.60 ± 0.22	0.711721 ± 0.000080
Grey 2	46.63493	-80.24853	-	-	-	4.90 ± 0.00	-
JN13	47.05850	-80.24853	-129.5 ± 0.7	-	-	1.50 ± 0.00	0.718154 ± 0.000080
JN14	46.95170	-79.77200	-118.8 ± 0.7	-	-	3.20 ± 0.40	-
KO1	47.31834	-81.76209	-144.0 ± 0.7	-30.50 ± 0.10	-2.40 ± 0.10	3.30 ± 0.00	0.714510 ± 0.000064
KO11	47.07022	-79.76510	-130.0 ± 0.7	-	-	2.60 ± 0.00	0.719980 ± 0.000067
KO12	47.34174	-79.80245	-	-	-	4.00 ± 0.40	-
KO13	46.52517	-79.55433	-112.5 ± 0.7	-	-	5.20 ± 0.40	0.729022 ± 0.000053
KO14	46.03226	-79.36216	-125.0 ± 0.7	-	-	4.00 ± 0.40	-
KO16	46.25990	-78.34390	-118.0 ± 0.7	-	-	5.10 ± 0.00	0.715973 ± 0.000058
KO2	47.31834	-81.58175	-145.0 ± 0.7	-31.10 ± 0.10	-6.40 ± 0.10	3.60 ± 0.40	-
KO3	48.43153	-81.68478	-135.0 ± 0.7	-29.00 ± 0.10	-5.10 ± 0.10	4.30 ± 0.00	0.715373 ± 0.000100
KO4	48.40571	-81.68267	-127.5 ± 0.7	-	-	4.20 ± 0.00	0.715954 ± 0.000042
KO5	49.12400	-81.36578	-156.0 ± 0.7	-31.00 ± 0.10	-1.60 ± 0.10	3.50 ± 0.00	0.714739 ± 0.000065
KO6	47.79829	-79.63181	-138.0 ± 0.7	-31.10 ± 0.10	-2.90 ± 0.10	3.70 ± 0.00	0.712536 ± 0.000053
Light Orange 3	46.87602	-79.76968	-148.0 ± 0.7	-	-	3.70 ± 0.40	0.716376 ± 0.000068
Neys	48.79333	-86.58409	-139.0 ± 0.7	-29.70 ± 0.10	-4.20 ± 0.10	4.30 ± 0.00	0.710910 ± 0.000071
Nipigon	49.01458	-88.18948	-148.0 ± 0.7	-32.00 ± 0.10	-5.70 ± 0.10	7.00 ± 0.00	0.717943 ± 0.000072
St Joes	46.24400	-83.93700	-113.0 ± 0.7	-	-	4.50 ± 0.40	0.714514 ± 0.000074
Trout lake	46.63427	-84.29080	-	-	-	3.50 ± 0.40	-
White river	48.61890	-85.33645	-	-	-	5.90 ± 0.40	-

Table S2– Known Origin SBW Samples

Site	Sample ID	Latitude	Longitude	$\delta^{2}H$ (‰)	$\delta^{13}C$ (‰)	$\delta^{15}N$ (‰)	$\delta^{34}S$ (‰)	$^{87}Sr/^{86}Sr$
block 101e	236_Bl101E_id1	50.879560	-56.917630	-	-	-	-	0.716210 ± 0.000430
block 101e	288_Bl101E_id7	50.879560	-56.917630	-	-	-	-	0.713383 ± 0.000273
block 101e	289_Bl101E_id8	50.879560	-56.917630	-	-	-	-	0.712257 ± 0.000269
block 101e	NFLD_Bl101E_id3_ko	50.879560	-56.917630	-	-	-	11.50 ± 0.20	-
block 101e	NFLD_Bl101E_id5_ko	50.879560	-56.917630	-	-	-	11.90 ± 0.20	-
block 101e	NFLD_Bl101E_id4_ko	50.879560	-56.917630	-	-	-	14.00 ± 0.20	-
block 322	243_Bl322_id1	49.252150	-57.877600	-	-	-	-	0.717182 ± 0.000467
block 322	292_Bl322_id7	49.390970	-57.661030	-	-	-	-	0.708252 ± 0.000480
block 322	293_Bl322_id8	49.390970	-57.661030	-	-	-	-	0.711481 ± 0.000175
block 322	NL_Blk322_id2_KO_H	49.390970	-57.661030	-85.1 ± 0.7	-	-	-	-
block 322	NL_Blk322_id1_KO_H	49.390970	-57.661030	-94.0 ± 0.7	-	-	-	-
block 322	NFLD_Bl322_id3_ko	49.390970	-57.661030	-97.0 ± 0.7	-	-	10.40 ± 0.20	-
block 322	NFLD_Bl322_id4_ko	49.390970	-57.661030	-94.0 ± 0.7	-	-	11.90 ± 0.20	-
block 322	NFLD_BL322_id5_ko	49.390970	-57.661030	-94.0 ± 0.7	-	-	12.30 ± 0.20	-
block 405	248_Bl405_id1	48.939610	-58.400580	-	-	-	-	0.712992 ± 0.000053
block 405	249_Bl405_id2	48.939610	-58.400580	-	-	-	-	0.712979 ± 0.000072
block 405	250_Bl405_id6	48.939610	-58.400580	-	-	-	-	0.714566 ± 0.000919
block 405	NL_Blk405_id2_KO_H	48.939610	-58.400580	-90.6 ± 0.7	-	-	-	-
block 405	NL_Blk405_id1_KO_H	48.939610	-58.400580	-97.2 ± 0.7	-	-	-	-
block 405	NFLD_405_id4_ko	48.939610	-58.400580	-91.0 ± 0.7	-	-	10.90 ± 0.20	-
block 405	NFLD_405_id3_ko	48.939610	-58.400580	-96.0 ± 0.7	-	-	12.30 ± 0.20	-
control 12	234_Ctrl12_id6	50.110000	-57.660000	-	-	-	-	0.710452 ± 0.000120
control 12	254_Ctrl12_id1	50.110000	-57.660000	-	-	-	-	0.710414 ± 0.000070
control 12	255_Ctrl12_id2	50.110000	-57.660000	-	-	-	-	0.712732 ± 0.000309
control 12	NL_ctrl12_id2_KO_H	50.110000	-57.660000	-90.1 ± 0.7	-	-	-	-
control 12	NL_ctrl12_id1_KO_H	50.110000	-57.660000	-95.1 ± 0.7	-	-	-	-
control 12	NFLD_C12_id4_ko	50.110000	-57.660000	-105.0 ± 0.7	-	-	15.20 ± 0.20	-
control 12	NFLD_C12_id3_ko	50.110000	-57.660000	-106.0 ± 0.7	-	-	15.30 ± 0.20	-
grey 2	G2_3/3_id1_ko	46.634930	-80.248530	-	-	-	3.90 ± 0.20	-
grey 2	G2_3/3_id2_ko	46.634930	-80.248530	-	-	-	4.30 ± 0.20	-

Site	Sample ID	Latitude	Longitude	$\delta^{2}H$ (‰)	$\delta^{13}C$ (‰)	$\delta^{15}N$ (‰)	$\delta^{34}S$ (‰)	$^{87}Sr/^{86}Sr$
grey 2	G2_3/3_id3_ko	46.634930	-80.248530	-	-	-	4.90 ± 0.20	-
jn13	263_JN13_id6	47.058500	-79.781700	-	-	-	-	0.716445 ± 0.000129
jn13	264_JN13_id7	47.058500	-79.781700	-	-	-	-	0.717837 ± 0.000171
jn13	265_JN13_id8	47.058500	-79.781700	-	-	-	-	0.717470 ± 0.000047
jn13	JN13_DO3_id7	47.058500	-79.781700	-90.0 ± 1.6	-	-	-	-
jn13	JN13_DO3_id6	47.058500	-79.781700	-99.0 ± 1.6	-	-	-	-
jn13	DO3_id4_ko	47.058500	-79.781700	-102.0 ± 0.7	-	-	0.90 ± 0.20	-
jn13	DO3_id5_ko	47.058500	-79.781700	-79.0 ± 0.7	-	-	1.20 ± 0.20	-
jn13	DO3_id3_ko	47.058500	-79.781700	-90.0 ± 0.7	-	-	1.20 ± 0.20	-
jn13	DO3_id2_ko	47.058500	-79.781700	-100.0 ± 0.7	-	-	1.30 ± 0.20	-
jn13	DO3_id1_ko	47.058500	-79.781700	-102.5 ± 0.7	-	-	2.00 ± 0.20	-
jn14	JN14_DR1_x_id6	46.951700	-79.772000	-79.0 ± 1.6	-	-	-	-
jn14	JN14_DR1_x_id4	46.951700	-79.772000	-88.0 ± 1.6	-	-	-	-
jn14	JN14_DR1_x_id5	46.951700	-79.772000	-92.0 ± 1.6	-	-	-	-
jn14	DR1_id2_ko	46.951700	-79.772000	-93.0 ± 0.7	-	-	2.50 ± 0.20	-
jn14	DR1_id1_ko	46.951700	-79.772000	-85.0 ± 0.7	-	-	2.90 ± 0.20	-
jn14	DR1_id3_ko	46.951700	-79.772000	-98.0 ± 0.7	-	-	4.20 ± 0.20	-
ko1	210_KO1_id4	47.318339	-81.762094	-	-	-	-	0.714072 ± 0.000069
ko1	211_KO1_id5	47.318339	-81.762094	-	-	-	-	0.714824 ± 0.000045
ko1	212_KO1_id6	47.318339	-81.762094	-	-	-	-	0.714769 ± 0.000038
ko1	KO1_x_x_id2_ko	47.318339	-81.762094	-101.0 ± 0.7	-	-	-	-
ko1	KO1_x_x_id1_ko	47.318339	-81.762094	-85.0 ± 0.7	-	-	-	-
ko1	KO1_x_x_id7	47.318339	-81.762094	-87.0 ± 1.6	-	-	-	-
ko1	KO1_x_x_id3_ko	47.318339	-81.762094	-88.0 ± 0.7	-	-	-	-
ko1	KO1_x_x_id6	47.318339	-81.762094	-91.0 ± 1.6	-	-	-	-
ko1	KO1_x_x_id5	47.318339	-81.762094	-94.0 ± 1.6	-	-	-	-
ko1	KO1_x_x_id4	47.318339	-81.762094	-96.0 ± 1.6	-	-	-	-
ko1	KO1_x_x_id8	47.318339	-81.762094	-98.0 ± 1.6	-	-	-	-
ko1	KO1_id11	47.318339	-81.762094	-	-29.00 ± 0.03	2.50 ± 0.01	-	-
ko1	KO1_id10	47.318339	-81.762094	-	-28.20 ± 0.03	2.90 ± 0.01	-	-
ko1	KO1_id13	47.318339	-81.762094	-	-28.80 ± 0.03	3.00 ± 0.01	-	-
ko1	KO1_x_x_id1	47.318339	-81.762094	-	-	-	3.50 ± 0.20	-
ko1	KO1_x_x_id3	47.318339	-81.762094	-	-	-	3.90 ± 0.20	-

Site	Sample ID	Latitude	Longitude	$\delta^{2}H$ (‰)	$\delta^{13}C$ (‰)	$\delta^{15}N$ (‰)	$\delta^{34}S$ (‰)	$^{87}Sr/^{86}Sr$
ko1	KO1_x_x_id2	47.318339	-81.762094	-	-	-	4.40 ± 0.20	-
ko11	222_KO11A_id4	47.070221	-79.765099	-	-	-	-	0.718858 ± 0.000112
ko11	223_KO11A_id5	47.070221	-79.765099	-	-	-	-	0.718905 ± 0.000087
ko11	224_KO11A_id6	47.070221	-79.765099	-	-	-	-	0.714635 ± 0.000370
ko11	282_KO11A_id7	47.070221	-79.765099	-	-	-	-	0.722321 ± 0.000251
ko11	283_KO11A_id8	47.070221	-79.765099	-	-	-	-	0.717332 ± 0.000096
ko11	284_KO11A_id9	47.070221	-79.765099	-	-	-	-	0.718332 ± 0.000058
ko11	KO11_LR1_B_id1_ko	47.070221	-79.765099	-94.5 ± 0.7	-	-	-	-
ko11	KO11_LR3_id3_ko	47.070221	-79.765099	-91.0 ± 0.7	-	-	0.90 ± 0.20	-
ko11	KO11_LR1_B_id1	47.070221	-79.765099	-	-	-	1.40 ± 0.20	-
ko11	KO11_LR3_id1_ko	47.070221	-79.765099	-101.5 ± 0.7	-	-	1.60 ± 0.20	-
ko11	KO11_LR1_A_id3	47.070221	-79.765099	-	-	-	1.80 ± 0.20	-
ko11	KO11_LR3_id2_ko	47.070221	-79.765099	-86.0 ± 0.7	-	-	2.20 ± 0.20	-
ko11	KO11_LR3_id5_ko	47.070221	-79.765099	-97.0 ± 0.7	-	-	2.20 ± 0.20	-
ko11	KO11_LR3_id4_ko	47.070221	-79.765099	-102.0 ± 0.7	-	-	2.50 ± 0.20	-
ko11	KO11_LR1_A_id2	47.070221	-79.765099	-	-	-	2.60 ± 0.20	-
ko11	KO11_LR1_A_id1	47.070221	-79.765099	-	-	-	4.20 ± 0.20	-
ko13	260_KO13_id3	46.525171	-79.554327	-	-	-	-	0.716959 ± 0.000049
ko13	261_KO13_id4	46.525171	-79.554327	-	-	-	-	0.723825 ± 0.000092
ko13	262_KO13_id5	46.525171	-79.554327	-	-	-	-	0.723634 ± 0.000335
ko13	KO13_Y1_x_id5	46.525171	-79.554327	-104.0 ± 1.6	-	-	-	-
ko13	KO13_Y1_x_id4	46.525171	-79.554327	-108.0 ± 1.6	-	-	-	-
ko13	KO13_Y1_x_id1_ko	46.525171	-79.554327	-88.5 ± 0.7	-	-	-	-
ko13	KO13_Y1_x_id3	46.525171	-79.554327	-96.0 ± 1.6	-	-	-	-
ko13	KO13_Y1_x_id2_ko	46.525171	-79.554327	-99.0 ± 0.7	-	-	-	-
ko13	KO13_Y1_x_id1	46.525171	-79.554327	-	-	-	3.70 ± 0.20	-
ko13	KO13_Y1_x_id2	46.525171	-79.554327	-	-	-	5.10 ± 0.20	-
ko14	KO14_Y2_x_id5	46.032261	-79.362155	-106.0 ± 1.6	-	-	-	-
ko14	KO14_Y2_x_id1_ko	46.032261	-79.362155	-79.0 ± 0.7	-	-	-	-
ko14	KO14_Y2_x_id3_ko	46.032261	-79.362155	-82.0 ± 0.7	-	-	-	-
ko14	KO14_Y2_x_id2_ko	46.032261	-79.362155	-92.0 ± 0.7	-	-	-	-
ko14	KO14_Y2_x_id4	46.032261	-79.362155	-96.0 ± 1.6	-	-	-	-
ko14	KO14_Y2_x_id1	46.032261	-79.362155	-	-	-	4.00 ± 0.20	-

Site	Sample ID	Latitude	Longitude	$\delta^{2}H$ (‰)	$\delta^{13}C$ (‰)	$\delta^{15}N$ (‰)	$\delta^{34}S$ (‰)	$^{87}Sr/^{86}Sr$
ko14	KO14_Y2_x_id2	46.032261	-79.362155	-	-	-	4.00 ± 0.20	-
ko14	KO14_Y2_x_id3	46.032261	-79.362155	-	-	-	4.10 ± 0.20	-
ko16	225_KO16_id4	46.259900	-78.343900	-	-	-	-	0.714112 ± 0.000098
ko16	226_KO16_id5	46.259900	-78.343900	-	-	-	-	0.712135 ± 0.000040
ko16	227_KO16_id6	46.259900	-78.343900	-	-	-	-	0.712442 ± 0.000038
ko16	KO16_Y3_x_id6	46.259900	-78.343900	-103.0 ± 1.6	-	-	-	-
ko16	KO16_Y3_x_id8	46.259900	-78.343900	-109.0 ± 1.6	-	-	-	-
ko16	KO16_Y3_x_id4	46.259900	-78.343900	-96.0 ± 1.6	-	-	-	-
ko16	KO16_Y3_x_id7	46.259900	-78.343900	-96.0 ± 1.6	-	-	-	-
ko16	KO16_Y3_x_id5	46.259900	-78.343900	-99.0 ± 1.6	-	-	-	-
ko16	KO16_Y3_id1_ko	46.259900	-78.343900	-86.0 ± 0.7	-	-	4.70 ± 0.20	-
ko16	KO16_Y3_id3_ko	46.259900	-78.343900	-116.0 ± 0.7	-	-	4.80 ± 0.20	-
ko16	KO16_Y3_id2_ko	46.259900	-78.343900	-130.0 ± 0.7	-	-	5.10 ± 0.20	-
ko2	KO2_x_3_id1_ko	47.318339	-81.581746	-100.0 ± 0.7	-	-	-	-
ko2	KO2_x_3_id3_ko	47.318339	-81.581746	-100.0 ± 0.7	-	-	-	-
ko2	KO2_x_3_id8	47.318339	-81.581746	-101.0 ± 0.7	-	-	-	-
ko2	KO2_x_3_id6	47.318339	-81.581746	-106.0 ± 0.7	-	-	-	-
ko2	KO2_x_3_id7	47.318339	-81.581746	-112.0 ± 0.7	-	-	-	-
ko2	KO2_x_3_id4	47.318339	-81.581746	-91.0 ± 0.7	-	-	-	-
ko2	KO2_x_3_id2_ko	47.318339	-81.581746	-99.0 ± 0.7	-	-	-	-
ko2	KO2_x_3_id5	47.318339	-81.581746	-99.0 ± 0.7	-	-	-	-
ko2	KO2_3_id9	47.318339	-81.581746	-	-27.10 ± 0.03	-0.20 ± 0.01	-	-
ko2	KO2_3_id10	47.318339	-81.581746	-	-27.40 ± 0.03	-0.50 ± 0.01	-	-
ko2	KO2_3_id13	47.318339	-81.581746	-	-27.90 ± 0.03	-0.60 ± 0.01	-	-
ko2	KO2_3_id11	47.318339	-81.581746	-	-27.90 ± 0.03	-0.70 ± 0.01	-	-
ko2	KO2_3_id12	47.318339	-81.581746	-	-27.20 ± 0.03	-0.80 ± 0.01	-	-
ko2	KO2_x_3_id3	47.318339	-81.581746	-	-	-	1.90 ± 0.20	-
ko2	KO2_x_3_id2	47.318339	-81.581746	-	-	-	2.30 ± 0.20	-
ko2	KO2_x_3_id1	47.318339	-81.581746	-	-	-	3.00 ± 0.20	-
ko3	213_KO3_id4	48.431525	-81.684781	-	-	-	-	0.715750 ± 0.000025
ko3	214_KO3_id5	48.431525	-81.684781	-	-	-	-	0.718739 ± 0.000034
ko3	215_KO3_id6	48.431525	-81.684781	-	-	-	-	0.715975 ± 0.000052
ko3	KO3_x_1_id6	48.431525	-81.684781	-102.0 ± 0.7	-	-	-	-

Site	Sample ID	Latitude	Longitude	$\delta^{2}H$ (‰)	$\delta^{13}C$ (‰)	$\delta^{15}N$ (‰)	$\delta^{34}S$ (‰)	$^{87}Sr/^{86}Sr$
ko3	KO3_x_1_id4	48.431525	-81.684781	-104.0 ± 0.7	-	-	-	-
ko3	KO3_x_1_id8	48.431525	-81.684781	-104.0 ± 0.7	-	-	-	-
ko3	KO3_x_1_id1_ko	48.431525	-81.684781	-118.0 ± 0.7	-	-	-	-
ko3	KO3_x_1_id3_ko	48.431525	-81.684781	-93.0 ± 0.7	-	-	-	-
ko3	KO3_x_1_id2_ko	48.431525	-81.684781	-97.0 ± 0.7	-	-	-	-
ko3	KO3_x_1_id5	48.431525	-81.684781	-99.0 ± 0.7	-	-	-	-
ko3	KO3_1_id15	48.431525	-81.684781	-	-25.90 ± 0.03	-0.80 ± 0.01	-	-
ko3	KO3_1_id16	48.431525	-81.684781	-	-25.70 ± 0.03	-1.20 ± 0.01	-	-
ko3	KO3_1_id17	48.431525	-81.684781	-	-25.80 ± 0.03	-1.20 ± 0.01	-	-
ko3	KO3_1_id19	48.431525	-81.684781	-	-26.00 ± 0.03	-1.40 ± 0.01	-	-
ko3	KO3_1_id18	48.431525	-81.684781	-	-25.60 ± 0.03	-1.50 ± 0.01	-	-
ko3	KO3_x_1_id1	48.431525	-81.684781	-	-	-	4.10 ± 0.20	-
ko3	KO3_x_1_id3	48.431525	-81.684781	-	-	-	4.10 ± 0.20	-
ko3	KO3_x_1_id2	48.431525	-81.684781	-	-	-	4.30 ± 0.20	-
ko4	216_KO4_id4	48.405714	-81.682667	-	-	-	-	0.716349 ± 0.000090
ko4	217_KO4_id5	48.405714	-81.682667	-	-	-	-	0.715831 ± 0.000089
ko4	218_KO4_id6	48.405714	-81.682667	-	-	-	-	0.717009 ± 0.000096
ko4	KO4_x_2_id4	48.405714	-81.682667	-101.0 ± 0.7	-	-	-	-
ko4	KO4_x_2_id8	48.405714	-81.682667	-103.5 ± 0.7	-	-	-	-
ko4	KO4_x_2_id2_ko	48.405714	-81.682667	-113.0 ± 0.7	-	-	-	-
ko4	KO4_x_2_id6	48.405714	-81.682667	-115.0 ± 0.7	-	-	-	-
ko4	KO4_x_2_id1_ko	48.405714	-81.682667	-120.0 ± 0.7	-	-	-	-
ko4	KO4_x_2_id3_ko	48.405714	-81.682667	-90.0 ± 0.7	-	-	-	-
ko4	KO4_x_2_id5	48.405714	-81.682667	-90.0 ± 0.7	-	-	-	-
ko4	KO4_x_2_id7	48.405714	-81.682667	-91.0 ± 0.7	-	-	-	-
ko4	KO4_x_2_id1	48.405714	-81.682667	-	-	-	4.90 ± 0.20	-
ko4	KO4_x_2_id2	48.405714	-81.682667	-	-	-	5.20 ± 0.20	-
ko4	KO4_x_2_id3	48.405714	-81.682667	-	-	-	5.30 ± 0.20	-
ko5	266_KO5(3)_id4	49.123997	-81.365782	-	-	-	-	0.713918 ± 0.000218
ko5	267_KO5(3)_id5	49.123997	-81.365782	-	-	-	-	0.715840 ± 0.000228
ko5	268_KO5(3)_id6	49.123997	-81.365782	-	-	-	-	0.717687 ± 0.000221
ko5	KO5_x_3_id5	49.123997	-81.365782	-100.0 ± 0.7	-	-	-	-
ko5	KO5_x_3_id3_ko	49.123997	-81.365782	-106.0 ± 0.7	-	-	-	-

Site	Sample ID	Latitude	Longitude	$\delta^{2}H$ (‰)	$\delta^{13}C$ (‰)	$\delta^{15}N$ (‰)	$\delta^{34}S$ (‰)	$^{87}Sr/^{86}Sr$
ko5	KO5_x_3_id8	49.123997	-81.365782	-107.0 ± 0.7	-	-	-	-
ko5	KO5_x_3_id1_ko	49.123997	-81.365782	-117.0 ± 0.7	-	-	-	-
ko5	KO5_x_3_id2_ko	49.123997	-81.365782	-121.0 ± 0.7	-	-	-	-
ko5	KO5_x_3_id7	49.123997	-81.365782	-97.0 ± 0.7	-	-	-	-
ko5	KO5_x_3_id6	49.123997	-81.365782	-99.0 ± 0.7	-	-	-	-
ko5	KO5_2_id15	49.123997	-81.365782	-	-28.50 ± 0.03	3.10 ± 0.01	-	-
ko5	KO5_2_id16	49.123997	-81.365782	-	-27.50 ± 0.03	3.50 ± 0.01	-	-
ko5	KO5_2_id17	49.123997	-81.365782	-	-27.50 ± 0.03	3.60 ± 0.01	-	-
ko5	KO5_1_id9	49.123997	-81.365782	-	-27.30 ± 0.03	3.70 ± 0.01	-	-
ko5	KO5_1_id12	49.123997	-81.365782	-	-27.30 ± 0.03	3.90 ± 0.01	-	-
ko5	KO5_1_id11	49.123997	-81.365782	-	-27.50 ± 0.03	3.90 ± 0.01	-	-
ko5	KO5_1_id10	49.123997	-81.365782	-	-27.70 ± 0.03	4.10 ± 0.01	-	-
ko5	KO5_2_id14	49.123997	-81.365782	-	-27.80 ± 0.03	4.10 ± 0.01	-	-
ko5	KO5_x_3_id3	49.123997	-81.365782	-	-	-	4.00 ± 0.20	-
ko5	KO5_x_3_id2	49.123997	-81.365782	-	-	-	4.20 ± 0.20	-
ko5	KO5_x_3_id1	49.123997	-81.365782	-	-	-	4.30 ± 0.20	-
ko6	219_KO6_id4	47.798294	-79.631813	-	-	-	-	0.714106 ± 0.000085
ko6	220_KO6_id5	47.798294	-79.631813	-	-	-	-	0.712401 ± 0.000278
ko6	221_KO6_id6	47.798294	-79.631813	-	-	-	-	0.714823 ± 0.000509
ko6	KO6_x_2_id1_ko	47.798294	-79.631813	-102.0 ± 0.7	-	-	-	-
ko6	KO6_x_2_id5	47.798294	-79.631813	-102.0 ± 1.6	-	-	-	-
ko6	KO6_x_2_id2_ko	47.798294	-79.631813	-89.0 ± 0.7	-	-	-	-
ko6	KO6_x_2_id3_ko	47.798294	-79.631813	-89.0 ± 0.7	-	-	-	-
ko6	KO6_x_2_id4	47.798294	-79.631813	-91.0 ± 1.6	-	-	-	-
ko6	KO6_x_2_id8	47.798294	-79.631813	-91.0 ± 1.6	-	-	-	-
ko6	KO6_x_2_id7	47.798294	-79.631813	-93.0 ± 1.6	-	-	-	-
ko6	KO6_x_2_id6	47.798294	-79.631813	-97.0 ± 1.6	-	-	-	-
ko6	KO6_1_id11	47.798294	-79.631813	-	-27.40 ± 0.03	2.90 ± 0.01	-	-
ko6	KO6_1_id13	47.798294	-79.631813	-	-27.00 ± 0.03	3.20 ± 0.01	-	-
ko6	KO6_1_id12	47.798294	-79.631813	-	-27.50 ± 0.03	3.20 ± 0.01	-	-
ko6	KO6_x_2_id1	47.798294	-79.631813	-	-	-	1.90 ± 0.20	-
ko6	KO6_x_2_id3	47.798294	-79.631813	-	-	-	2.20 ± 0.20	-
ko6	KO6_x_2_id2	47.798294	-79.631813	-	-	-	2.30 ± 0.20	-

Site	Sample ID	Latitude	Longitude	$\delta^{2}H$ (‰)	$\delta^{13}C$ (‰)	$\delta^{15}N$ (‰)	$\delta^{34}S$ (‰)	$^{87}Sr/^{86}Sr$
light orange 3	273_LO3_id4	46.876020	-79.769680	-	-	-	-	0.715684 ± 0.000041
light orange 3	274_LO3_id5	46.876020	-79.769680	-	-	-	-	0.713944 ± 0.000133
light orange 3	LO3_x_x_id1_ko	46.876020	-79.769680	-100.0 ± 0.7	-	-	-	-
light orange 3	LO3_x_x_id7_ko	46.876020	-79.769680	-100.0 ± 0.7	-	-	-	-
light orange 3	LO3_x_x_id5	46.876020	-79.769680	-105.0 ± 1.6	-	-	-	-
light orange 3	LO3_x_x_id4	46.876020	-79.769680	-109.0 ± 1.6	-	-	-	-
light orange 3	LO3_x_x_id3	46.876020	-79.769680	-115.0 ± 1.6	-	-	-	-
light orange 3	LO3_x_x_id6	46.876020	-79.769680	-121.0 ± 1.6	-	-	-	-
light orange 3	LO3_x_x_id2_ko	46.876020	-79.769680	-97.0 ± 0.7	-	-	-	-
light orange 3	LO3_x_x_id2	46.876020	-79.769680	-	-	-	3.40 ± 0.20	-
light orange 3	LO3_x_x_id7	46.876020	-79.769680	-	-	-	3.40 ± 0.20	-
light orange 3	LO3_x_x_id1	46.876020	-79.769680	-	-	-	3.50 ± 0.20	-
neys	231_NY_id4	48.793329	-86.584093	-	-	-	-	0.711381 ± 0.000127
neys	232_NY_id5	48.793329	-86.584093	-	-	-	-	0.710287 ± 0.000091
neys	233_NY_id6	48.793329	-86.584093	-	-	-	-	0.710373 ± 0.000127
neys	285_NY1_id7	48.793329	-86.584093	-	-	-	-	0.711116 ± 0.000120
neys	286_NY1_id8	48.793329	-86.584093	-	-	-	-	0.711726 ± 0.000096
neys	NY1_x_x_id1_ko	48.793329	-86.584093	-101.0 ± 0.7	-	-	-	-
neys	NY1_x_x_id5	48.793329	-86.584093	-102.0 ± 1.6	-	-	-	-
neys	NY1_x_x_id3_ko	48.793329	-86.584093	-105.0 ± 0.7	-	-	-	-
neys	NY1_x_x_id7	48.793329	-86.584093	-108.0 ± 1.6	-	-	-	-
neys	NY1_x_x_id6	48.793329	-86.584093	-110.0 ± 1.6	-	-	-	-
neys	NY1_x_x_id8	48.793329	-86.584093	-113.0 ± 1.6	-	-	-	-
neys	NY1_x_x_id4	48.793329	-86.584093	-96.0 ± 1.6	-	-	-	-
neys	NY1_x_x_id2_ko	48.793329	-86.584093	-98.0 ± 0.7	-	-	-	-
neys	NY1_id14	48.793329	-86.584093	-	-26.40 ± 0.03	1.10 ± 0.01	-	-
neys	NY3_id19	48.793329	-86.584093	-	-28.50 ± 0.03	1.50 ± 0.01	-	-
neys	NY3_id16	48.793329	-86.584093	-	-28.70 ± 0.03	1.50 ± 0.01	-	-
neys	NY3_id18	48.793329	-86.584093	-	-27.90 ± 0.03	1.70 ± 0.01	-	-
neys	NY1_id11	48.793329	-86.584093	-	-26.00 ± 0.03	1.80 ± 0.01	-	-
neys	NY1_id13	48.793329	-86.584093	-	-26.40 ± 0.03	1.80 ± 0.01	-	-
neys	NY1_id10	48.793329	-86.584093	-	-26.00 ± 0.03	2.00 ± 0.01	-	-
neys	NY3_id15	48.793329	-86.584093	-	-27.70 ± 0.03	2.10 ± 0.01	-	-

Site	Sample ID	Latitude	Longitude	$\delta^{2}H$ (‰)	$\delta^{13}C$ (‰)	$\delta^{15}N$ (‰)	$\delta^{34}S$ (‰)	$^{87}Sr/^{86}Sr$
neys	NY3_id17	48.793329	-86.584093	-	-28.90 ± 0.03	2.20 ± 0.01	-	-
neys	NY1_id12	48.793329	-86.584093	-	-26.20 ± 0.03	2.60 ± 0.01	-	-
neys	NY1_x_x_id3	48.793329	-86.584093	-	-	-	3.10 ± 0.20	-
neys	NY1_x_x_id2	48.793329	-86.584093	-	-	-	3.20 ± 0.20	-
neys	NY1_x_x_id1	48.793329	-86.584093	-	-	-	4.00 ± 0.20	-
nipigon	269_NP3_id4	49.014580	-88.189483	-	-	-	-	0.714955 ± 0.000165
nipigon	271_NP3_id6	49.014580	-88.189483	-	-	-	-	0.718208 ± 0.000241
nipigon	NP3_x_x_id2_ko	49.014580	-88.189483	-101.0 ± 0.7	-	-	-	-
nipigon	NP3_x_x_id8	49.014580	-88.189483	-101.0 ± 1.6	-	-	-	-
nipigon	NP3_x_x_id3_ko	49.014580	-88.189483	-102.0 ± 0.7	-	-	-	-
nipigon	NP3_x_x_id7	49.014580	-88.189483	-102.0 ± 1.6	-	-	-	-
nipigon	NP3_x_x_id5	49.014580	-88.189483	-108.0 ± 1.6	-	-	-	-
nipigon	NP3_x_x_id4	49.014580	-88.189483	-109.0 ± 1.6	-	-	-	-
nipigon	NP3_x_x_id6	49.014580	-88.189483	-109.0 ± 1.6	-	-	-	-
nipigon	NP3_x_x_id1_ko	49.014580	-88.189483	-98.0 ± 0.7	-	-	-	-
nipigon	NP3_id11	49.014580	-88.189483	-	-30.10 ± 0.03	-0.10 ± 0.01	-	-
nipigon	NP3_id9	49.014580	-88.189483	-	-30.50 ± 0.03	-0.60 ± 0.01	-	-
nipigon	NP3_id10	49.014580	-88.189483	-	-29.80 ± 0.03	-0.90 ± 0.01	-	-
nipigon	NP3_id12	49.014580	-88.189483	-	-29.90 ± 0.03	-1.40 ± 0.01	-	-
nipigon	NP3_x_x_id2	49.014580	-88.189483	-	-	-	5.30 ± 0.20	-
nipigon	NP3_x_x_id3	49.014580	-88.189483	-	-	-	5.50 ± 0.20	-
nipigon	NP3_x_x_id1	49.014580	-88.189483	-	-	-	7.40 ± 0.20	-
st joes	275_StJoe_id4	46.244000	-83.937000	-	-	-	-	0.717765 ± 0.000345
st joes	276_StJoe_id5	46.244000	-83.937000	-	-	-	-	0.714385 ± 0.000148
st joes	277_StJoe_id6	46.244000	-83.937000	-	-	-	-	0.714426 ± 0.000110
st joes	SJ_x_x_id4	46.244000	-83.937000	-84.0 ± 1.6	-	-	-	-
st joes	SJ_x_x_id5	46.244000	-83.937000	-87.0 ± 1.6	-	-	-	-
st joes	SJ_x_x_id6	46.244000	-83.937000	-91.0 ± 1.6	-	-	-	-
st joes	SJ_x_x_id7	46.244000	-83.937000	-97.0 ± 1.6	-	-	-	-
st joes	StJoe_id2_ko	46.244000	-83.937000	-91.0 ± 0.7	-	-	2.50 ± 0.20	-
st joes	StJoe_id1_ko	46.244000	-83.937000	-97.0 ± 0.7	-	-	3.30 ± 0.20	-
st joes	StJoe_id3_ko	46.244000	-83.937000	-103.0 ± 0.7	-	-	4.20 ± 0.20	-
trout lake	Trout_lake_id1_ko	46.634270	-84.290800	-	-	-	2.30 ± 0.20	-

Site	Sample ID	Latitude	Longitude	$\delta^{2}H$ (‰)	$\delta^{13}C$ (‰)	$\delta^{15}N$ (‰)	$\delta^{34}S$ (‰)	$^{87}Sr/^{86}Sr$
trout lake	Trout_lake_id2_ko	46.634270	-84.290800	-	-	-	3.00 ± 0.20	-
trout lake	Trout_lake_id3_ko	46.634270	-84.290800	-	-	-	4.50 ± 0.20	-
white river	WR1_x_x_id3	48.618903	-85.336450	-	-	-	4.10 ± 0.20	-
white river	WR1_x_x_id1	48.618903	-85.336450	-	-	-	4.30 ± 0.20	-
white river	WR1_x_x_id2	48.618903	-85.336450	-	-	-	4.30 ± 0.20	-

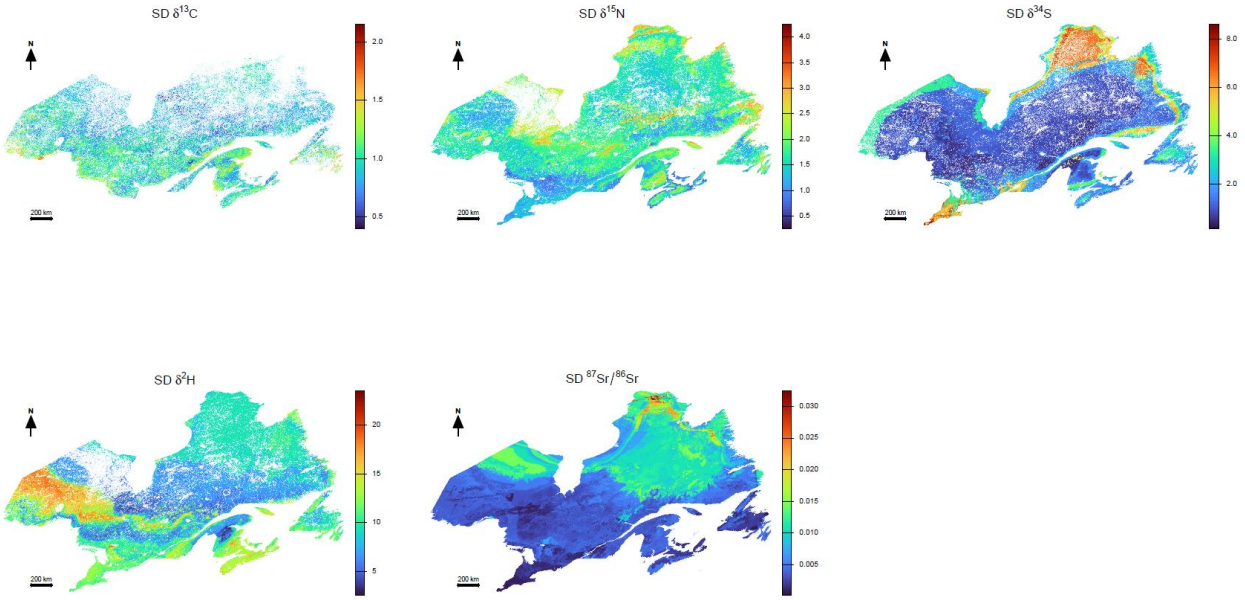

Figure S1 - Spatial distribution of predictive uncertainty (standard deviation) associated with the mean foliar isoscapes for carbon (δ^{13}C), nitrogen (δ^{15}N), sulfur (δ^{34}S), hydrogen (δ^{2}H), and strontium (^{87}Sr/^{86}Sr) across eastern Canada. Uncertainty estimates were derived from quantile random forest models and represent the expected pixel-wise variability of isotope predictions.

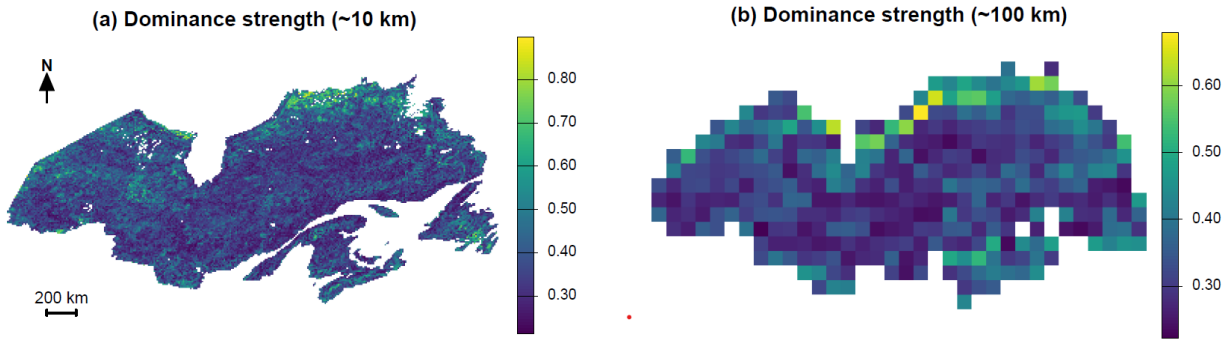

Figure S2 - Dominance strength of isotope geolocation potential at two spatial scales.
Maps show the dominance strength, defined as the maximum fractional separability across all isotope systems (C, N, S, H, and Sr) at each pixel. Dominance strength quantifies how strongly the top-ranked isotope outperforms all alternatives at a given location. Panel (a) displays dominance strength evaluated at a ~10 km spatial scale, and panel (b) at a ~100 km scale. Values approaching 1 indicate areas where a single isotope provides strongly dominant geolocation information, whereas lower values indicate regions where multiple isotopes contribute comparably to geolocation potential.

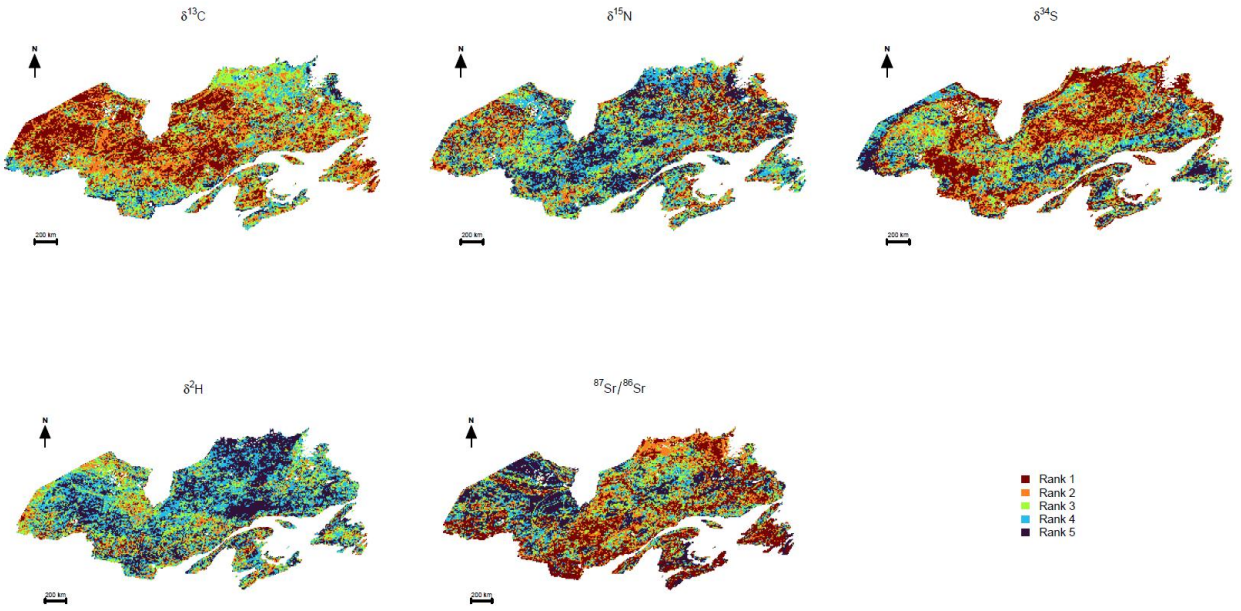

Figure S3- Spatial distribution of isotope rank based on fractional separability evaluated at a 10 km spatial scale. Each panel shows, for an individual isotope system (carbon, nitrogen, sulfur, hydrogen, or strontium), its rank relative to all other isotopes at each pixel (rank 1 = highest geolocation potential; rank 5 = lowest). Ranks were derived by ordering isotope-specific fractional separability values from highest to lowest at each location.

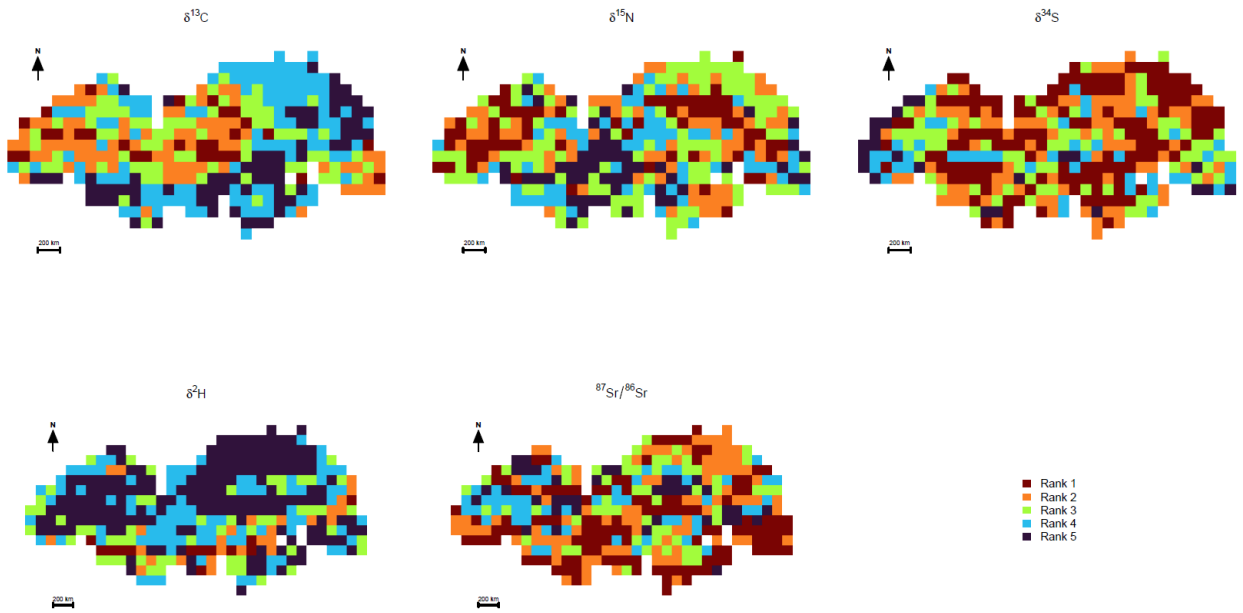

Figure S4 - Spatial distribution of isotope rank based on fractional separability evaluated at a 100 km spatial scale. Each panel shows, for an individual isotope system (carbon, nitrogen, sulfur, hydrogen, or strontium), its rank relative to all other isotopes at each pixel (rank 1 = highest geolocation potential; rank 5 = lowest). Ranks were derived by ordering isotope-specific fractional separability values from highest to lowest at each location.